

Investigations on the role of **GILZ in statin therapy and the influence of glucocorticoid metabolism in age-related inflammation**

Dissertation
zur Erlangung des Grades
des Doktors der Naturwissenschaften
der Naturwissenschaftlich-Technischen Fakultät
der Universität des Saarlandes

von
Jenny Vanessa Valbuena Pérez

Saarbrücken
2019

Tag des Kolloquiums: 16.07.2019

Dekan: Univ.-Prof. Dr. rer. nat. Guido Kickelbick

Berichterstatter: Prof. Dr. Alexandra K. Kiemer

Prof. Dr. Thorsten Lehr

Vorsitz: Prof. Dr. Claus Jacob

Akad. Mitarbeiter: Dr. Jennifer Herrmann

To the memory of my Abuelita

I love you, my angel

Contents

Abbreviations and Symbols	i
List of Figures	v
List of Tables	vii
Abstract	1
Zusammenfassung	2
1. Introduction	3
1.1 Cardiovascular disease	4
1.2 Statins	4
1.2.1 Pharmacological and pharmacokinetic aspects	4
1.2.2 Pleiotropic effects of statins.....	6
1.2.3 Statin-associated muscle symptoms.....	6
1.3 The glucocorticoid-induced leucine zipper (GILZ)	7
1.4 Aging and age-related diseases.....	8
1.4.1 Inflammaging	9
1.5 Glucocorticoid function and metabolism.....	9
1.5.1 Regulation of glucocorticoid response and function	9
1.5.2 Glucocorticoids in inflammation	10
1.6 Aim of the present work	12
2. Materials and Methods	13
2.1 Chemicals and reagents	14
2.1.1 General Buffers	14
2.2 Cell culture.....	15
2.2.1 Cell lines.....	15
2.2.2 Cell freezing / thawing.....	15
2.2.3 Primary cells	15
2.3 Bacterial culture.....	17
2.3.1 Generation of competent E. Coli	18
2.3.2 Plasmid isolation	18

2.4	Mice.....	18
2.5	RNA isolation and reverse transcription.....	18
2.6	Quantitative Polymerase Chain Reaction (qPCR)	19
2.7	Western blot	21
2.7.1	Near-Infrared detection	22
2.7.2	Chemiluminescent detection.....	22
2.8	Cytotoxicity measurement	23
2.9	Effects of statins on C2C12 differentiation.....	23
2.10	Jenner-Giemsa staining.....	24
2.11	Immunofluorescence	24
2.11.1	Whole-zebrafish immunofluorescence.....	25
2.12	GILZ induction under statin treatment	25
2.13	Gene expression in zebrafish embryos under statin treatment	26
2.14	Chromatin immunoprecipitation (ChIP).....	26
2.15	Lentiviral transductions and stable cell line generation	27
2.15.1	Lentivirus generation	27
2.15.2	Lentiviral titre	27
2.15.3	Antibiotic kill curve	28
2.15.4	Generation of C2C12shGILZ stable cell lines	29
2.15.5	KLF2 overexpression.....	29
2.15.6	Generation of RAW 264.7 ^{Cas9} cells	29
2.16	Short interfering (si) RNA-mediated gene knockdown.....	30
2.17	Morpholino-mediated Gilz silencing and mRNA-mediated overexpression in zebrafish.....	30
2.17.1	Morpholino (MO) design and mRNA synthesis	30
2.17.2	MO and mRNA Injection	30
2.18	CRISPR/Cas9-mediated GILZ knockout.....	31
2.18.1	Verification of editing efficiency	31
2.18.2	Sequencing analysis.....	31
2.19	Serum Analysis.....	32
2.20	Thiobarbituric acid reactive substances (TBARS) assay.....	32

2.21	Determination of 11 β -HSD1 activity in peritoneal macrophages.....	32
2.22	Determination of steroid levels via LC-HRMS/MS.....	32
2.23	Statistics.....	33
3.	Chapter I.....	34
3.1	Introduction.....	35
3.2	Results.....	37
3.2.1	Statins are toxic towards skeletal muscle cells.....	37
3.2.2	Non-toxic concentrations of statin induce GILZ in skeletal muscle cells.....	37
3.2.3	Toxic concentrations of statin induce GILZ expression.....	38
3.2.4	GILZ induction can be reversed by geranylgeranyl pyrophosphate.....	38
3.2.5	Statin-induced impairment of myogenesis is accompanied by GILZ induction.....	39
3.2.6	GILZ knockout abolishes the cytotoxic effects of statins.....	41
3.2.7	GILZ contributes to statin-induced inhibition of myogenesis.....	44
3.2.8	FoxO3 mediates GILZ induction by statins in muscle.....	48
3.2.9	Statins induce Gilz in zebrafish embryos, and deregulation of Gilz expression impairs somitogenesis.....	48
3.3	Discussion.....	51
4.	Chapter II.....	55
4.1	Introduction.....	56
4.2	Results.....	57
4.2.1	Statin cytotoxicity towards endothelial cells and macrophages.....	57
4.2.2	Atorvastatin induces GILZ expression in endothelial cells and macrophages.....	57
4.2.3	Statin-induced GILZ expression in HUVECs is mevalonate-dependent.....	59
4.2.4	KLF2 is not involved in the regulation of GILZ expression in endothelial cells.....	59
4.2.5	Development of a GILZ-KO endothelial cell line model via CRISPR/Cas9 editing.....	60
4.3	Discussion.....	64
5.	Chapter III.....	66
5.1	Introduction.....	67
5.2	Results.....	69
5.2.1	Lipid peroxidation and clinical chemistry analysis.....	69
5.2.2	Cytokine expression in tissues from aged mice.....	70

5.2.3 Altered glucocorticoid homeostasis in myeloid cells from aged mice.....	70
5.2.4 Reduced corticosterone levels and 11 β -HSD1 activity in aged mice	74
5.2.5 Upstream regulators of 11 β -HSD1 are downregulated in aged macrophages	74
5.3 Discussion.....	76
6. Summary and Conclusions.....	79
7. References.....	82
Appendix.....	95
Appendix 1	96
Appendix 2	98
Appendix 3	100
Acknowledgments.....	101

Abbreviations and Symbols

11-DHC	11-dehydrocorticosterone
aa	amino acids
ACTH	adrenocorticotropic hormone
Akt	RAC-alpha serine/threonine-protein kinase
ALT	alanine transaminase
ANOVA	analysis of variance
AP-1	activator protein 1
AST	aspartate transaminase
ATCC	American Type Culture Collection
AVP	arginine vasopressin
BCA	bicinchoninic acid
BMM	bone marrow-derived macrophages
bp	base pairs
BSA	bovine serum albumin
Ca(NO ₃) ₂	calcium nitrate
CaCl ₂	calcium chloride
Cas9	CRISPR associated protein 9
CBG	corticosteroid-binding globulin
cDNA	complementary DNA
ChIP	chromatin immunoprecipitation
CI	confidence interval
CRH	corticotropin-releasing hormone
CRISPR	clustered regularly interspaced short palindromic repeats
CRP	C-reactive protein
CVD	cardiovascular disease
DAPI	4',6-diamidino-2-phenylindole
DHEA	dehydroepiandrosterone
DM	differentiation medium
DMEM	Dulbecco's Modified Eagle's Medium
DMSO	dimethyl sulfoxide
DNA	deoxyribonucleic acid
DPBS	Dulbecco's Phosphate-Buffered Saline
ECACC	European Collection of Authenticated Cell Cultures
ECGM	endothelial cell growth medium
ECL	enhanced chemiluminescence

Abbreviations

EDTA	ethylene diamine tetracetic acid
ELISA	enzyme-linked immunosorbent assay
FBS	foetal bovine serum
FDB	<i>flexor digitorum brevis</i>
FHRE	forkhead response element
FoxO3a	forkhead box O3
FPP	farnesyl pyrophosphate
GADPH	glyceraldehyde 3-phosphate dehydrogenase
GC	glucocorticoid
gDNA	genomic DNA
GGPP	geranylgeranyl pyrophosphate
GILZ	glucocorticoid-induced leucine zipper
GM	growth medium
GR	glucocorticoid receptor
GRE	glucocorticoid response element
GTP	guanosine triphosphate
H ₃ BO ₃	boric acid
HCl	hydrochloric acid
HEPES	hydroxyethyl piperazineethanesulfonic acid
HESI	heated electrospray ionization
HIV	human immunodeficiency virus
HMG-CoA	3-hydroxy-3-methylglutaryl coenzyme A
HPA	hypothalamic-pituitary-adrenal
hpf	hours post-fertilization
HRP	horseradish peroxidase
HSD	hydroxysteroid dehydrogenase
HUVEC	human umbilical endothelial vein cells
ICE	inference of CRISPR Edits
IF	immunofluorescence
IGF-1	insulin-like growth factor-1
IgG	immunoglobulin G
IL	interleukin
IQR	interquartile range
IRE	insulin response element
KCl	potassium chloride
KH ₂ PO ₄	potassium dihydrogen phosphate
KHCO ₃	potassium bicarbonate
KLF2	Krüppel-like factor 2
KD	knockdown

Abbreviations

KO	knockout
LB	lysogeny broth
LC-HRMS/MS	liquid chromatography-high resolution mass spectrometry
LDL-C	low-density lipoprotein cholesterol
LPS	lipopolysaccharide
mAb	monoclonal antibody
Mcl-1	induced myeloid leukaemia cell differentiation protein
M-CSF	macrophage colony-stimulating factor
MDA	malondialdehyde
MgSO ₄	magnesium sulphate
MHC	major histocompatibility complex
MHC	myosin heavy chain
MMP	matrix metalloproteinase
MO	morpholino
MOI	multiplicity of infection
MRF	myogenic regulatory factor
mRNA	messenger RNA
mTOR	mammalian target of rapamycin
MTT	3-(4,5-dimethylthiazol-2-yl)-2,5-diphenyltetrazolium bromide
MVA	mevalonic acid
Na ₂ HPO ₄	sodium hydrogen phosphate
NaCl	sodium chloride
NADH	nicotinamide adenine dinucleotide
NADPH	nicotinamide adenine dinucleotide phosphate
NaH ₂ PO ₄	sodium dihydrogen phosphate
NCE	normalised collision energy
NF-κB	nuclear factor kappa B
NH ₄ Cl	ammonium chloride
NHEJ	non-homologous end joining
NO	nitric oxide
NOS	nitric oxide synthase
PBL	peripheral blood leukocytes
PBS	phosphate buffered saline
PCR	polymerase chain reaction
PER	proline/glutamate-rich
PGC-1α	peroxisome-proliferator-activated receptor coactivator-1α
PI3K	phosphoinositide 3 kinase
PM	peritoneal macrophages

Abbreviations

PRR	pattern recognition receptors
PVDF	polyvinylidene difluoride
RBB	Rockland blocking buffer
RIPA	radio Immunoprecipitation Assay
RNA	ribonucleic acid
RNase	ribonuclease
ROS	reactive oxygen species
RT-qPCR	reverse transcription – quantitative PCR
SAMS	statin-associated muscle symptoms
SDS	sodium dodecyl sulphate
SDS-PAGE	SDS-polyacrylamide gel electrophoresis
SEM	standard error of the mean
sgRNA	single guide RNA
shRNA	short hairpin RNA
SINE	short interspersed elements
siRNA	small interfering RNA
TBARS	thiobarbituric acid reactive substances
TBE	Tris/Borate/EDTA
TGF- β	transforming growth factor β
TNF- α	tumour necrosis factor α
tSIM	targeted single ion monitoring
TU	transducing units
UA	uric acid
UHPLC	ultra-high-performance liquid chromatography
VP	viral particles
WT	wildtype

List of Figures

Figure 1.1. General aspects of statins.	5
Figure 1.2. GILZ structure and functional domains.	7
Figure 1.3. The seven pillars of aging.	8
Figure 1.4. Regulation of cortisol levels.	10
Figure 3.1. Analysis of the publicly available ArrayExpress dataset E-TABM-116:	36
Figure 3.2. Statin cytotoxicity towards muscle cells.	37
Figure 3.3. Effect of statin treatment on <i>Gilz</i> mRNA expression in C2C12.	38
Figure 3.4. Effect of statin treatment at toxic concentrations on GILZ expression in muscle cells.	39
Figure 3.5. Effect of statins on C2C12 differentiation.	40
Figure 3.6. Effect of statins on GILZ expression during myogenesis.	41
Figure 3.7. Effect of GILZ knockout on statin-induced myotoxicity.	42
Figure 3.8. Effect of GILZ knockout on statin-induced FDB myofibre toxicity.	43
Figure 3.9. Effect of GILZ knockout on statin-induced anti-myogenic effects	44
Figure 3.10. <i>Gilz</i> expression in stable C2C12sh <i>Gilz</i> cell lines.	45
Figure 3.11. Effect of GILZ absence on statin-induced anti-myogenic effects, as measured by MHC IF.	46
Figure 3.12. Effect of GILZ absence on statin-induced anti-myogenic effects, as measured by Jenner-Giemsa staining.	47
Figure 3.13. Involvement of FoxO3 in statin-induced GILZ expression.	49
Figure 3.14. Effect of statins on gene expression in zebrafish, and effect of <i>gilz</i> deregulation in zebrafish muscle development.	50
Figure 4.1. Statin cytotoxicity towards endothelial cells.	57
Figure 4.2. Effect of statin treatment on mRNA expression in endothelial cells and macrophages.	58
Figure 4.3. Effect of mevalonate on statin-induced <i>GILZ</i> expression in endothelial cells.	59
Figure 4.4. Effect of KLF2 knockdown and overexpression on GILZ expression in endothelial cells.	60
Figure 4.5. Effect of statin treatment on GILZ expression in an endothelial cell line.	61
Figure 4.6. CRISPR/Cas9 – mediated GILZ knockout in cell lines.	62
Figure 4.7. Validation of CRISPR/Cas9-mediated genome editing in HMEC-1 and C2C12 clones <i>via</i> Sanger sequencing.	63
Figure 5.1. Aged mice show a pro-inflammatory phenotype.	68
Figure 5.2. Oxidative stress levels in livers from young and aged mice.	69

List of Figures

Figure 5.3. Expression of pro-inflammatory cytokines in tissues from young and aged mice.	71
Figure 5.4. Expression of GC-responsive genes in PM/PBL from young and aged mice.	72
Figure 5.5. Alterations in glucocorticoid metabolism in aged mice.	73
Figure 5.6. Differences in serum glucocorticoids and 11 β -HSD1 activity in young and aged mice.	74
Figure 5.7. Gene expression of upstream regulators of 11 β -HSD1.	75

List of Tables

Table 2.1. Primer sequences and annealing conditions for the transcripts evaluated in this study	20
Table 2.2. Antibodies used in this study for western blot	22
Table 2.3. Primers used in the ChIP assay	26
Table 5.1. Clinical chemistry analysis in serum from young and aged C57BL/6 mice.	69

Abstract

The glucocorticoid-induced leucine zipper (GILZ) is an immunomodulatory, ubiquitously expressed protein, with multiple roles in different pathophysiological processes. Aim of the present study was to evaluate the role of GILZ and glucocorticoid (GC) metabolism in two different settings:

Statins, the most prescribed class of drugs for prevention of cardiovascular disease, exert beneficial lipid-lowering independent effects, as well as muscle-related adverse effects, by mechanisms not fully understood. The role of GILZ in these mechanisms was investigated. Statins were able to induce GILZ expression in skeletal muscle, endothelial cells, and macrophages. Moreover, using *in vitro*, *ex vivo* and *in vivo* approaches, we demonstrated that GILZ is an important mediator of statin-induced muscle damage.

The second part of this study focused on aging, which is characterised by a chronic, low-grade inflammatory state —termed “inflammaging”— that contributes to age-related pathogenesis. The elucidation of the mechanisms that modulate this state is of interest to geroscience. Evaluation of the age-associated changes in the myeloid compartment of mice, focusing on glucocorticoid metabolism, showed reduced levels of circulating GCs that, together with perturbations in GC pre-receptor metabolism in aged macrophages, result in dysregulation of the anti-inflammatory networks in these innate immune cells and, thus, might promote the inflammaging phenotype.

Zusammenfassung

Der Glukokortikoid-induzierte Leucin Zipper (GILZ) stellt ein ubiquitär exprimiertes Protein dar und spielt eine Rolle in verschiedenen pathophysiologischen Prozessen. Ziel der vorliegenden Studie war es, die Beteiligung von GILZ und des Glukokortikoid (GC)-Metabolismus in zwei Ansätzen zu untersuchen.

In der Prävention kardiovaskulärer Erkrankungen stellen Statine die meistverordnete Substanzklasse dar. Neben ihrer Lipid-senkenden Wirkung zeichnen sie pleiotrope Effekte sowie muskelschädigende Nebenwirkungen aus. Zunächst wurde die Hypothese überprüft, dass GILZ für die Vermittlung dieser Prozesse eine Rolle spielt, die nicht in direktem Zusammenhang mit der Lipid-Senkung stehen. Statine führten zu einer Erhöhung der GILZ-Expression in Muskelzellen, Endothelzellen und Makrophagen. Darüber hinaus konnte gezeigt werden, dass GILZ als wichtiger Mediator in der Statin-induzierten Muskelschädigung agiert. Der zweite Teil der Studie fokussierte auf Alterungsprozesse, die sich durch eine chronische, Entzündung auszeichnen. Die Untersuchung alterungsbedingter Änderungen im myeloiden Kompartiment von Mäusen zeigte im Hinblick auf deren GC Metabolismus reduzierte Spiegel zirkulierender GCs. Zusammen mit Störungen im GC Prä-Rezeptor Metabolismus, wie er in alten Mäusen zu finden ist, führt dies zu einer Dysregulation des anti-inflammatorischen Netzwerks dieser Immunzellen, welches zum entzündlichen Phänotyp des Alterns beitragen könnte.

1. Introduction

1.1 Cardiovascular disease

The term cardiovascular disease (CVD) comprises a group of disorders of the heart, brain vasculature, and blood vessels, such as ischaemic heart disease (or coronary artery disease), stroke, and hypertension (Mendis et al., 2011). CVD is the leading cause of mortality and disability worldwide, accounting for an estimated 31% of global deaths per year (World Health Organization, 2018).

The main pathophysiological condition leading to CVD is atherosclerosis, a chronic inflammatory process that occurs in medium and large blood vessels (Mendis et al., 2011). The pathogenesis of atherosclerosis involves lipid deposition, activation of dysfunctional endothelium, and release of pro-inflammatory cytokines and chemoattractant molecules; subsequent leukocyte recruitment, activation and transmigration (primarily monocyte-derived macrophages that later form foam-cells, and T-cells); platelet aggregation; and smooth-muscle cell migration and proliferation as a result of cytokine and growth factor secretion (Tousoulis et al., 2014). Among the most important risk factors for atherosclerosis and CVD are advancing age and high atherogenic lipid burden, *i.e.* cholesterol and its lipoprotein carriers (Catapano et al., 2016; Grundy et al., 2018; Mendis et al., 2011).

1.2 Statins

Statins are the first line of treatment in the management of hyperlipidaemias and prevention of CVD (Catapano et al., 2016; Stone et al., 2014). Since their introduction in 1987, statin prescription has risen, as shown by several studies in different populations (Nolte et al., 2010; Salami et al., 2017; Vancheri et al., 2016). Thus, statins are positioned among the most prescribed drug classes worldwide, in a tendency that seems to be maintained.

1.2.1 Pharmacological and pharmacokinetic aspects

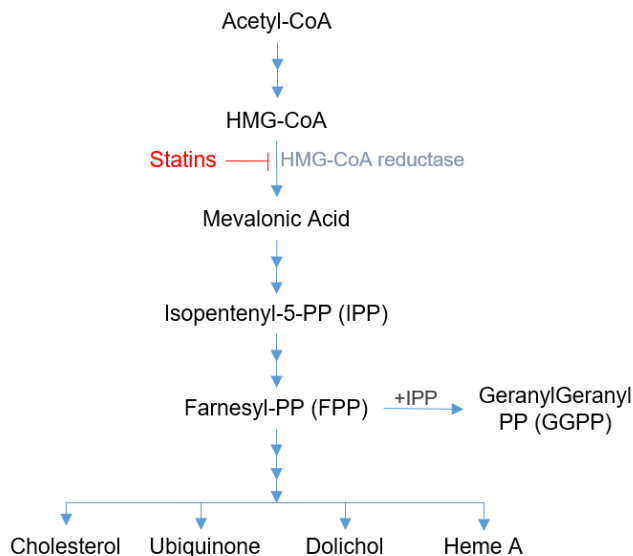
Statins are competitive inhibitors of the 3-hydroxy-3-methylglutaryl coenzyme A (HMG-CoA) reductase enzyme, the rate-limiting enzyme in the mevalonate biosynthetic pathway. As a consequence, they block the biosynthesis of cholesterol in the liver, enhancing clearance of circulating low density lipoprotein (LDL)-cholesterol (Sirtori, 2014). Inhibition of the mevalonate pathway by statins also impairs biosynthesis of its other products, such as isoprenoid metabolites, important for the post-translational modifications of several proteins, and ubiquinone (Figure 1.1 A).

First discovered as fungal secondary metabolites (Endo, 2010), statins are either classified according to their origin in natural/semi-synthetic (lovastatin, simvastatin and pravastatin), and synthetic statins (atorvastatin, rosuvastatin, fluvastatin, pitavastatin, and cerivastatin); or

Introduction

according to their lipophilicity. They are administered as the active hydroxy-acid, except for lovastatin and simvastatin, which are lactone prodrugs (Gazzerro et al., 2012; Sirtori, 2014). The chemical structure and lipophilic properties of statins are summarised in Figure 1.1 B.

A



B

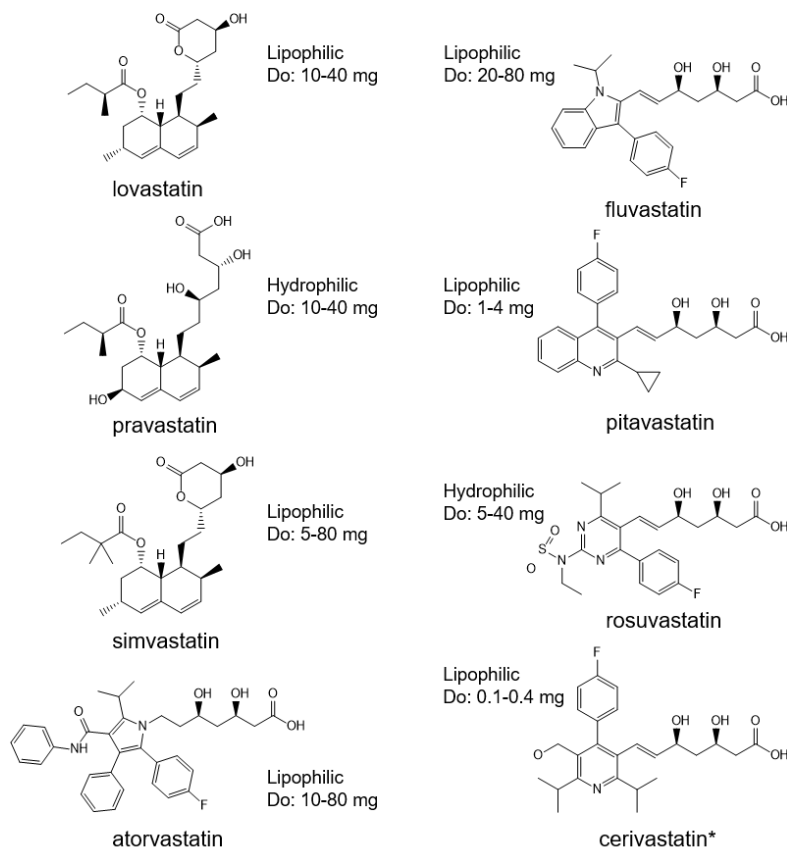


Figure 1.1. General aspects of statins. The mevalonate pathway, simplified schema (A). Statins inhibit HMG-CoA reductase, the rate limiting enzyme of the pathway. PP, pyrophosphate. The structure of the 8 therapeutically approved statins (B). The lipophilic properties and standard daily dose are specified. *Withdrawn from the market.

1.2.2 *Pleiotropic effects of statins*

Extended research has shown that statins exert beneficial effects independent from their lipid-lowering action. In the cardiovascular system, these so called “pleiotropic” effects include improvement of endothelial function, inhibition of vascular inflammation and thrombogenesis, and atherosclerotic plaque stabilisation (Almeida and Budoff, 2019). Furthermore, statins showed immunomodulatory and antioxidant actions, neuroprotective effects, and beneficial effects in lipid-independent diseases, such as rheumatoid arthritis, multiple sclerosis, bone loss, and cancer (Gazzerro et al., 2012; Margaritis et al., 2014; Oesterle et al., 2017).

Several cellular and molecular mechanisms underlie statin pleiotropy, the majority of them attributed to inhibition of Ras, Rho and Rac small GTPase function, as a result of reduced isoprenylation (Huacuja Álvarez et al., 2006). Studies have shown that statins increase the expression of the atheroprotective transcription factor Krüppel-like factor 2 (KLF2) and improve nitric oxide (NO) activity in the vascular endothelium, inhibit nuclear factor (NF)- κ B transcriptional activity in different cell types, inhibit cell proliferation, decrease reactive oxygen species (ROS) generation, and inhibit the major histocompatibility complex (MHC) II in T-cells, among other effects (Gazzerro et al., 2012; Margaritis et al., 2014; Oesterle et al., 2017).

1.2.3 *Statin-associated muscle symptoms*

It is generally considered that the benefits of statin therapy largely outweigh the risks of adverse effects (Collins et al., 2016), of which the most relevant are newly diagnosed type 2 diabetes mellitus, hepatotoxicity, and statin-associated muscle symptoms (SAMS) (Newman et al., 2019). SAMS are a class effect, dose-dependent and not correlated to the hypolipidemic effect of the statin (Kobayashi et al., 2008; Vaklavas et al., 2009). They constitute one of the principal causes of non-adherence to treatment, in fact, muscle toxicity was the reason for cerivastatin withdrawal from the market in 2001 (Taha et al., 2014). With a prevalence of 5–29% in clinical practice, SAMS can range from mild myalgia without elevation of creatine kinase (CK) to, in very rare cases, fatal rhabdomyolysis (Grundy et al., 2018; Stroes et al., 2015).

The molecular mechanisms that lead to muscle impairment are still not fully understood. Several HMG-CoA-related and non-related mechanisms have been proposed (recently reviewed by du Souich et al., 2017): isoprenoid depletion (particularly of GGPP) cause apoptosis and proteolysis mediated by inhibition of the protein kinase Akt and the transcriptional coactivator peroxisome-proliferator-activated receptor coactivator (PGC)-1 α ; direct impairment of mitochondrial respiration, ROS production, and calcium homeostasis in the myocyte also trigger apoptosis. Moreover, reduced resting chloride channel conductance and decreased lactate efflux could cause muscle fatigue. In addition to their myotoxicity, statins impair muscle regeneration *via* GGPP depletion, and impaired insulin-like growth factor-1

(IGF-1) signalling (Baba et al., 2008; Ogura et al., 2007; Trapani et al., 2012). Further research in the field can improve the understanding of these mechanisms and allow for identification of risks and biomarkers associated with SAMS (Muntean et al., 2017).

1.3 The glucocorticoid-induced leucine zipper (GILZ)

GILZ was first identified as a dexamethasone-inducible gene (*Tsc22d3*) encoding for a 137-amino acid (aa) protein in murine thymocytes (D'Adamio et al., 1997). Later, other splice variants of murine GILZ were described, encoding for proteins of 201 aa, 43 aa, 80 aa (Soundararajan et al., 2007), and 234 aa (Bruscoli et al., 2010). Human GILZ is a 134-aa protein with 97% similarity in the coding region with its murine orthologue (Cannarile et al., 2001). Different transcript variants coding for other isoforms are also annotated for the *GILZ* gene and have been observed experimentally (NCBI "Gene"; Köberle et al., 2012).

GILZ consists of three domains: The N-terminal domain (residues 1–75), a central leucine zipper (LZ) domain (residues 76–97), and the C-terminal domain, which includes a proline/glutamate-rich (PER) region (residues 98–137). The N- and C-terminal regions are responsible for the interaction of GILZ with its targets, while the LZ-domain mediates the protein homodimerization (Figure 1.2 Ayroldi et al., 2014; Fan and Morand, 2012a).

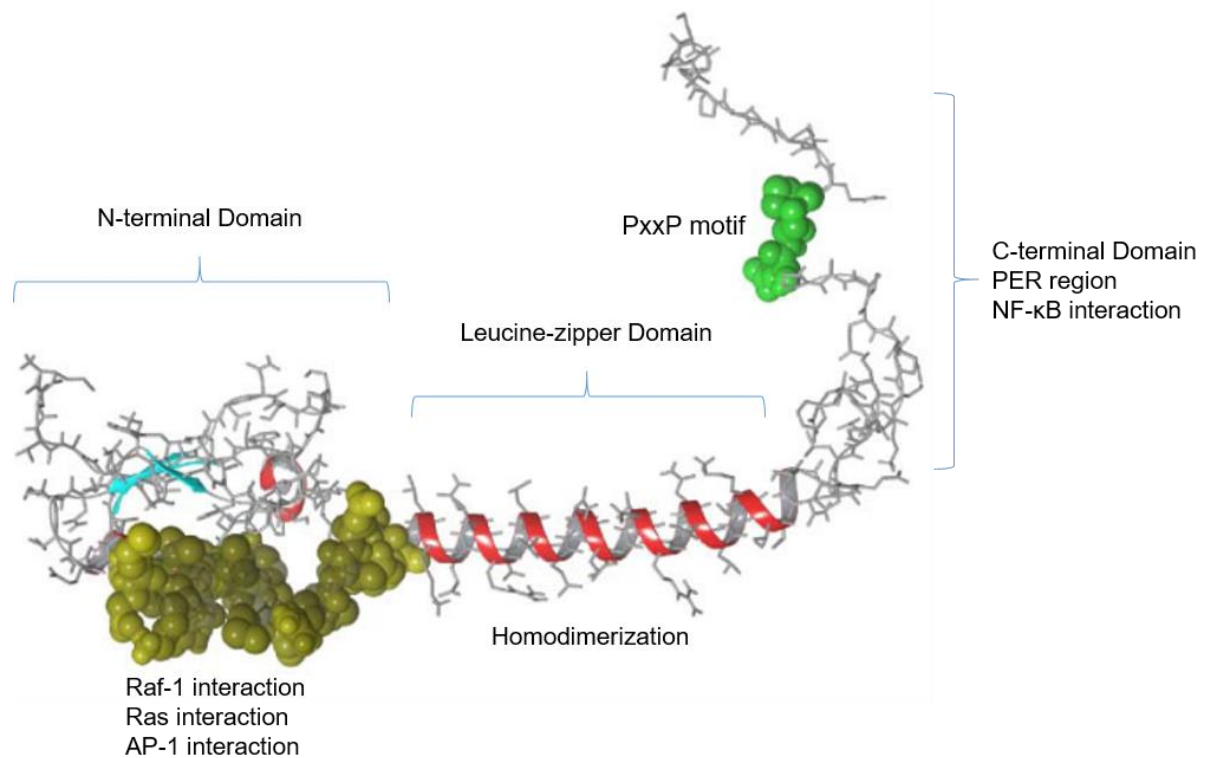


Figure 1.2. GILZ structure and functional domains. Modified from (Ayroldi et al., 2014).

GILZ is ubiquitously expressed in human and mouse tissues (Cannarile et al., 2001; Soundararajan et al., 2007). Besides its immunomodulatory function, it plays multiple roles in other glucocorticoid (GC)-mediated as well as non-GC-mediated cellular processes. The anti-inflammatory action of GILZ is mainly exerted *via* inhibition of NF- κ B transcriptional activity, as well as interaction with activator protein (AP)-1. Anti-proliferative, anti-oncogenic, pro-apoptotic and anti-apoptotic functions of GILZ in different cell types have also been reported (reviewed by Ayroldi et al., 2014).

1.4 Aging and age-related diseases

Aging, defined as the functional decline that occurs during the lifespan of an organism, constitutes a risk factor for several human pathologies (López-Otín et al., 2013). For instance, the prevalence and mortality associated with CVD is expected to grow exponentially, as the world population continues to age (Costantino et al., 2016). The recent field of geroscience intends to understand the mechanisms driving aging and age-related chronic disease, how they interact and overlap, in order to provide therapeutic opportunities to extend human lifespan by targeting aging itself (Kennedy et al., 2014). In this context, seven pillars of aging have been identified (Figure 1.3). These are not independent factors, but rather constitute an integrated network that, interestingly, converge on inflammation (Franceschi et al., 2018; Kennedy et al., 2014). Indeed, longitudinal studies have shown a correlation between inflammation and longevity, capability, and cognition in the aged population (Arai et al., 2015).

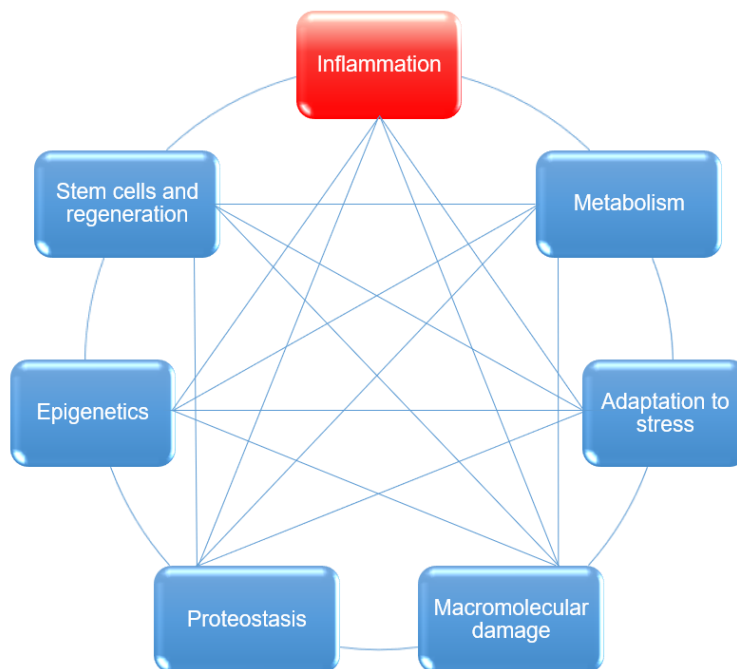


Figure 1.3. The seven pillars of aging. After Kennedy et al., 2014.

1.4.1 Inflammaging

The changes in the immune system associated with aging, globally known as immunosenescence, affect both innate and adaptive immunity. Rather than solely detrimental, such changes represent an adaptive/remodelling response that results in dysregulated homeostasis not only of immunity, but of other systems that influence and are influenced by the immune system, like the nervous and endocrine systems (Fulop et al., 2018).

The chronic, low-grade systemic inflammatory state observed with advancing age, termed “Inflammaging” (Franceschi et al., 2000), involves functional alteration of immune cells as a consequence of different mechanisms, including cellular senescence, oxidative stress, mitochondrial dysfunction, defective autophagy and mitophagy, inflammasome activation, and dysbiosis (Franceschi et al., 2018). Population studies have shown that aged individuals have elevated circulating levels of pro-inflammatory mediators/markers, such as tumour necrosis factor α (TNF- α), interleukin (IL)-6 and C-reactive protein (CRP), that correlate with increased risk of morbidity and mortality (Bandaranayake and Shaw, 2016; Minciullo et al., 2016). The global pro-inflammatory state, however, is not the only determinant of successful/unsuccessful aging, as a compensatory, anti-inflammatory response, is observed in parallel to inflammaging, particularly in very long-lived individuals (centenarians). The mediators associated with anti-inflammaging include transforming growth factor (TGF)- β , IL-10, dehydroepiandrosterone (DHEA), and cortisol (Baylis et al., 2013; Minciullo et al., 2016). It is considered that, ultimately, the ability of the anti-inflammatory network to cope with and modulate chronic inflammation is determinant to either attain healthy aging and longevity, or for the onset of chronic inflammatory diseases.

1.5 Glucocorticoid function and metabolism

1.5.1 Regulation of glucocorticoid response and function

Endogenous GCs are master regulators of several physiological functions, including metabolism, development, cardiovascular function, response to stress, and immune function (Kharwanlang and Sharma, 2017). The synthesis of GCs is regulated in a circadian manner, and in response to stressors (including pro-inflammatory cytokines), by the hypothalamic-pituitary-adrenal (HPA) axis, a component of the neuroendocrine system (Gupta and Morley, 2014). Activation of the HPA axis starts with release of corticotropin-releasing hormone (CRH) and arginine vasopressin (AVP) from the hypothalamus, which stimulate the secretion of adrenocorticotrophic hormone (ACTH) from the anterior pituitary gland. ACTH enters the circulation and stimulates synthesis of GCs through steroidogenesis in the adrenal cortex. Secreted GCs, in turn, cause a decrease in the release of CRH and ACTH, in a negative feedback loop (Figure 1.4 A). GCs circulate bound in a 95% to corticosteroid-binding globulin (CBG).

Free GCs can diffuse through cell membranes and exert their action by binding to the widely expressed glucocorticoid receptor (GR) through genomic mechanisms (transactivation, transrepression, and composite glucocorticoid response element (GRE) binding), or non-genomic effects (Cain and Cidlowski, 2017).

While the HPA axis controls systemic GC release, the bioavailability and activity of GCs is controlled at the intracellular, pre-receptor level, by two enzymes: 11 β -hydroxysteroid dehydrogenase (11 β -HSD) 1 and 2, that catalyse the interconversion of active cortisol and inactive cortisone (Chapman et al., 2013). 11 β -HSD1 functions mainly as a reductase, catalysing the NADPH-dependent reduction of cortisone to cortisol in the endoplasmic reticulum, although it can also act as an NADP-dependent dehydrogenase, inactivating cortisol. 11 β -HSD2, on the contrary, functions solely as a NAD-dependent reductase (Figure 1.4 B).

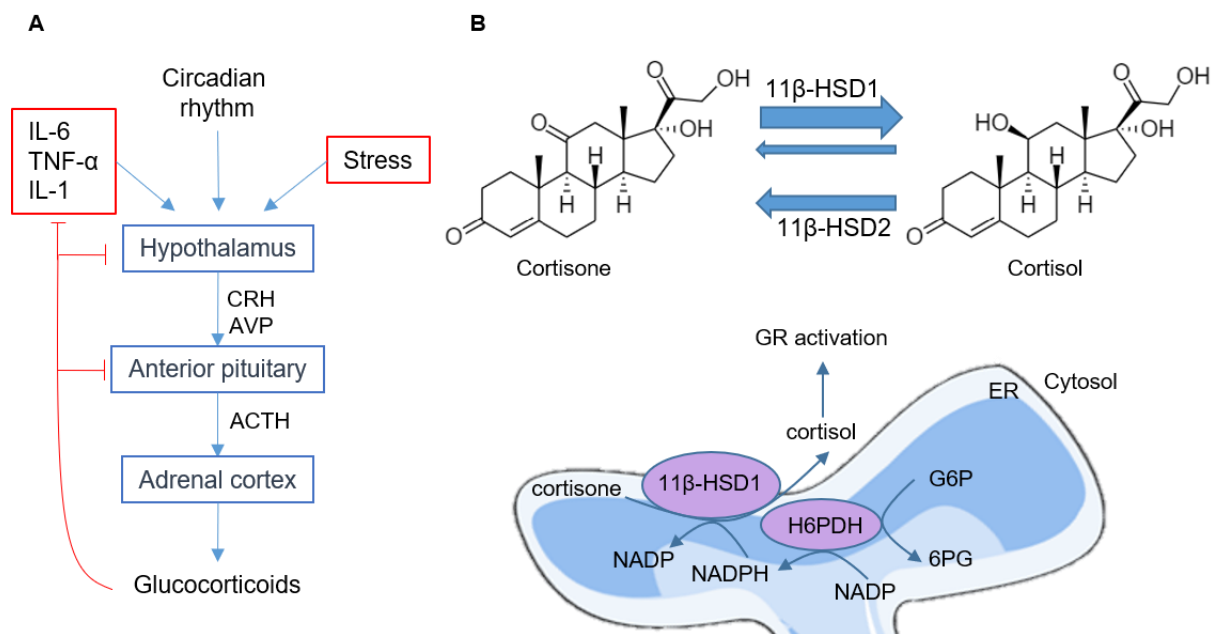


Figure 1.4. Regulation of cortisol levels. The HPA axis, see text for details (A). Intracellular levels of cortisol are controlled by the interconversion of cortisone and cortisol by 11 β -HSD isozymes (B). In the endoplasmic reticulum (ER), 11 β -HSD1 reduces cortisone to cortisol using the NADPH generated by hexose 6-phosphate dehydrogenase (H6PDH) as cofactor. H6PDH catalyses the conversion of glucose-6-phosphate (G6P) to 6-phosphogluconate (6PG).

1.5.2 Glucocorticoids in inflammation

Although GCs are well established anti-inflammatory agents in pharmacological therapy, they cannot be defined as strictly immunosuppressive in normal physiology. The anti-inflammatory action of GCs occurs at all stages of inflammation. During the alarm phase, GCs attenuate the secretion of pro-inflammatory mediators by inhibiting NF- κ B and AP-1 activity, decrease histamine release by mast cells, and reduce vascular permeability. In the mobilization phase,

they attenuate leukocyte extravasation by reducing the secretion of chemokines and adhesion molecules. Finally, during the resolution phase, they promote an anti-inflammatory, phagocytic phenotype in macrophages, to allow for tissue clearance (Cain and Cidlowski, 2017). On the other hand, GCs can also increase the expression of genes associated with the detection of insult and initiation of the inflammatory response, *i.e.* pattern recognition receptors (PRRs), chemokine/cytokine receptors, and complement factors, in what is thought to be a mechanism to sensitise immune cells so that they respond rapidly and effectively to insult. Once the inflammatory response is triggered, elevated concentrations of GCs (in response to stress) restrain the extent of inflammation, suppress the adaptive immune response, and help restore homeostasis (Busillo and Cidlowski, 2013; Cain and Cidlowski, 2017). This biphasic immunostimulant/immunosuppressive action highlights the main role of endogenous GCs in regulation of immunity, and how the dysregulation of GC secretion and function (*e.g.* during chronic stress associated with aging) might directly impair immune function.

1.6 Aim of the present work

Statins are the cornerstone of CVD prevention and treatment. As CVD remains the leading cause of morbidity and mortality worldwide, and a growing portion of the population already is or will be under statin treatment, the study of the molecular mechanisms that mediate their beneficial and deleterious effects remains of importance. In the first part of this work, we aimed to elucidate such mechanisms, focusing on the role of GILZ. First, its potential role in the onset of SAMS, the most common adverse effect associated with statin use, was investigated. Secondly, its potential role as an anti-inflammatory mediator of the pleiotropic effects of statins in vascular inflammation was evaluated.

The aging population is at high risk of suffering from cardiovascular events, as well as other age-related diseases. Chronic inflammation is one of the pillars that underlie the functional decline associated with age, thus, identification of the pathways that control/fuel the so called “inflammaging” process is relevant for the design of preventive and therapeutic strategies for age-related diseases. Aim of the second part of this work was to evaluate the age-associated changes in gene expression and glucocorticoid metabolism across tissues, as well as in the myeloid compartment of mice, to improve the current understanding of the molecular mechanisms that modulate inflammaging.

2. Materials and Methods

2.1 Chemicals and reagents

Cell-culture grade dimethyl sulfoxide (DMSO), atorvastatin, simvastatin, cerivastatin, pravastatin, and mevalonic acid lithium salt were obtained from Sigma-Aldrich (St Louis, MO, USA). Simvastatin sodium salt, geranylgeranyl pyrophosphate (GGPP), and farnesyl pyrophosphate (FPP) were obtained from Cayman Chemicals (Ann Arbor, MI, USA). 20 mM statin stock solutions were prepared in DMSO and stored at -20 °C. Unless stated otherwise, experiments performed with simvastatin refer to the active acid form of the drug. 100 mM stock solution from mevalonic acid was prepared in sterile water and stored at -20 °C. Foetal bovine serum (FBS), horse serum, trypsin-EDTA, accutase, high glucose DMEM, and RPMI 1640 were from Sigma-Aldrich. Penicillin/streptomycin and glutamine were from PAA (Pasching, Austria). MCDB 131 medium was from Thermo Fisher Scientific (Waltham, MA, USA). Endothelial Cell Growth Medium (ECGM) and endothelial cell growth medium SupplementMix were obtained from PromoCell (Heidelberg, Germany). DNA oligos and Sanger sequencing services were provided by Eurofins Genomics (Ebersberg, Germany). All other chemicals were obtained either from Sigma Aldrich or Carl Roth (Karlsruhe, Germany), unless stated otherwise.

2.1.1 General Buffers

PBS: 2.7 mM KCl, 1.8 mM KH_2PO_4 , 137 mM NaCl and 10 mM Na_2HPO_4 in distilled water. The pH was adjusted to 7.4 and the solution was adjusted to a final volume of 1 l. PBST was prepared by adding 0.1% tween-20 to PBS.

TBS: 20 mM Tris and 137 mM NaCl in distilled water. The pH was adjusted to 7.6 and the solution was adjusted to a final volume of 1 l. TBST was prepared by adding 0.1% tween-20 to TBS.

TBE: 90 mM Tris, 90 mM H_3BO_3 , 2 mM EDTA disodium in distilled water, in a final volume of 1 l.

Sodium phosphate buffer, 1 mM, pH 5.6: 65.05 mg $\text{NaH}_2\text{PO}_4 \cdot \text{H}_2\text{O}$, 4.05 mg Na_2HPO_4 in distilled water. The pH was adjusted to 5.6 and the solution was adjusted to a final volume of 500 ml.

Electrophoresis buffer: 25 mM Tris, 192 mM glycine, 0.1% SDS in distilled water, to a final volume of 1 l.

Blotting buffer: 25 mM Tris, 192 mM glycine, and 5% methanol in distilled water, to a final volume of 1 l.

2.2 Cell culture

2.2.1 Cell lines

C2C12 cells (ECACC 91031101) were maintained in high glucose DMEM (growth medium, GM) at a maximum confluency of 65%, HEK-293T cells (ATCC® CRL-3216) were maintained in high glucose DMEM, RAW 264.7 cells (ATCC® TIB-71) were maintained in RPMI 1640, and HMEC-1 cells (ATCC® CRL-3243) in MCDB 131 medium. All cell culture media were supplemented with 10% FBS, penicillin/streptomycin (100 U / 100 µg/ml), and 2.0 mM glutamine, unless stated otherwise. For inducing differentiation of C2C12 into myotubes, confluent cell layers were cultured in high glucose DMEM supplemented with 2% horse serum, penicillin/streptomycin and glutamine (differentiation medium, DM), with medium change every other day. All cells were cultured at 37 °C in a humidified atmosphere with 5% CO₂. Cells were subcultured according to the ATCC recommendations. Briefly, cells were washed with PBS and detached with trypsin-EDTA. Digestion was stopped with culture medium, the cell suspension was centrifuged for 5 minutes at 200 x g and resuspended in medium. The resulting suspension was used for seeding cells for experiments, and appropriate aliquots were used for passaging.

2.2.2 Cell freezing / thawing

For freezing, cells were washed and detached as for splitting. The cell suspension was centrifuged for 5 minutes at 200 x g and cells were resuspended in freezing medium (FBS with 10% DMSO). Cells were aliquoted into cryovials, frozen at -80 °C for 2 days, and transferred to liquid nitrogen for long-term storage.

For thawing, frozen cells were warmed up in a 37 °C water bath, and quickly transferred into pre-warmed medium. The resulting suspension was centrifuged for 10 minutes at 200 x g, the cell pellet was resuspended in culture medium and cells were cultured as described above.

2.2.3 Primary cells

Isolation of primary cells in the laboratory was performed with technical assistance from Theo Ranßweiler, Dr. Jessica Hoppstädter, and Anna Dembek.

Human umbilical endothelial vein cells (HUVECs): HUVECs were isolated from umbilical cords as described previously (Weber et al., 2003). In brief, the umbilical cord vein was digested with a 0.01% collagenase A solution (#10103586001, Roche, Basel, Switzerland) for 45 minutes. Cells were suspended in ECGM supplemented with endothelial cell growth medium SupplementMix, 10% FBS, penicillin/streptomycin (100 U / 100 µg/ml), and kanamycin (50 µg/ml), and plated in a 25 cm² cell culture flask. On the next day, cells were washed twice

with PBS, the medium was renewed, and cells were cultured as described above. Cells were used for experiments in passages 2–3.

Murine bone marrow-derived macrophages (BMMs): BMMs were isolated from male C57BL/6J wildtype (WT) or GILZ knockout (KO) mice, following a previously published method (Hoppstädter et al., 2015). In brief, femurs and tibias were flushed with RPMI 1640 medium supplemented with penicillin/streptomycin. After centrifugation for 10 minutes at 200 x g, the cell pellet was resuspended in hypotonic buffer (155 mM NH₄Cl, 10 mM KHCO₃ and 0.1 mM EDTA disodium in distilled water, to a final volume of 1 l) for erythrocyte lysis, during 3 minutes in a 37 °C water bad. Cells were centrifuged and resuspended in RPMI 1640 medium supplemented with 10% FBS (PAN Biotech, Aidenbach, Germany), penicillin/streptomycin, glutamine, and 50 ng/ml M-CSF (#99906, Biomol, Hamburg, Germany), plated in a 75 cm² cell culture flask, and allowed to adhere overnight. Non-adherent cells were then transferred into a 175 cm² cell culture flask and cultured for another 5 days before use in experiments.

Murine peripheral blood leukocytes (PBL): whole blood from young and aged C57BL/6 mice was collected in PBS-EDTA (5 mM EDTA in PBS) containing tubes, and centrifuged for 20 minutes at 500 x g and 4 °C. The cell pellet was resuspended in 1 ml erythrocyte lysis buffer and incubated for 15 minutes on ice. After 5 minutes of centrifugation at 500 x g and 4 °C, the supernatant was discarded and the PBL pellet was frozen at -80 °C.

Murine peritoneal macrophages (PMs): PMs were isolated from young and aged C57BL/6J mice by washing the peritoneal cavity with cold PBS-EDTA. The fluid was collected and centrifuged for 10 minutes at 350 x g and 4 °C. Cells were resuspended in RPMI-1640 medium supplemented with 10% FBS (PAN Biotech), penicillin/streptomycin, and glutamine, seeded in a 35 mm cell culture dish, and allowed to adhere for 2 hours. After this time, non-adherent cells were removed by washing with PBS and PMs were detached with accutase. The cell suspension was centrifuged, and the pellets were frozen at -80 °C. When used for treatment, cells were resuspended and plated in RPMI-1640 medium without FBS and, after removing the non-adherent cells at the end of 1 hour, treated as specified below.

Flexor digitorum brevis (FDB) muscle fibres: FDB fibres were isolated from WT or GILZ KO C57BL/6J mice by Dr. Jessica Hoppstädter in the laboratory of Professor Carlo Riccardi (Department of Medicine, University of Perugia), following a protocol adapted from the literature (Keire et al., 2013; Park et al., 2014; Weisleder et al., 2012). The FDB muscles were dissected under a stereo microscope and digested in a 0.2% collagenase A solution in DMEM for 60 minutes. Then, the myofibres were carefully separated under a stereo dissecting microscope, dispersed in DMEM containing 10% horse serum by drawing through a series of

pipette tips with gradually decreasing diameter, and purified by sedimentation steps. Pure fibres were plated in laminin (#L2020, Sigma Aldrich)-coated cell culture dishes, and cultured in DMEM supplemented with 20% serum replacement 2 (#S9388, Sigma Aldrich), 1% horse serum, penicillin/streptomycin, and glutamine.

Murine primary myoblasts: Primary myoblasts were isolated from hindlimbs of male 3-day-old WT or GILZ KO C57BL/6J mice by Dr. Jessica Hoppstädter in the laboratory of Professor Carlo Riccardi (Department of Medicine, University of Perugia). The muscle was dissected and shredded, washed in PBS and digested with trypsin-EDTA for 60 minutes. After filtering through a 70 µm cell strainer, the cell suspension was diluted in DMEM supplemented with 10% FBS and centrifuged for 20 minutes at 200 x g and 4 °C. The resuspended cells were pre-plated for 1 hour to allow fibroblast adhesion. Non-adherent cells were collected, centrifuged for 10 minutes at 200 x g and 4 °C, resuspended in F-10-based primary myoblast growth medium (Ham's F-10 nutrient mixture, #N6013, Sigma-Aldrich, supplemented with 20% FBS, penicillin/streptomycin, and glutamine), and plated onto collagen I (#C3867, Sigma-Aldrich)-coated cell culture dishes. Further enrichment of the myoblasts was achieved by dislodging and pre-plating the cells onto collagen-coated dishes every fourth day for 1-2 weeks. Afterwards, myoblasts were cultured in growth medium (40% DMEM, 40% Ham's F-10 nutrient mixture, 20% FBS), supplemented with penicillin/streptomycin and glutamine.

2.3 Bacterial culture

The following *E. coli* strains were used as host organisms for plasmid amplification:

TOP10 (Invitrogen, Carlsbad, CA, USA). Genotype: F⁻ mcrA Δ(mrr-hsdRMS-mcrBC) ϕ80lacZΔM15 ΔlacX74 nupG recA1 araD139 Δ(ara-leu)7697 galE15 galK16 rpsL(StrR) endA1 λ-

GT116 (Invivogen, San Diego, CA, USA). Genotype: F⁻ mcrA Δ(mrr-hsdRMS-mcrBC) ϕ80lacZΔM15 ΔlacX74 recA1 endA1 Δdcm ΔsbcC-sbcD.

Plasmids obtained from Addgene (Cambridge, MA, USA) were received and cultured in DH5α strain. Genotype: F⁻ ϕ80lacZΔM15 Δ(lacZYA-argF) U169 recA1 endA1 hsdR17 (rk⁻, mk⁺) phoA supE44 thi-1 gyrA96 relA1 λ-

Liquid cultures of bacteria were prepared in lysogeny broth medium (LB, 10% tryptone, 5% yeast extract, 5% NaCl, in water, pH 7.5), with or without antibiotic selection marker (ampicillin 100 µg/ml, Sigma-Aldrich), and cultured at 37 °C in an incubator shaker. Agar plates were prepared by adding 30% of agar to the culture medium.

2.3.1 Generation of competent *E. Coli*

Competent *E. coli* were generated using the calcium chloride method. Briefly, 5 ml of an overnight culture were diluted to 100 ml with LB and allowed to grow to an $OD_{600} = 0.4$. The culture was then placed on ice for 30 min, centrifuged at 2,000 x g and 4 °C, and resuspended in 10 ml ice cold $CaCl_2$ solution (75 mM $CaCl_2$, 15% glycerol, in water). After 30 minutes of incubation on ice, cells were centrifuged at 2,000 x g and 4°C, resuspended in 2.5 ml $CaCl_2$, aliquoted, and stored at -80 °C.

2.3.2 Plasmid isolation

Plasmids were isolated from overnight liquid cultures using either the High Pure Plasmid Isolation Kit (#11754777001, Roche), or the QIAprep Spin Miniprep Kit (#27106 Qiagen, Hilden, Germany), following the manufacturer's instructions.

2.4 Mice

Mice were housed in a 12/12 hours light/dark cycle with food and water ad libitum. GILZ KO mice were generated as previously described (Bruscoli et al., 2012; Hoppstädter et al., 2015). For aging studies, young (10 weeks) or aged (80–100 weeks) C57BL/6 mice were either non-treated or treated with one intraperitoneal injection of 5 mg/kg LPS (#tlrl-smlps, InvivoGen, San Diego, CA, USA) or vehicle (DPBS) for 4 hours before sacrifice (approval number from animal welfare committee GB 3-2.4.2.2-06/2016). Tissues were removed and stored at -80 °C for RT-qPCR analysis. Serum, BMMs, PBLs, and PMs were also collected for analysis

2.5 RNA isolation and reverse transcription

Total RNA from cultured cells was isolated using the High Pure RNA Isolation Kit (#11828665001, Roche), following the manufacturer's instructions. The RNA concentration was measured using a NanoDrop™ Lite spectrophotometer (Thermo Fisher Scientific). Samples with an A260/A280 ratio higher than 1.8 were used for further analysis.

Total RNA from murine tissue was isolated using the QIAzol lysis reagent (#79306, Qiagen) following the manufacturer's instructions. Residual genomic (g) DNA contamination was removed using the DNA-free™ DNA Removal Kit (#AM1906, Thermo Fisher Scientific). To verify the absence of gDNA, a SINE-PCR was performed using the GenScript Taq DNA polymerase (#E00007, GenScript Inc., Piscataway, NJ, USA). The primer sequences were: forward 5'-CTTCTGGAGTGTTTGAAGAC-3', reverse 5'-CTGGAACTCACTCTGAAGAC-3'. The reaction was carried out in a T100 thermal cycler (Bio-Rad Laboratories, Hercules, CA, USA) using the following program:

Denaturation	5 min 94 °C	} 30 cycles
Denaturation	1 min 94 °C	
Annealing	1 min 56 °C	
Elongation	1 min 72 °C	
Final elongation	10 min 72 °C	

RNA was considered free of gDNA contamination when no product was detected by agarose gel electrophoresis. A 2% agarose gel containing 0.04% ethidium bromide was used for detection. Upon addition of a suitable volume of 10 x loading buffer (40 mM EDTA disodium, 0.05% bromophenol blue, 0.05% xylene cyanol, 70% glycerol, in water ad 50 ml), DNA was loaded onto a gel and separated in TBE at 100 V. To determine the DNA fragment sizes, a 50 bp ladder (#SM0372, Thermo Fisher Scientific) was used. The DNA bands were detected using a UV transilluminator and the software ArgusX1 (Biostep, Stollberg, Germany).

RNA was reverse transcribed using the High Capacity cDNA Reverse Transcription Kit (#4368813, Thermo Fisher Scientific), in the presence of RNase inhibitor (RNaseOUT™, #10777019, Thermo Fisher Scientific), following the manufacturer’s instructions.

2.6 Quantitative Polymerase Chain Reaction (qPCR)

qPCR was performed on cDNA samples using the 5xHotFirePol EvaGreen qPCR Mix (no ROX, #08-25-00020, Solis BioDyne, Tartu, Estonia) in a 20 µl format. The primer sequences and annealing temperatures for each transcript are detailed in table 2.1. The reaction was conducted in a CFX96 touch™ Real-Time PCR detection system running the CFX Manager 2.1 software (Bio-Rad Laboratories), using the following program:

Denaturation	15 min 95 °C	} 40 cycles
Denaturation	0:15 min 94 °C	
Annealing	0:20 min	
Elongation	0:20 min 72 °C	
Plate read		
Melt curve	65 °C – 95 °C	

Data were analysed either by absolute quantification, using a standard curve of the PCR product cloned into the pGEM-T Easy vector (Promega, Madison, WI, USA), or with the comparative $\Delta\Delta C_t$ method. Housekeeping genes were chosen based on the literature, or after evaluating the expression stability of at least three candidate genes under the experimental conditions, using the geNorm, NormFinder, and BestKeeper Software tools. Absolute amounts of transcript were normalised to the corresponding housekeeping genes.

Table 2.1. Primer sequences and annealing conditions for the transcripts evaluated in this study

Gene	NCBI Accession number	Forward primer sequence 5'-3'	Reverse primer sequence 5'-3'	µl primer [10 µM] / reaction	Annealing T (°C)
<i>Human</i>					
<i>ACTB</i>	NM_001101.3	TGCGTGACATTAAGG AGAAG	GTCAGGCAGCTCGTA GCTCT	0.5	60
<i>KLF2</i>	NM_016270.2	AGACCACGATCCTCCT TGAC	AAGGCATCACAAGCC TCGAT	0.5	60
<i>NOS3</i> (<i>eNOS</i>)	NM_00603.4	CCTCACCGCTACAACA TCCT	ACGTTGATTTCCACTG CTGC	0.5	60
<i>TSC22D3</i> (<i>GILZ</i>)	NM_004089.3	TCCTGTCTGAGCCCTG AAGAG	AGCCACTTACACCGCA GAAC	0.5	60
<i>Mouse</i>					
<i>Anxa1</i>	NM_010730.2	TGGAAAGCCCTTGGAT GAAGT	AAGTCCCTTCATGGCA CCAC	0.5	60
<i>Cdkn1a</i>	NM_007669.5	GACCAGCCTGACAGA TTTCTA	TGGGCACTCAGGGTT TTCT	0.5	60
<i>Cdkn2a</i>	NM_009877.2	CGGGGACATCAAGAC ATCGT	GCCGGATTTAGCTCTG CTCT	0.5	60
<i>Cebpa</i>	NM_0012875 23.1	TTCGGGTCTGCTGGATC TCTA	TCAAGGAGAAACCAC CACGG	0.5	60
<i>Cebpb</i>	NM_0012877 39.1	GGAGACGCAGCACAA GGT	AGCTGCTTGAACAAG TTCCG	0.5	60
<i>Csnk2a2</i>	NM_009974.3	GTAAAGGACCCTGTGT CAAAGA	GTCAGGATCTGGTAG AGTTGCT	0.8	60
<i>GR-β</i>	HM236293.1	AAAGAGCTAGGAAAA GCCATTGTC	CTGTCTTTGGGCTTTT GAGATAGG	0.5	61
<i>H19</i>	NR_130973.1	CAGAGGTGGATGTGC CTGCC	CGGACCATGTCATGTC TTTCTGTC	0.5	60
<i>H6pd</i>	NM_173371.4	ATAGATGCGGAAGGT CGGGC	ACCAGCGTGAGGATC TCAGT	0.5	60
<i>Hdac3</i>	NM_010411.2	GCATTTCGAGGACATG GGGAA	TTTCGGACAGTGTAGC CACC	0.5	60
<i>Hsd11b1</i>	NM_008288.2	GGAACCCAGGAAGGA AGATCA	CAGGCAGGACTGTTCT AAGAC	0.5	60
<i>Hsd11b2</i>	NM_008289.2	AACCTCTGGGAGAAA CGCAAG	GGCATCTACAAGTGG GCTAAGG	0.5	60
<i>Il1b</i>	NM_008361.3	CCAAAAGATGAAGGG CTGCTT	GGAAGGTCCACGGGA AAGAC	0.5	60
<i>Il6</i>	NM_031168.2	AAGAAATGATGGATG CTACCAAAGTCTG	GTACTCCAGAAGACC AGAGGAAATT	0.4	60
<i>Klf2</i>	NM_008452.2	CCTTGCACATGAAGCG ACAC	ACTTGTCCGGCTCTGT CCTA	0.5	60
<i>Mkp1</i>	NM_013642.3	CTCCAAGGAGGATAT GAAGCG	ACTAGTACTCAGGGG GAGGC	0.5	60
<i>Mmp9</i>	NM_013599.3	GCCGACTTTTGTGGTC TTCC	TACAAGTATGCCTCTG CCAGC	0.5	60
<i>Nr3c1</i>	NM_008173.3	AAAGAGCTAGGAAAA GCCATTGTC	TCAGCTAACATCTCTG GGAATTCA	0.5	61

Materials and Methods

<i>Ppia</i>	NM_008907.1	GGCCGATGACGAGCC C	TGTCTTTGGAAC TTTG TCTGC	0.5	58
<i>Rn18s</i>	NR_003278.3	AGGTCTGTGATGCCCT TAGA	GAATGGGGTTCAACG GGTTA	0.5	61
<i>Sgk1</i>	NM_0011618 45.2	GAGGCCATGTGTCAAT CATGC	TTCTTTCACTTCACAC CCAGGTT	0.5	60
<i>Sirt1</i>	NM_019812.3	TGGAGCAGGTTGCAG GAATC	GGCACCGAGGAACTA CCTGAT	0.5	60
<i>Tnf</i>	NM_013693.2	CCATTCCTGAGTTCTG CAAAGG	AGGTAGGAAGGCCTG AGATCTTATC	0.5	60
<i>Tsc22d3</i>	NM_010286.4	GGGATGTGGTTTCCGT TAAACTGGA	TGCTCAATCTTGTTGT CTAGGGCCA	0.4	61
<i>Tsc22d3</i>	NM_010286.4	GCTGCTTGAGAAGAA CTCCCA	GAAC TTTTCCAGTTGC TCGGG	0.5	60
<i>Zebrafish</i>					
<i>actb2</i>	NM_181601.4	AAATTGCCGCACTGGT T	ACGATGGATGGGAAG ACA	0.5	60
<i>elf1</i>	NM_131159.2	CTCAAATGGCATGGAT GTTGCCCA	GGTCTTGGTTTGCGCA CTTTGGTT	0.5	60
<i>fbxo32</i>	NM_200917.1	GGAGCACCAAAGAGC GTCAT	AGTTGGGACTTGCGG ATGAG	0.5	60
<i>hatn10</i>	NA	TGAAGACAGCAGAAG TCAATG	CAGTAAACATGTCAG GCTAAATAA	0.5	60
<i>rn18s</i>	KY486501.1	CCGCTAGAGGTGAAA TTCTTG	CAGCTTTGCAACCATA CTCC	0.5	60
<i>tsc22d3</i>	NM_200569.2	AACAACCAGCTGGAG CGCGAA	GCAGAGCCCGTGCTG CTGTATT	0.5	60

2.7 Western blot

Protein lysates were prepared either in SB lysis buffer (50 mM Tris-HCl, 1% SDS, 10% glycerol, 5% β -mercaptoethanol, 0.004% bromophenol blue, in water) or RIPA buffer (50 mM Tris-HCl, 1% triton X-100, 0.1% SDS, 0.5% sodium deoxycholate, 150 mM NaCl, in water), supplemented with a protease inhibitor cocktail (cOmplete® Mini, # 04693124001, Roche). Samples were sonicated for 5 s and stored at -80 °C for further analysis. The protein concentration in RIPA lysates was measured using the Pierce™ BCA Protein Assay Kit (#23225, Thermo Fisher Scientific).

SDS-polyacrylamide gel electrophoresis (SDS-PAGE) was performed using polyacrylamide gels (4% stacking gel and 12% resolving gel) and the Mini PROTEAN system (Bio-Rad Laboratories). Samples were thawed on ice and denatured at 95 °C for 5 minutes before loading into the gel. For samples prepared in RIPA buffer, an appropriate volume of loading buffer (Roti®-Load 1, #K929, Carl-Roth) was added before denaturation. To estimate protein size, a prestained protein ladder was run in parallel to the samples (PageRuler™, #26616, Thermo Fisher Scientific). Samples were transferred onto an Immobilon®-FL PVDF membrane (#IPFL00010, Merck, Darmstadt, Germany) using a Mini Trans-Blot® cell (Bio-Rad

Laboratories). After blotting, the membrane was allowed to air-dry. Afterwards, it was soaked in methanol and rinsed with distilled water, before continuing with the immunodetection.

2.7.1 Near-Infrared detection

The membrane was blocked for 1 to 2 hours in blocking buffer for fluorescent western blotting (RBB, #MB-070, Rockland Immunochemicals, Limerick, PA, USA) before incubation with primary antibody at 4 °C overnight. Antibody sources and dilutions are indicated in table 2.2. The membrane was washed 4 times for 5 minutes with PBST (or TBST) and incubated with the appropriate IRDye-conjugated secondary antibody, at room temperature for 90 minutes. After washing, the signal was detected using an Odyssey® Near-Infrared Imaging System and software (LI-COR Biosciences, Lincoln, NE, USA).

2.7.2 Chemiluminescent detection

Chemiluminescent immunodetection was performed in the laboratory of Professor Carlo Riccardi (Department of Medicine, University of Perugia), using the HRP-coupled secondary antibodies listed in table 2.2 and the Clarity™ Western ECL Blotting Substrate (Bio-Rad Laboratories), according to the manufacturer's instructions.

Table 2.2. Antibodies used in this study for western blot

Antibody	Dilution	Cat. Number	Supplier
Mouse anti α -tubulin [DM1A] mAb	1:1,000 in 5% milk powder – PBST	T 9026	Sigma-Aldrich
Polyclonal goat anti 11 β -HSD1	1:400 in RBB	AF3397	R&D Systems, Minneapolis, MN, USA
Rat anti GILZ [CFMKG15] mAb	1:1,000 in 5% milk powder – TBST	14-4033-80	Thermo Fisher Scientific
Mouse anti GADPH [OTI2D9]	1:2,000 in 5% milk powder – TBST	TA802519	OriGene Technologies, Rockville, MD, USA
Mouse anti Akt (pan) [40D4] mAb	1:2,000 in 5% milk powder – TBST	2920	Cell Signalling Technology Danvers, MA, USA
Rabbit anti phospho-Akt (Ser473) [D9E] XP® mAb	1:2,000 in 5% milk powder – TBST	4060	
Polyclonal rabbit anti phospho-FoxO3a (Ser253)	1:2,000 in 5% milk powder – TBST	9466	
Mouse anti FoxO3a [D12] mAb	1:1,000 in gelatine buffer (0.75% gelatine A, 0.1% tween-20, 20 mM Tris, 137 mM NaCl, pH 7.5)	sc-48348 X	Santa Cruz Biotechnology Dallas, TX, USA
Mouse anti myogenin [5FD] mAb	1:200 in TBST	sc52903	Santa Cruz Biotechnology
Polyclonal rabbit anti cleaved Caspase-3	1:1,000 in TBST	ALX-210-807-C100	Enzo Life Sciences Farmingdale, NY, USA

IRDye® 680RD goat anti rabbit IgG	1:10,000 in RBB	926-68071	LI-COR Biosciences, Lincoln, NE, USA
IRDye® 800CW goat anti mouse IgG	1:10,000 in RBB	926-32210	
IRDye® 800CW donkey anti goat IgG	1:10,000 in RBB	926-32214	
Goat anti rat IgG (H+L), HRP	1:5,000 in TBST	31470	Thermo Fisher Scientific
Goat anti mouse IgG (H+L), HRP	1:5,000 in TBST	31430	
Goat anti rabbit IgG, HRP	1:10,000 in TBST	12-348	Merck

2.8 Cytotoxicity measurement

The 3-(4,5-dimethylthiazol-2-yl)-2,5-diphenyltetrazolium bromide (MTT) reduction assay was used to determine cell viability after statin treatment. Cells were seeded in 96-well plates at a density of 1×10^4 cells/well (or 2×10^4 cells/well for C2C12 differentiation), allowed to adhere overnight, and treated with test compounds at the indicated concentrations. Cells incubated without any treatment were used as growth controls, cells incubated with solvent at the maximum concentration present in the assay (0.25%) served as negative controls, and wells with treatment but without cells were used as blank. At the end of treatment, cells were incubated for 3 hours with MTT solution (0.5 mg/ml in medium) and lysed. The absorbance was measured at 550 nm in a microplate reader (XFluor4 Sunrise™, TECAN), using a reference wavelength of 690 nm. The relative viabilities were calculated related to the negative control; the comparison between the viability of growth control and negative control showed that the solvent had no statistically significant effect on cell viability (data not shown).

For evaluating the cell viability in FDBs treated with statin, fibres isolated from 2 mice were pooled and treated with test compounds at the indicated concentrations. At the end of treatment, the number of living and non-living myofibres was evaluated using the trypan blue exclusion method.

2.9 Effects of statins on C2C12 differentiation

C2C12 myoblasts were seeded at a density of 1.0×10^5 cells/well in 24-well plates and induced to differentiate in the absence or presence of non-toxic concentrations of atorvastatin (5 μ M), pravastatin (50 μ M), simvastatin (1 μ M) and cerivastatin (0.1 μ M) for 5–6 days. Myotube formation was evaluated *via* Jenner-Giemsa staining and IF of myosin heavy chain. Similarly, primary myoblasts of WT and GILZ KO mice, as well as stable C2C12^{scr} or C2C12^{shGILZ} cells (see 2.15) were induced to differentiate in the absence or presence of statins.

2.10 Jenner-Giemsa staining

To measure the myogenic differentiation of C2C12 myotubes Jenner-Giemsa staining was performed, following a previously published protocol (Veliça and Bunce, 2011). In brief, cells were fixed in ice-cold methanol for 5 minutes, air-dried, and stored at 4 °C until analysis. For staining, wells were incubated with Jenner's stain solution (Santa Cruz Biotechnology; diluted 1:3 in 1 mM sodium phosphate buffer pH 5.6) for 5 minutes at room temperature, washed with distilled water, and subsequently incubated with Giemsa solution (Carl Roth, diluted 1:20 in the same buffer) for 10 minutes at room temperature. Wells were observed in a phase contrast microscope equipped with a digital camera (ZEISS Axiovert 40 CFL with Canon EOS 400D), and each well was photographed in 3 randomly selected regions. Images were analysed using the free image-processing software Fiji ("Fiji Is Just ImageJ", Schindelin et al. 2012).

2.11 Immunofluorescence

Myosin heavy chain immunofluorescence (MHC IF) was performed on C2C12 myotubes. Cells were cultured and differentiated onto glass coverslips that were previously treated for 10 minutes in a 1:1 mixture of 70% ethanol and 0.1 N HCl (Andrés and Walsh, 1996). At the end of treatment, cells were pre-fixed by adding paraformaldehyde solution (4% in PBS) directly into the culture medium. After 2 minutes, the pre-fixation culture medium was replaced with paraformaldehyde solution and cells were fixed for 15 minutes at room temperature. Cells were washed with PBS and permeabilized with an 0.2% triton X-100 solution in PBS for 10 minutes at room temperature, washed, blocked in a 5% BSA solution in PBS for 1 hour at room temperature, and incubated with primary monoclonal anti-myosin heavy chain antibody (MF20, deposited by Donald A. Fischman to the Developmental Studies Hybridoma Bank, The University of Iowa, Department of Biology, Iowa City, IA, USA) diluted 1:50 in dilution buffer (1% BSA in PBS), at 4 °C overnight. After washing, cells were incubated with Alexa Fluor® 488 goat anti-mouse secondary antibody (#A11017, Thermo Fisher Scientific) diluted 1:800 in dilution buffer, for 1 hour at room temperature. Then, cells were washed and counterstained with DAPI (#D9542, Sigma-Aldrich) for 15 minutes at room temperature, mounted with FluorSave™ (Merck) and observed with an Axio Observer Z1 epifluorescence microscope, equipped with an AxioCam Mr3 and AxioVision software (Zeiss, Oberkochen, Germany). Photographs from randomly selected regions were analysed using the Fiji software, and the fusion index was calculated as the percentage of total nuclei incorporated into myotubes, defined as myosin-expressing cells containing 3 or more nuclei.

2.11.1 Whole-zebrafish immunofluorescence

Whole zebrafish embryos were stained following a protocol based on the literature (Cao et al., 2009). Zebrafish embryos were fixed in paraformaldehyde solution at 4 °C overnight, and then stored in methanol at -20 °C for at least four hours. Embryos were permeabilized in acetone for 30 minutes at -20 °C, washed, blocked in a 1% BSA solution in PBST for 2 hours at room temperature, and incubated with primary monoclonal anti-myosin heavy chain antibody (F59, deposited by Frank E. Stockdale to the Developmental Studies Hybridoma Bank, The University of Iowa, Department of Biology, Iowa City, IA, USA) diluted 1:100 in blocking buffer at 4 °C overnight. After washing in PBST, the embryos were incubated with Alexa Fluor® 594 goat anti-mouse secondary antibody (1:200; # A-11005 Thermo Fisher Scientific) at room temperature for 4 hours, washed again, and observed on a Leica SP8 Confocal microscope using the 40X magnification.

2.12 GILZ induction under statin treatment

To evaluate the ability of statins to induce GILZ in different cell types, HUVECs and C2C12 cells were seeded in 12-well plates at a density of 1.5×10^5 and 1.0×10^5 cells/well, respectively, and BMMs were seeded at 2.5×10^5 cells/well in 24-well plates. Cells were treated with 3 μ M atorvastatin and frozen at different time points for RT-qPCR analysis.

In a second set of experiments, C2C12 or primary murine myoblasts were seeded at 2.0×10^5 cells/well in 12-well plates and induced to differentiate in the absence or presence of non-toxic concentrations of atorvastatin (5 μ M), pravastatin (50 μ M), simvastatin (1 μ M) and cerivastatin (0.1 μ M) for up to 72 hours. Cells were frozen at different time points for RT-qPCR or western blot analysis.

For evaluating the effect of toxic concentrations of statins on GILZ expression levels, C2C12 myoblasts (5×10^4 cells/well) and 72-hour myotubes (1×10^5 cells/well) seeded in 24-well plates were treated with 50 μ M statins for 6 hours, in the absence or presence of mevalonate (100 μ M). Gene expression was evaluated *via* RT-qPCR, and protein *via* western blot. Primary murine myoblasts were similarly treated with atorvastatin and harvested for western blot analysis. In an analogue experiment, C2C12 myoblasts were treated with statin in the absence or presence of GGPP and FPP (10 μ M).

HUVECs were seeded in 24-well plates at 7×10^4 cells/well and treated with statins in the absence or presence of mevalonate (100 μ M) for 24 hours. HMEC-1 cells were seeded in 24-well plates at a density of 1×10^5 cells/well and treated with statins for 24 hours. Cells were frozen for RT-qPCR analysis.

2.13 Gene expression in zebrafish embryos under statin treatment

Zebrafish embryos from the AB wildtype strain were obtained from the laboratory of Professor Rolf Müller (Helmholtz Institute for Pharmaceutical Research Saarland). The developmental stage was determined by embryo morphology, in hours post fertilization (hpf, Kimmel et al. 1995) by observation under a stereo microscope. To examine the effects of statins, embryos at 19–22 hpf were sorted and placed at a density of 2–3 embryos/cm² in 6-well plates, and incubated at 28 °C in Danieus' solution (17 mM NaCl, 2.0 mM KCl, 1.5 mM HEPES pH 7.1–7.3, 1.8 mM Ca(NO₃)₂, 1.2 mM MgSO₄, 1.2 µM methylene blue, in water) containing 1 µM statin or solvent control. 12 hours after treatment, 10–20 embryos were pooled, flash-frozen in liquid nitrogen, and stored at -80 °C for RNA isolation and RT-qPCR analysis.

2.14 Chromatin immunoprecipitation (ChIP)

The ChIP assay was performed by Dr. Jessica Hoppstädter in the laboratory of Professor Carlo Riccardi (Department of Medicine, University of Perugia), using the EZ-ChIP™ Kit (#17-371, Merck) according to the manufacturer's instructions. In brief, C2C12 cells were fixed in 1% paraformaldehyde for 10 minutes, lysed, and sonicated on ice. Precleared lysates from 1x10⁶ myoblasts in a volume of 100 µl were incubated overnight at 4 °C with 10 µg monoclonal anti-FoxO3 antibody (D12, #sc-48348 X, Santa Cruz Biotechnology) or 10 µg normal mouse IgG (#12-371B, Merck). Immunocomplexes were purified, and qPCR analysis was performed using the SYBR® Select Master Mix (#4472908, Thermo Fisher Scientific) and The Applied Biosystems 7300 qPCR system to determine the abundance of specific *Gilz* promoter regions. The primers used to quantify forkhead response elements (FHRE)-containing sequences and a non-FHRE sequence within the *Gilz* promoter are listed in table 2.3.

Table 2.3. Primers used in the ChIP assay

	Forward primer sequence 5'-3'	Reverse primer sequence 5'-3'
FHRE1	TGGCCAGTTAAACCACATCC	GCTGAACTGTTTACAGTCCCTGA
FHRE2	TAACCGTGTAACAGGAGCCAG	GGAACCTCTGGGGAAATCCTA
FHRE3	AGCATGGGCAGAAAAAGGAATAAG	CTGGTTTGGTTGGTGTAACAGT
FHRE4 (IRE, insulin-response element,)	AGAGCTTTCTTGGTCTGAGAGAAT	AATTTTGAGGTGAGTAGCAGTAGT
non-FHRE	GTATTCGGCCTTCTCCTTGC	CTGCTGCGTGGTGAAAAACA

2.15 Lentiviral transductions and stable cell line generation

All lentiviral plasmids were obtained from Addgene. The packaging plasmid psPAX2 (#12260), and the envelope plasmid pMD2.G (#12259), were a gift from Didier Trono. FUW-tetO-loxP-hKLF2 was a gift from Rudolf Jaenisch (#60850, Theunissen et al., 2014). The pLKO.1-TRC cloning vector was a gift from David Root (#10878, Moffat et al., 2006). pLKO.1-scramble shRNA was a gift from David Sabatini (#1864, Sarbassov et al., 2005). LentiCas9-Blast was a gift from Feng Zhang (#52962, Sanjana et al. 2014).

Two different sequences of short hairpin (sh) RNA targeting murine GILZ were used for generating lentiviral particles. shGILZ1 (5'-GGAGTACTGACTGGTCTCTTA-3') was designed using the siRNA Wizard™ v3.1 software tool (InvivoGen). shGILZ2 (5'-ACAGCTT CACCTGACAATG-3') was previously published (Bruscoli et al., 2010). Sequences were cloned into the pLKO.1-TRC cloning vector, following the protocol available from Addgene (Addgene, 2006), with minor modifications. In brief, the cloning vector was digested with AgeI-HF and EcoRI-HF (New England BioLabs, Ipswich, MA, USA) and purified from an agarose gel using the NucleoSpin® Gel and PCR Clean-up Kit (#740609, Macherey-Nagel, Düren, Germany). The annealed oligos were then ligated into the vector using T4 DNA ligase (#M0202, New England BioLabs) overnight at room temperature. The ligation mix was transformed into GT116 *E. coli*, and ampicillin-resistant clones were screened for inserts by sequencing, using the pLKO.1 sequencing primer (5'-GACTATCATATGCTTACCGT-3').

2.15.1 Lentivirus generation

Lentiviral particles were produced following Addgene's protocol. Briefly, 5×10^5 HEK-293T cells plated onto 6-cm cell culture dishes in medium without antibiotics were transfected at 50–80% confluency with the transfer, packaging and envelope plasmids (1000:750:250) using the fuGENE® 6 Transfection Reagent (#E2691, Promega). 12–15 hours after transfection, the medium was replaced with complete DMEM. The lentivirus-containing media were then harvested at 24 and 48 hours, pooled, centrifuged at $200 \times g$ for 5 minutes, aliquoted, and stored at -20°C .

2.15.2 Lentiviral titre

Non-biological titration of the lentiviral vectors was performed by determining the viral particle content in the harvested supernatants, using a protocol adapted from the literature (Geraerts et al., 2006; Scherr et al., 2001). Genomic viral RNA was purified from 200 μl of freshly harvested lentivirus stock using the High Pure Viral RNA Kit (#11858882001, Roche), following the manufacturer's instructions. After digestion of residual DNA with the DNA-free™ DNA Removal Kit (Thermo Fisher Scientific), 10-fold serial dilutions of the purified viral RNA were

reverse transcribed and amplified *via* qPCR, using primers for the 5'LTR region (forward 5'-AGCTTGCCTTGAGTGCT TCA-3', reverse 5'-TGACTAAAAGGGTCTGAGGGA-3'), and the 5'-end of the *gag* gene (forward 5'-GGAGCTAGAACGATTCGCAGTTA-3', reverse 5'-TGTAGCTGTCCCAGTATTTGTC-3'). The copy number (viral particles, VP) contained in the supernatant was calculated from comparison against a plasmid standard curve, and the titre calculated as viral particles per ml of supernatant (VP/ml).

The biological titration of the vectors was performed either *via* limiting dilution, following the protocol developed by the MISSION® RNAi Team (Sigma-Aldrich); or by qPCR, following a procedure modified from the protocol of the Laboratory of Virology and Genetics at the EPFL (*École Polytechnique Fédérale De Lausanne*), as follows: HEK-293T cells were seeded in 12-well plates at a density of 8×10^4 cells/well and transduced with increasing amounts of lentiviral supernatant in the presence of 8 μ g/ml polybrene (#H9268, Sigma-Aldrich). 96 hours after transduction, gDNA was extracted using the GenElute Mammalian gDNA Miniprep Kit (#G1N70, Sigma Aldrich) according to the manufacturer's recommendations, and qPCR of 5'LTR and *gag* was performed, using *ACTB* as housekeeping gene. For each dilution, the HIV copy number integrated per genome was calculated as the ratio of 5'LTR or *gag* copies to *ACTB*, and the viral titre was determined as the number of transducing units per ml of supernatant (TU/ml).

For each lentivirus, the ratio from biological to non-biological titre was established and used for estimation of the functional titre (TU/ml) for all further preparations that were only titrated *via* the gRNA method. This functional titre was then used to determine the volume of viral supernatant needed for infecting cells at a given multiplicity of infection (MOI, defined as the number of TU per cell).

2.15.3 Antibiotic kill curve

The optimal concentration of antibiotic needed for selection of transduced cells was determined by performing an antibiotic kill curve. In brief, cells seeded at the same relative densities used for transduction in 24-well plates, were treated with increasing antibiotic concentrations. Cells were cultured with medium change every-other day and observed daily. The minimum concentration of antibiotic that resulted in complete cell death after 3–5 days was chosen for selection in the experiments.

To determine whether the cells were able to grow starting as single cells, the kill curve was performed on a 96-well plate, in a matrix that combined decreasing concentrations of antibiotic (in rows) with decreasing cell numbers (in columns), from 1,000 to 1 cell/well. Cells were

considered to be able to grow as single clones when growth was observed after 10 days in the antibiotic control wells containing less than 4 cells on average.

2.15.4 Generation of C2C12shGILZ stable cell lines

Stable, polyclonal C2C12 cell lines were generated by reverse transducing 7.5×10^4 cells in 6-well plates with scramble shRNA, shGILZ1, or shGILZ2 lentiviral particles at an MOI of 10 in the presence of polybrene, following the protocol for generation of stable cell lines available from Addgene. 24 hours after transduction the medium was changed, and 48 hours after infection puromycin (2 $\mu\text{g/ml}$, #540411, Merck) was added to select for transduced cells. The puromycin resistant cells were expanded for 2 to 3 weeks, after which they were harvested for analysis of gene and protein expression, and cell stocks were frozen. Further culture and experiments were done in 1 $\mu\text{g/ml}$ puromycin-containing medium. A non-transduced control was run in parallel to confirm no viable cells were present after selection.

2.15.5 KLF2 overexpression

The FUW-tetO-loxP-hKLF2 transfer vector uses the Tet-On system to allow for doxycycline-inducible overexpression of human KLF2. For overexpression in HUVECs, cells were seeded at 2×10^4 cells/well in a 24-well plate and transduced with hKLF2 lentivirus at an MOI of 10 and 20 in the presence of polybrene. 24 hours after transduction, medium containing 2 $\mu\text{g/ml}$ doxycycline (#ab141091, Abcam, Cambridge, UK) was added to the cells, to induce expression of the transgene. 72 hours after doxycycline addition, cells were harvested for RT-qPCR analysis.

2.15.6 Generation of RAW 264.7^{Cas9} cells

A RAW 264.7 macrophage cell line stably expressing Cas9 was generated for further use in CRISPR/Cas9 mediated gene editing experiments (see 2.18), following a protocol adapted from the literature (Joung et al., 2017). 5×10^5 cells were placed in a 6-well plate, Cas9 lentiviral particles were added at an MOI of 0.4 in the presence of polybrene, and cells were spininfected by spinning the plate at 1,000 x g for 2 hours at 33 °C. After 24 hours the medium was changed, and 48 hours after infection blasticidin S (12.5 $\mu\text{g/ml}$, #10264913, Fisher Scientific) was added to select for transduced cells. The blasticidin resistant cells were expanded for 2 to 3 weeks, after which cells stocks were frozen. A non-transduced control was run in parallel to confirm no viable cells were present after selection.

2.16 Short interfering (si) RNA-mediated gene knockdown

For silencing KLF2 expression in HUVECs, 5×10^4 cells were transfected in a 24-well format with an siPOOLTM targeting the KLF2 gene, or a negative control siPOOLTM (siTools Biotech, Planegg/Martinsried, Germany), using the riboxxFECT transfection reagent (Ribox, Radebeul, Germany). A reverse transfection protocol, according to the manufacturer's instructions, was followed. The final concentration of siRNA was 3–10 nM.

2.17 Morpholino-mediated *Gilz* silencing and mRNA-mediated overexpression in zebrafish

The gene silencing/overexpression experiments in zebrafish were performed by the research group of Professor William K.F. Tse (Faculty of Agriculture, Kyushu University, Fukuoka, Japan). Zebrafish from the AB wildtype strain were raised and staged as previously described (Kimmel et al., 1995). All experimental procedures were approved by the Animal Experimental Committee, Kyushu University.

2.17.1 Morpholino (MO) design and mRNA synthesis

The *Gilz* MO and mRNA experiments were performed as previously published (Tse et al., 2013). The sequence of *tsc22d3* MO, targeting the ATG site, was 5'-GATTTTTGAACATCTCCGTGCTCAT-3' (Gene Tools, Philomath, OR, USA). Its efficiency and specificity were confirmed by splicing MO, mRNA rescue, and Western blot analysis.

tsc22d3 mRNA was amplified from full-length cDNA using Pfu DNA polymerase (Agilent Technologies, Santa Clara, CA, USA) and the following primers: forward 5'-CCGAATTCATGAGCACAGAGATGTTCAA-3', reverse 5'-CCCTCGAGTTATACAGCAGAGCCCCGT-3', that contain EcoRI and XhoI restriction sites, respectively. The digested PCR products were ligated into the pCS2+ vector to generate the pCS2+*tsc22d3* expression construct. The construct vector was linearized by digestion with NotI, and capped RNA was *in vitro* transcribed with the mMACHINETM SP6 Transcription Kit (#AM1340, Thermo Fisher Scientific), following the manufacturer's instructions.

2.17.2 MO and mRNA Injection

Two pmol of *tsc22d3* MO or 1,200 pg of mRNA were injected into 1- or 2-cell stage embryos. Embryos from 4 different fish pairings were used for each injection. At 24 hpf, embryos were collected and fixed for whole-mount immunofluorescence staining, as described under 2.11.

2.18 CRISPR/Cas9-mediated GILZ knockout

The clustered regularly interspaced short palindromic repeats (CRISPR) / CRISPR-associated (Cas) 9 technique was used to disrupt the GILZ gene in HMEC-1 and C2C12 cells, using a transient transfection and clonal expansion approach. Validated synthetic TrueGuide™ single guide (sg) RNAs were obtained from Thermo Fisher Scientific. Target sequences were for *TSC22D3* 5'-ACTTACACCGCAGAACCACC-3', and for *Tsc22d3* 5'-GATGTACGCTGTGAGAGAGG-3'.

Cells at 30–70% confluency were transfected in a 12-well format with the synthetic sgRNA and a recombinant Cas9 protein (TrueCut™ Cas9 Protein v2, #A36496, Thermo Fisher Scientific), using the Lipofectamine™ CRISPRMAX™ Cas9 transfection reagent (#CMAX00001, Thermo Fisher Scientific), following the manufacturer's instructions. 48 hours after transfection, cells were detached and counted. A fraction of the cells was used for clonal expansion, following the limiting dilution cloning procedure for HMEC-1 (seeding cells at 0.8 cells/well in 96-well plates), or using cloning discs for isolation of single colonies from C2C12 seeded at low density (50, 250, 1,000 and 5,000 cells) in 6 cm cell culture dishes (Domann and Martinez, 1995). The remaining cells were used for gDNA extraction and verification of editing efficiency. The surviving clones after clonal expansion were harvested for gDNA extraction, PCR amplification of the edited region and sequencing analysis, amplified and kept either in culture or frozen, until confirmation of the knockout was achieved.

2.18.1 Verification of editing efficiency

The T7E1 endonuclease assay was performed on gDNA from control and transfected cells to verify the CRISPR genome editing in the mixed population. The assay is based on the ability of T7E1 to cleave mismatched DNA heteroduplexes, formed between WT and CRISPR-mutated DNA strands after denaturation and reannealing of a PCR product amplified from the genomic target region. To this end, the Alt-R™ Genome Editing Detection Kit (#1075931, Integrated DNA Technologies, Skokie, IL, USA) was used according to the manufacturer's instructions. The primers used for PCR amplification of the edited region were: *TSC22D3* forward 5'-GCTTGGTGTTACTAGGCCCC-3', reverse 5'-AGGATAGAGCTTCAGGCA CAA-3', *Tsc22d3* forward 5'-ACAGAAGGCTGACTTGGCTC-3', reverse 5'-GGCCAC GATGGCTAAGGAAT-3'. The annealing temperature for the PCR, run with the 5xHotFirePOI EvaGreen qPCR Mix under the program described in 2.6, was set at 64.4 °C.

2.18.2 Sequencing analysis

gDNA was extracted with QuickExtract® DNA Extraction Solution (#101094, Biozym, Hessisch Oldendorf, Germany). PCR of the edited region was performed as mentioned above,

the PCR products were purified and sent for analysis *via* Sanger sequencing. The sequencing primer sequences were: *TSC22D3* 5'-GCCACGATGGCTAAGGAATG-3', *Tsc22d3* 5'-GATAGAGCTTCAGGCACAATATAG-3'. Analysis of the sequencing files for indel detection was performed with assistance of the CRISP-ID web application (Dehairs et al., 2016), and the ICE analysis tool (Synthego, Redwood City, CA, USA).

2.19 Serum Analysis

Serum collected from young and aged mice was sent to the “*Zentrallabor des Universitätsklinikums des Saarlandes*” for clinical chemistry analysis. The determination of corticosterone and 11-dehydrocorticosterone (11-DHC) levels in serum was performed by the research group of Professor Markus Meyer (Centre for Molecular Signalling (PZMS), Saarland University), as described under 2.22.

2.20 Thiobarbituric acid reactive substances (TBARS) assay

Products of lipid peroxidation were measured in liver tissue from young and aged mice, following a previously described protocol (Simon et al., 2014). The total TBARS are expressed as μmol malondialdehyde (MDA) equivalents per μg of total protein, quantified using the Pierce™ BCA Protein Assay Kit.

2.21 Determination of 11 β -HSD1 activity in peritoneal macrophages

The determination of 11 β -HSD1 activity was performed by Rebecca Linnenberger and Dr. Jessica Hoppstädter. The activity of 11 β -HSD1 in PMs from young and aged mice was measured incubating cells with 0.1 μM or 1 μM cortisone-D₈ for 24 hours. At the end of treatment, supernatants were collected and analysed as described under 2.22 to measure cortisone-D₈ and cortisol-D₈ levels. The conversion to cortisol-D₈ was expressed as percentage of the total steroid measured, and is presented per μg of total protein, quantified using the Pierce™ BCA Protein Assay Kit.

2.22 Determination of steroid levels via LC-HRMS/MS

The determination of steroid levels was performed by the research group of Professor Markus R. Meyer (Centre for Molecular Signalling (PZMS), Saarland University), using liquid chromatography–high resolution mass spectrometry (LC-HRMS/MS). Samples were mixed 1:1 with an internal standard (cortisol-D₄, 100 $\mu\text{g}/\text{ml}$ in acetonitrile containing 0.1% formic acid), and centrifuged for 10 min at 18,407 x g and -10 °C. The supernatant was transferred into an MS vial and a volume of 5 μl was used for analysis.

Chromatographic separation of the analytes was carried out on a Dionex Ultimate UHPLC System (Thermo Fisher Scientific) using an Accucore™ Phenyl Hexyl LC column (100 mm x 2.1 mm, 2.6 µm) heated to 40 °C. Mobile phase A was water with 0.1% formic acid and ammonium formate, mobile phase B was acetonitrile with 0.1% formic acid. The LC gradient was as follows: starting with 2% solvent B over 0.1 min, the gradient was increased to 98% solvent B until 5 min, maintained at 98% until 7.5 min, and decreased to 2% until 10 min. The flow rate was set to 600 µl/min. Detection of analytes was achieved *via* high resolution mass spectrometry on a ThermoFisher Q-Exactive Plus equipped with a heated electrospray ionization (HESI)-II source. The HESI-II source conditions were as follows: sheath gas, nitrogen, at 55 arbitrary units; auxiliary gas, nitrogen, at 15 arbitrary units; temperature, 450 °C; spray voltage, 3.50 kV; ion transfer capillary temperature, 275 °C; and S-lens RF level, 55.0. Mass spectrometry was done in positive polarity mode using targeted single ion monitoring (tSIM) mode. The settings for tSIM mode were as follows: resolution, 35,000; microscans, 1; AGC target, 5e4; maximum IT, 200 ms; isolation window, 2.0 m/z; normalised collision energy (NCE), 35; scan range, m/z 150–900; spectrum data type, profile; and underfill ratio, 0.5%. The peak areas of the analytes were normalised using the internal standard peak area ratio.

2.23 Statistics

Results are expressed as mean ± SEM (standard error of the mean). Statistically significant differences between means were determined using the GraphPad Prism 6.0 or Origin 2019 software. Unless stated otherwise, an unpaired Welch's *t*-test was performed for the comparison of two groups, and the comparison of three or more groups was carried out by one or two-way analysis of variance (ANOVA) followed by Bonferroni's post-hoc analysis for individual differences. Where specified, median comparison of two groups was performed using Mann Whitney U Test; and median comparison of three or more groups was carried out by Kruskal-Wallis test followed by Dunn's post-hoc analysis. Results were considered significant at $P < 0.05$.

3. Chapter I

The glucocorticoid-induced leucine zipper (GILZ) mediates statin-induced muscle damage

3.1 Introduction

Statins are the first line of treatment in the management of hyperlipidaemia and prevention of CVD (Catapano et al., 2016; Grundy et al., 2018). These drugs are inhibitors of the HMG-CoA reductase enzyme, preventing the biosynthesis of cholesterol in the liver by blocking the mevalonate pathway and, as a consequence, enhancing clearance of circulating LDL-cholesterol (Sirtori, 2014). Since their introduction in 1987, statin prescription rates have risen, as shown by several studies in different populations (Nolte et al., 2010; Salami et al., 2017; Vancheri et al., 2016), positioning them among the most prescribed drug classes worldwide. Given the high prevalence of CVD, and the favourable data on CVD prevention by statins (Heller et al., 2017; Taylor et al., 2013), this tendency seems to be maintained.

Statins have a satisfactory safety profile, their most relevant adverse effect being skeletal muscle toxicity (Grundy et al., 2018). SAMS have an incidence of 5–29% in clinical practice (Grundy et al., 2018; Stroes et al., 2015), can range from mild myalgia to, in rare cases, fatal rhabdomyolysis (Moßhammer et al., 2014), and are a frequent cause for non-adherence to treatment or its discontinuation (Laufs et al., 2017). Although several studies have been conducted, and a number of risk factors that contribute to the onset of SAMS have been described, such as sex, pharmacokinetic differences, or genetic factors (Needham and Mastaglia, 2014; du Souich et al., 2017), the molecular mechanisms leading to myopathy are still not fully understood.

GILZ was first described as a dexamethasone-induced, immunomodulatory protein (D'Adamio et al., 1997). Since then, it has been shown that GILZ expression is not restricted to immune cells but is extended to several tissues and cell types, including skeletal muscle (Cannarile et al., 2001). GILZ plays multiple roles in both, glucocorticoid and non-glucocorticoid-mediated cellular processes (Ayroldi and Riccardi, 2009) beyond its immune-modulating function. For instance, studies demonstrated a role for GILZ in inhibition of adipocyte differentiation (Shi et al., 2003), in sodium homeostasis in the kidney, where it is robustly induced by aldosterone (Rashmi et al., 2017; Soundararajan et al., 2005), and in spermatogenesis, where lack of GILZ leads to hyperactivity of Ras signalling pathway and apoptosis during meiosis (Bruscoli et al., 2012). Of particular interest is the role described for GILZ in the regulation of skeletal muscle differentiation: it was shown that GILZ is strongly induced after dexamethasone treatment. In this setting, GILZ mediated dexamethasone anti-myogenic action *via* inhibition of the transcriptional activity of an early myogenic regulatory factor (MRF), MyoD (Bruscoli et al., 2010).

We analysed different publicly available gene expression profiling datasets that suggest statins were able to induce *GILZ* in different cell types (GEO accession numbers GDS2987, GSE32547, GSE4883). Interestingly, the analysis of a transcription profiling of human *quadriceps femoris* muscle following statin treatment suggested a moderate increase in *GILZ* expression in biopsies from patients receiving atorvastatin and simvastatin for 8 weeks, compared with those receiving placebo (ArrayExpress dataset E-TABM-116 (Laaksonen et al., 2006), Figure 3.1). In the present study, we aimed to test the hypothesis that *GILZ* plays a role in the onset of SAMS, focusing on both, myotoxic and anti-myogenic effects.

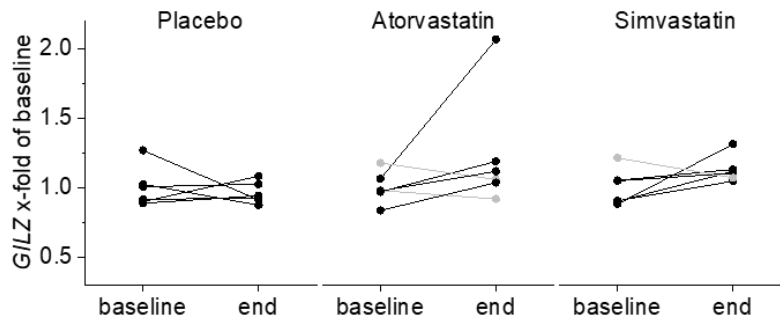


Figure 3.1. Analysis of the publicly available ArrayExpress dataset E-TABM-116: transcription profiling of human quadriceps femoris muscle following statin treatment. *GILZ* mean expression (NCBI RefSeq NM_004089.3; scan REFs GI_37622900-A, GI_37622900-I) is shown as fold of baseline. Connected data points represent patients before and after intervention.

3.2 Results

3.2.1 Statins are toxic towards skeletal muscle cells

We used the MTT assay to measure cell viability of C2C12 myoblasts and differentiating myotubes treated with increasing concentrations of atorvastatin, cerivastatin, simvastatin in its lactone and acid forms, and pravastatin, for 24 hours. All statins were toxic towards myoblasts, although higher concentrations of the hydrophilic statin pravastatin were needed to cause a significant decrease in cell viability (Figure 3.2 A). In myotubes, neither pravastatin nor simvastatin acid was significantly toxic at the evaluated concentrations (Figure 3.2 B).

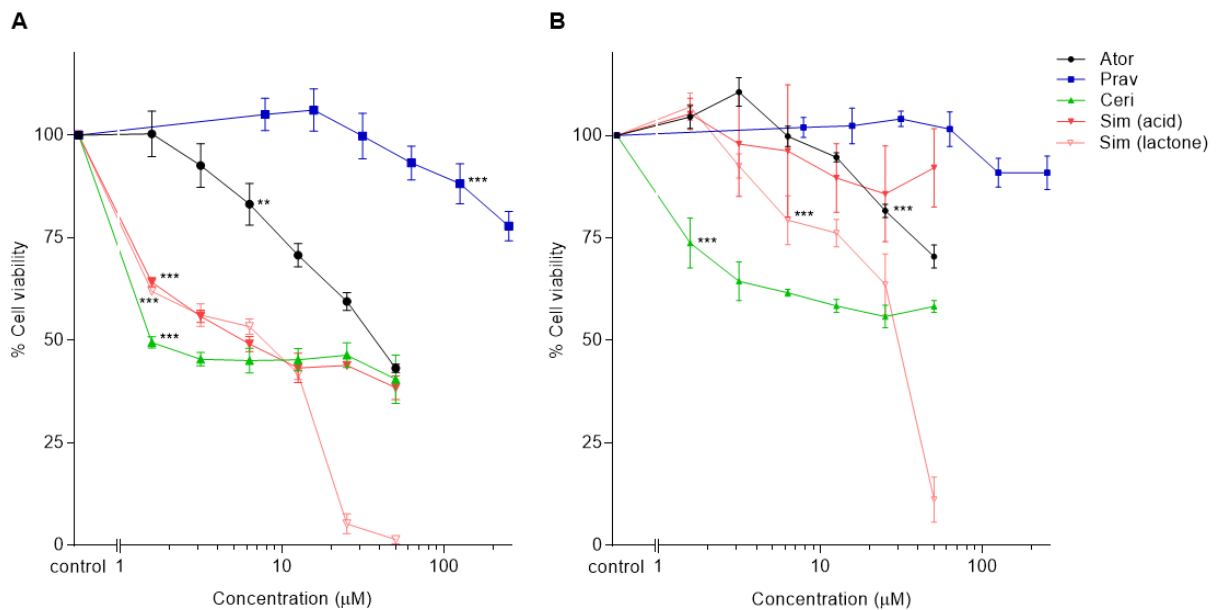


Figure 3.2. Statin cytotoxicity towards muscle cells. C2C12 myoblasts (**A**) or 48-hours myotubes (**B**) were treated with increasing concentrations of atorvastatin (Ator), cerivastatin (Ceri), pravastatin (Prav), simvastatin (Sim) acid or simvastatin lactone for 24 hours. The cell viability was measured via MTT assay. Data show the mean of three independent experiments performed in replicates \pm SEM. ** $P < 0.01$, *** $P < 0.001$ for the lowest concentration that caused a significant decrease in viability relative to the control.

In accordance with the literature (Skottheim et al., 2008; Taha et al., 2016), comparison of the dose-response curves also showed that the lactone form of simvastatin was more toxic towards muscle cells than the active acid form of the drug [statin main effect, myoblasts $F(1,24)=115.8$, $P < 0.001$; myotubes $F(1,24)=21.16$, $P < 0.001$].

3.2.2 Non-toxic concentrations of statin induce GILZ in skeletal muscle cells

To first evaluate whether GILZ expression was modified in muscle cells in the presence of statins, we treated C2C12 myoblasts with a non-toxic concentration of atorvastatin (3 μ M) for up to 24 hours and measured the levels of *Gilz* mRNA at different time points. A significant

increase compared with the control was detected after 8 hours of treatment, to a level of induction that was maintained until the end of treatment (Figure 3.3).

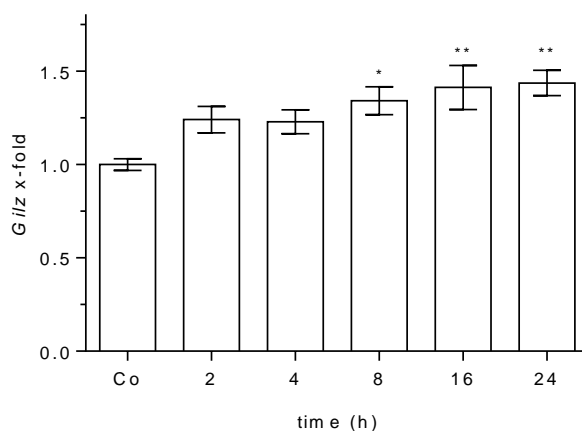


Figure 3.3. Effect of statin treatment on *Gilz* mRNA expression in C2C12. C2C12 myoblasts were treated with atorvastatin (3 μ M) for up to 24 hours. *Gilz* expression was normalised against the housekeeping gene (*Rn18s*) and is presented as fold change of control. Data show the mean of 3 independent experiments performed in replicates \pm SEM. * $P < 0.05$, ** $P < 0.01$, relative to the control.

3.2.3 Toxic concentrations of statin induce GILZ expression

Next, we treated myoblasts and myotubes with 50 μ M atorvastatin, simvastatin, or cerivastatin. At this concentration all statins were cytotoxic after 24 hours, but not at 6 hours (Figure 3.2 and data not shown). We detected an increase in *Gilz* mRNA expression after 6 hours of treatment with all statins, which was reversed by the addition of mevalonate (100 μ M) to the medium, indicating that the mechanism of GILZ induction relates to the inhibition of HMG-CoA reductase (Figure 3.4 A–B). In myotubes, the increase in *Gilz* expression was modest compared with that of myoblasts. Western blot analysis showed an elevated expression of GILZ protein in both, C2C12 and primary murine myoblasts treated with toxic concentrations of statins (Figure 3.4 C–F).

3.2.4 GILZ induction can be reversed by geranylgeranyl pyrophosphate

The inhibition of HMG-CoA by statins not only impairs cholesterol biosynthesis, but also other biosynthetic pathways. Of main importance is the inhibition of protein prenylation resulting from decreased synthesis of the isoprenoid derivatives GGPP and FPP. Thus, we evaluated whether GILZ induction could be reversed by the addition of any, or both, of these mediators to the medium. Co-treatment of C2C12 myoblasts with 10 μ M GGPP in addition to simvastatin completely reversed *Gilz* induction, while FPP had no effect (Figure 3.4 G).

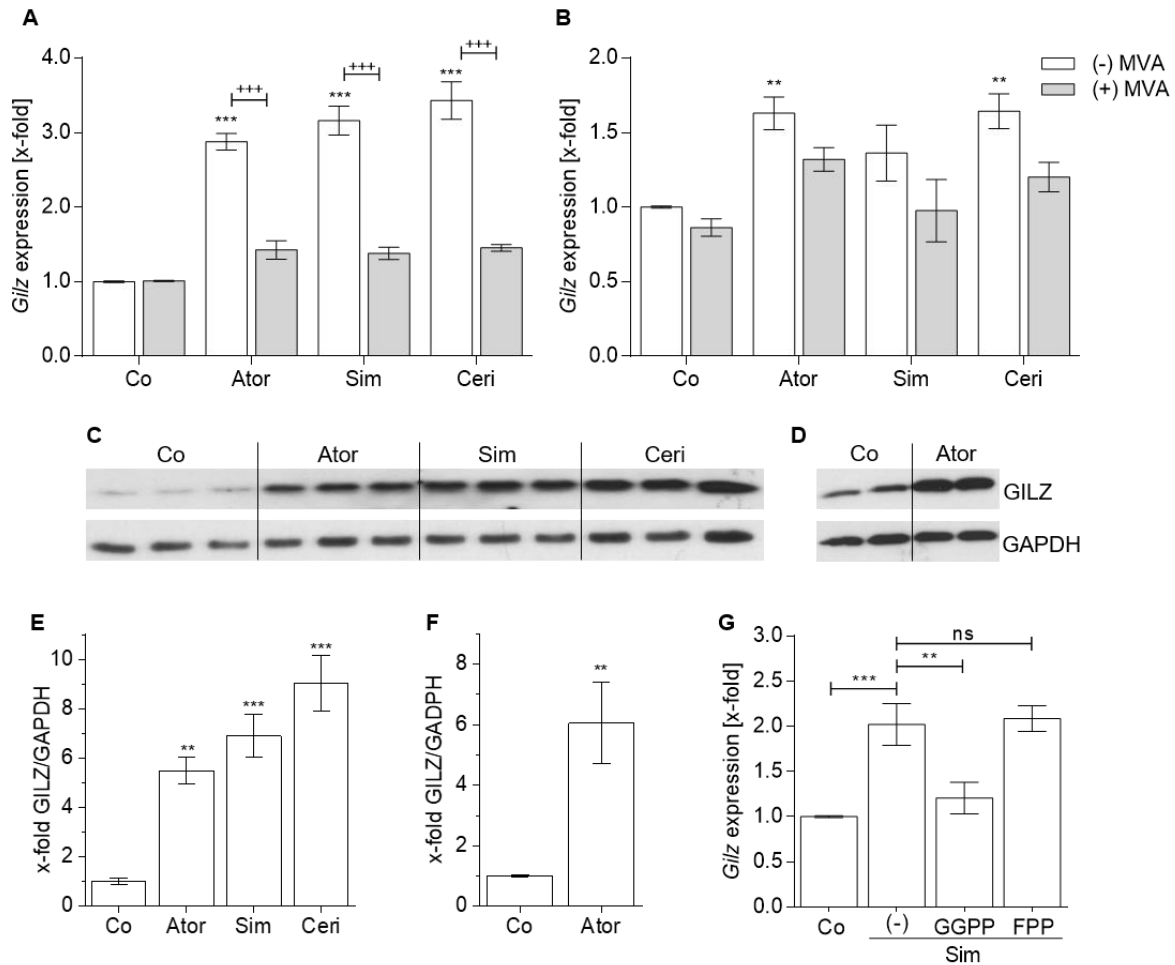


Figure 3.4. Effect of statin treatment at toxic concentrations on GILZ expression in muscle cells. C2C12 myoblasts (A) or 72-hour myotubes (B) were treated with 50 μ M statin in the absence or presence of mevalonate (MVA, 100 μ M) for 6 hours, *Gilz* mRNA expression was measured. GILZ protein expression was measured in C2C12 (C) and primary murine (D) myoblasts after treatment with 50 μ M statin for 6 hours. One representative blot is shown. Densitometric analysis, normalised to the housekeeping protein (E,F). C2C12 myoblasts were treated with 50 μ M simvastatin in the absence or presence of GGPP and FPP (10 μ M) for 6 hours, *Gilz* mRNA levels were measured (G). mRNA expression was normalised against the housekeeping gene (*Csnk2a2*) and is presented as fold change of control. Data show the mean of at least 2 independent experiments performed in replicates \pm SEM. ** $P < 0.01$, *** $P < 0.001$ relative to the corresponding control, +++ $P < 0.001$ relative to the non-MVA condition.

3.2.5 Statin-induced impairment of myogenesis is accompanied by GILZ induction

Myogenesis is a multistep, tightly regulated process that leads to the formation of skeletal muscle, both during embryonic development as well as in adult life, to maintain muscle homeostasis and repair muscle after injury (Bentzinger et al., 2012). Statins are not only toxic towards skeletal muscle fibres but might also impair the muscle regeneration process (Baba et al., 2008; Ogura et al., 2007; Trapani et al., 2012). To examine these effects, we induced differentiation of C2C12 myoblasts by switching confluent cell layers to differentiation medium (DM) in the absence or presence of statins, and evaluated myotube formation by Jenner-Giemsa staining and myosin heavy chain (MHC) immunofluorescence. We observed that treatment of C2C12 cells with sub-toxic concentrations of statins during differentiation resulted in less

myotube formation, and a significantly reduced fusion index after 6 days, where fully differentiated myotubes were visible in the control (Figure 3.5).

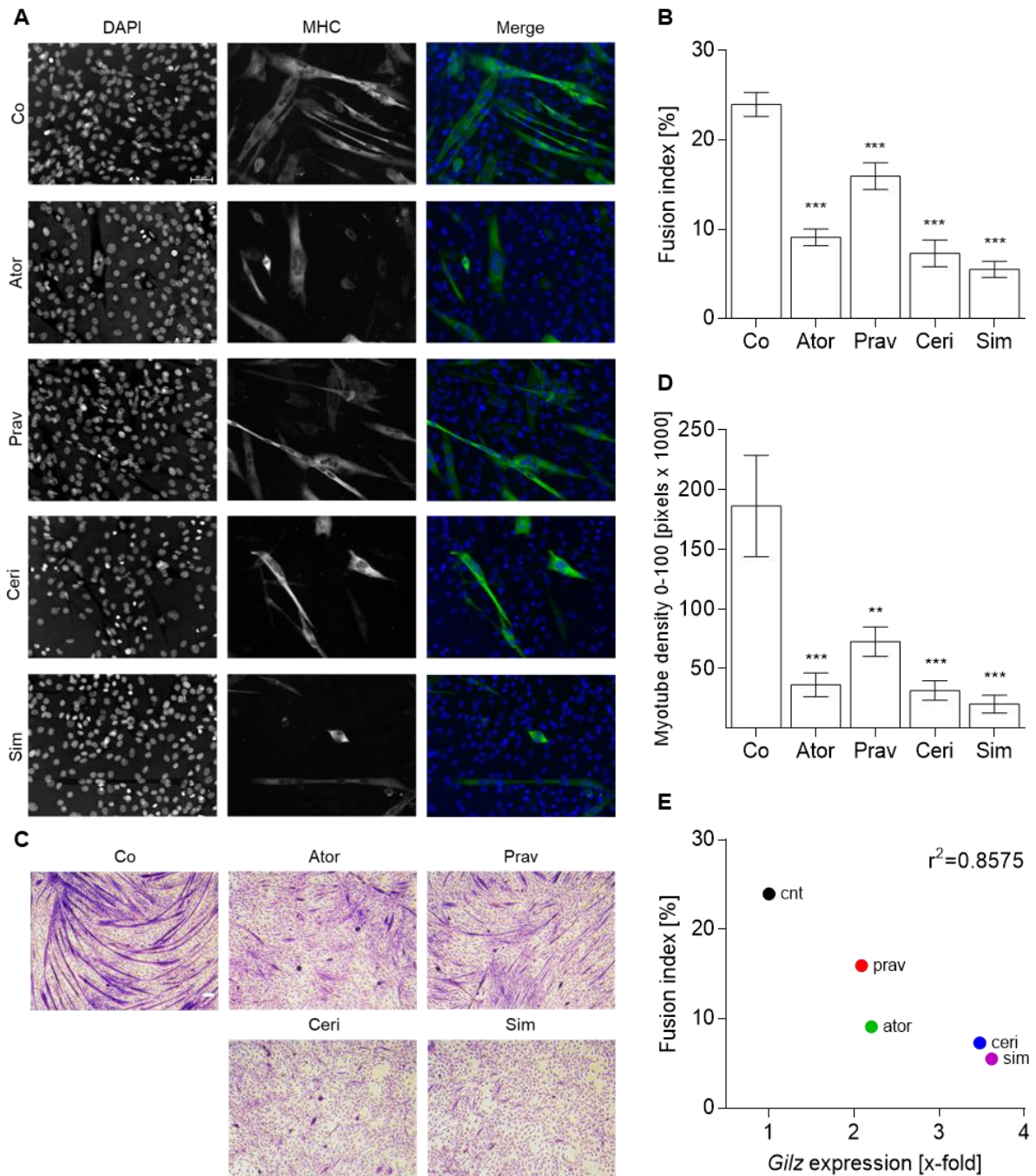


Figure 3.5. Effect of statins on C2C12 differentiation. C2C12 were induced to differentiate for 6 days in the absence or presence of atorvastatin (5 μ M), pravastatin (10 μ M), cerivastatin (0.1 μ M), and simvastatin (1 μ M), and subjected to MHC IF (A, scale bar, 50 μ m) or Jenner-Giemsa staining (C, scale bar, 100 μ m). Representative images are shown. The degree of differentiation was quantified by measuring the fusion index in IF images (B), and myotube density in Jenner-Giemsa images (D). Correlation between the degree of *Gilz* mRNA induction after 72 hours of statin stimulation (Figure 3.6 A) and fusion index (E). Data show the mean of 3 independent experiments performed in replicates \pm SEM. * $P < 0.05$, ** $P < 0.01$, *** $P < 0.001$ relative to the control.

We analysed GILZ expression levels in differentiating C2C12 and primary murine myotubes treated with statins, finding that the impairment in myogenesis was also accompanied by GILZ induction on both, mRNA and protein level (Figure 3.6). Pearson correlation analysis showed a negative correlation between the fold increase in *Gilz* mRNA levels, and the fusion index ($r^2=0.8575$). Since GILZ has been shown to mediate the anti-myogenic effects of dexamethasone (Bruscoli et al., 2010), we hypothesised that it might also be involved in the effects observed after statin treatment.

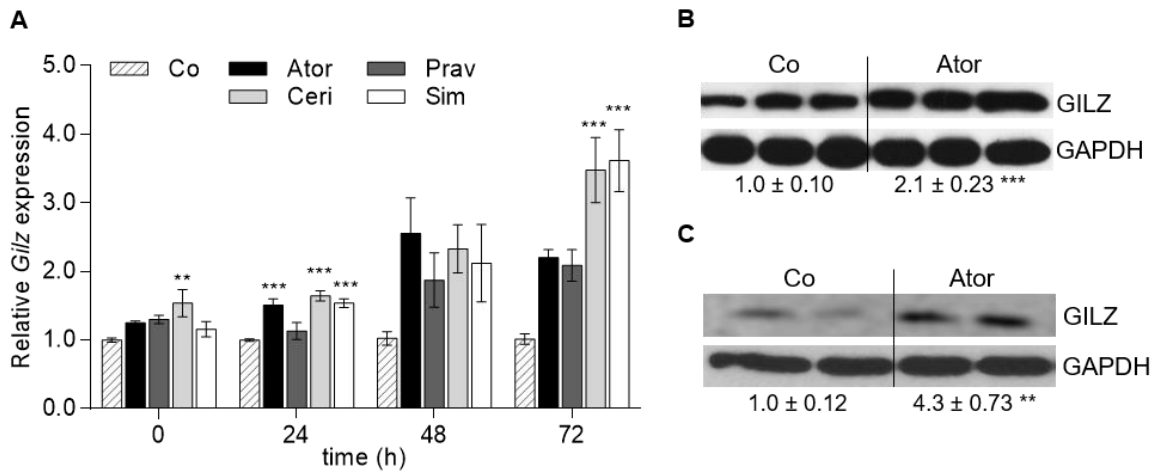


Figure 3.6. Effect of statins on GILZ expression during myogenesis. C2C12 were induced to differentiate for 72 hours in the absence or presence of atorvastatin (5 μ M), pravastatin (10 μ M), cerivastatin (0.1 μ M), and simvastatin (1 μ M). *Gilz* expression data was normalised against the housekeeping gene (*Csnk2a2*) and is presented as fold change of control (A). GILZ protein levels in C2C12 (B) and primary murine (C) myotubes treated with atorvastatin (5 μ M) during myogenesis. Representative blots are shown. Data show the mean of 3 independent experiments \pm SEM. * $P < 0.05$; ** $P < 0.01$, *** $P < 0.001$ relative to the control.

3.2.6 *GILZ* knockout abolishes the cytotoxic effects of statins

To assess whether loss of GILZ could rescue statin-induced cytotoxicity, we isolated primary myoblasts from WT and GILZ KO mice, treated them with increasing doses of statins, and measured cell viability after 24 hours. Comparison of the dose-response curves obtained showed significant differences between genotypes: GILZ KO myoblasts were significantly less sensitive towards atorvastatin, cerivastatin, and simvastatin treatment than their WT counterparts [cell type main effect $F(1,124)=10.06$, $P=0.002$; $F(1,124)=26.24$, $P<0.0001$; and $F(1,116)=24.18$, $P<0.0001$, respectively, Figure 3.7 A–C].

Due to the importance of the PI3K/Akt signalling pathway in statin-induced myotoxicity (Bonifacio et al., 2015; Mallinson et al., 2009), we hypothesised that the resistance to cell death from GILZ KO myoblasts might be related to modulation of the Akt phosphorylation status. Indeed, atorvastatin treatment induced dephosphorylation of Akt and activated the apoptotic pathway, as observed by cleaved caspase-3 detection, in WT myoblasts.

On the other hand, Akt phosphorylation levels were restored to that of the control in statin-treated GILZ KO cells, and the active form of caspase-3 was undetectable (Figure 3.7 D–E).

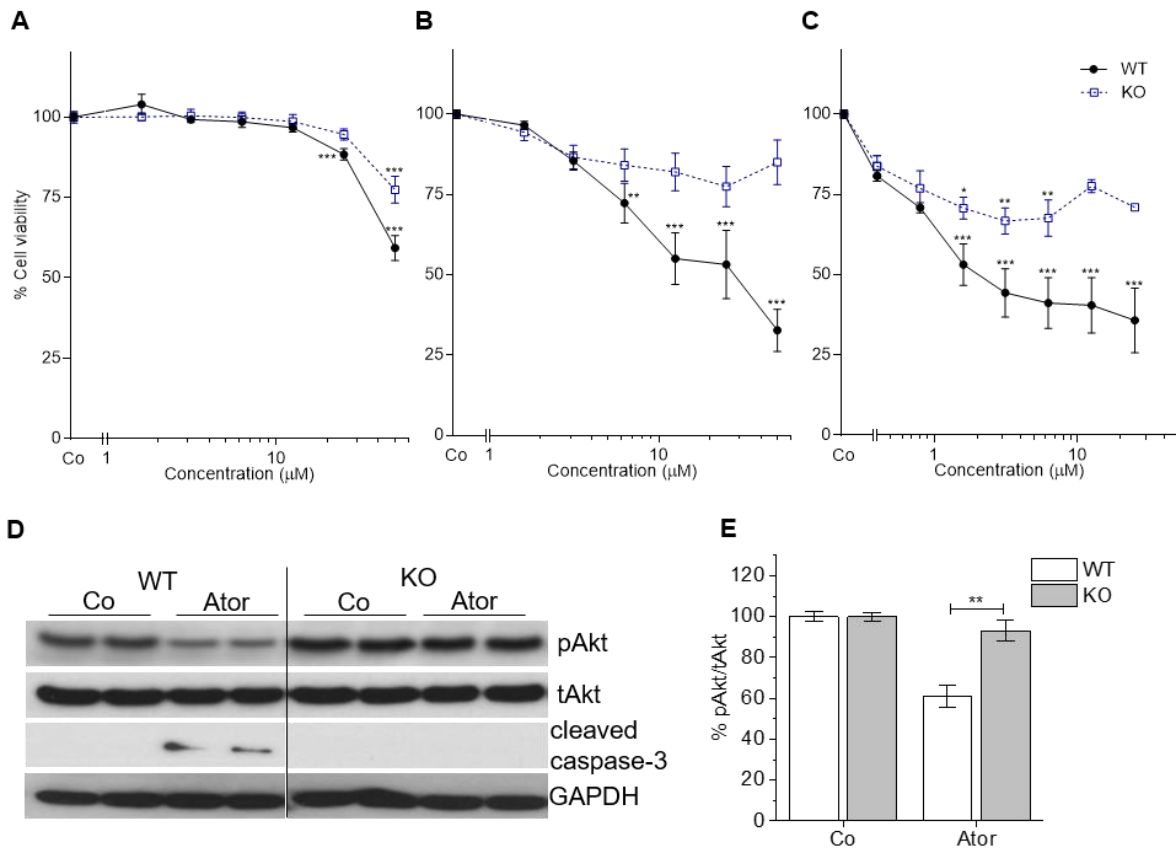


Figure 3.7. Effect of GILZ knockout on statin-induced myotoxicity. WT and GILZ KO primary murine myoblasts were treated with atorvastatin (A), simvastatin (B) or cerivastatin (C) in increasing concentrations for 24 hours. The cell viability was measured *via* MTT assay and differences between curves were analysed by two-way ANOVA. Myoblasts were treated with atorvastatin (50 μM) for 6 hours, Akt phosphorylation and caspase-3 activation were measured by western blot. One representative blot is shown (D). The ratio of phosphorylated to total Akt was measured by densitometric analysis and normalised to the corresponding control (E). Data show the mean of at least 3 independent experiments performed in replicates \pm SEM. * $P < 0.05$, ** $P < 0.01$, *** $P < 0.001$ relative to the control.

As an *ex vivo* model for the evaluation of statin myotoxicity, we used *flexor digitorum brevis* myofibres isolated from WT and KO animals. These short fibres can be isolated, dissociated, and cultured, representing a more mature system for evaluation of statin effects than cell culture systems, since myoblasts *in vitro* can differentiate to myotubes but are unable to form fully differentiated myocytes and, therefore, do not exactly resemble the features of mature muscle (Ravenscroft et al., 2007; Sakamoto and Kimura, 2013). Treatment of FDB fibres from WT mice with atorvastatin, simvastatin, and cerivastatin induced vacuolation at 72 hours. After 5 days the sarcomere structures were no longer visible, the fibres were swollen, ruptured, and blebs appeared (Figure 3.8 A and data not shown). Viability analysis using the trypan blue exclusion method after 5 days indicated that statins induced fibre death in a dose-dependent

manner. Loss of GILZ prevented the morphological changes indicative of myotoxicity and made the fibres resistant towards statins: in KO fibres, there were no significant differences in viability between the control and treatments at any of the concentrations evaluated (Figure 3.8 A–B).

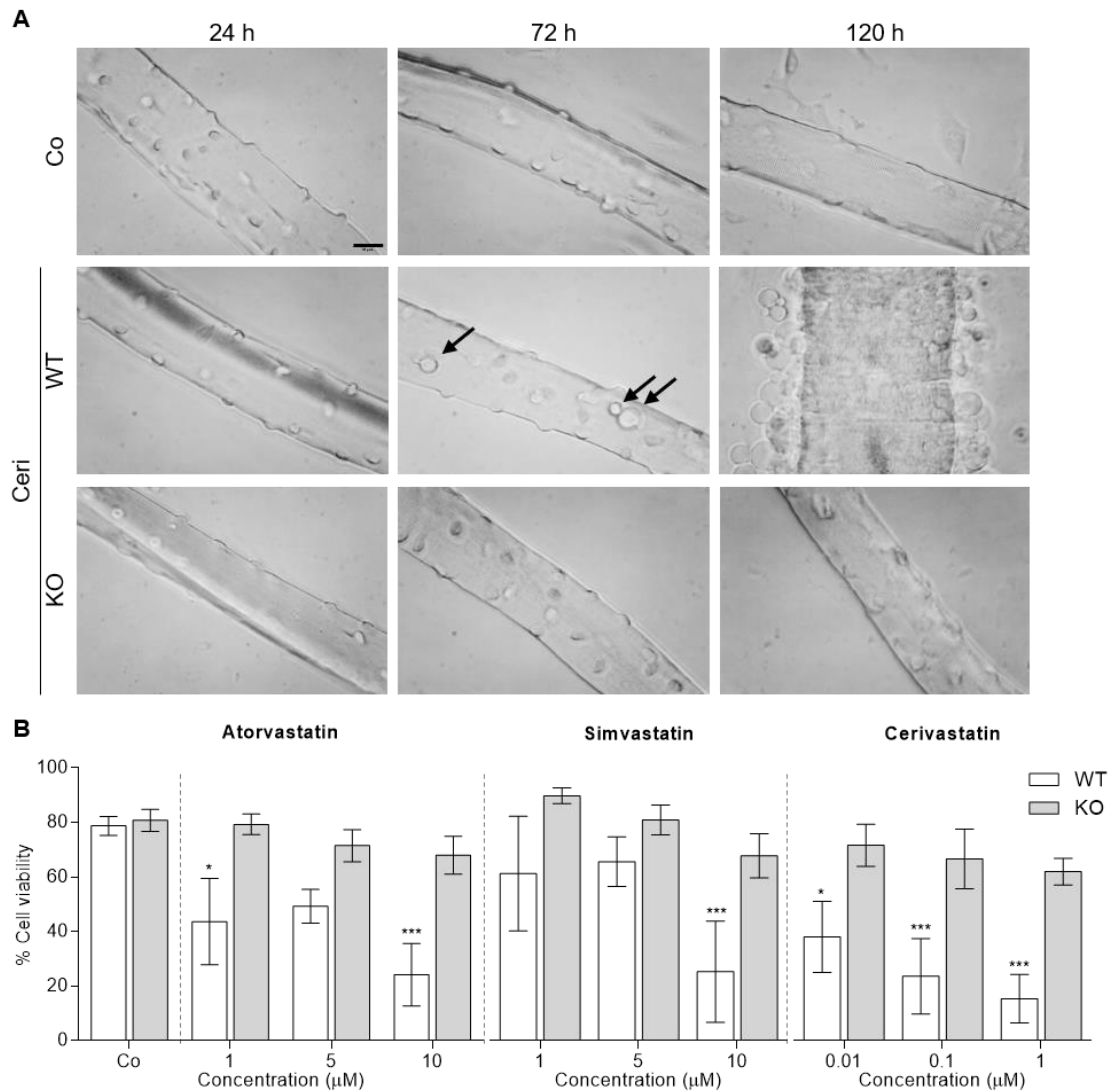


Figure 3.8. Effect of GILZ knockout on statin-induced FDB myofibre toxicity. WT and GILZ KO FDB myofibres were treated with cerivastatin (1 μ M) for up to 120 hours and imaged for morphological analysis, representative pictures are shown (A). Scale bar, 20 μ m. Cell viability was measured after 120 h of treatment, using the trypan blue exclusion method (B). Data show the mean of 4 independent experiments performed in replicates \pm SEM. * $P < 0.05$, *** $P < 0.001$ relative to the corresponding control.

3.2.7 *GILZ* contributes to statin-induced inhibition of myogenesis

To investigate the contribution of *GILZ* to statin-induced inhibition of myogenesis, we differentiated WT and *GILZ* KO myoblasts in the presence of statins and evaluated the expression of the MRF myogenin, which is required in cells committed to the myogenic program for driving their fusion and terminal differentiation (Bentzinger et al., 2012). We observed a decrease in myogenin protein levels in WT primary murine myoblasts induced to differentiate for 72 hours in the presence of atorvastatin. By contrast, the expression of myogenin in atorvastatin treated *GILZ* KO cells was restored to that of the control (Figure 3.9), providing evidence that *GILZ* acts as a mediator of the anti-myogenic effects of statins.

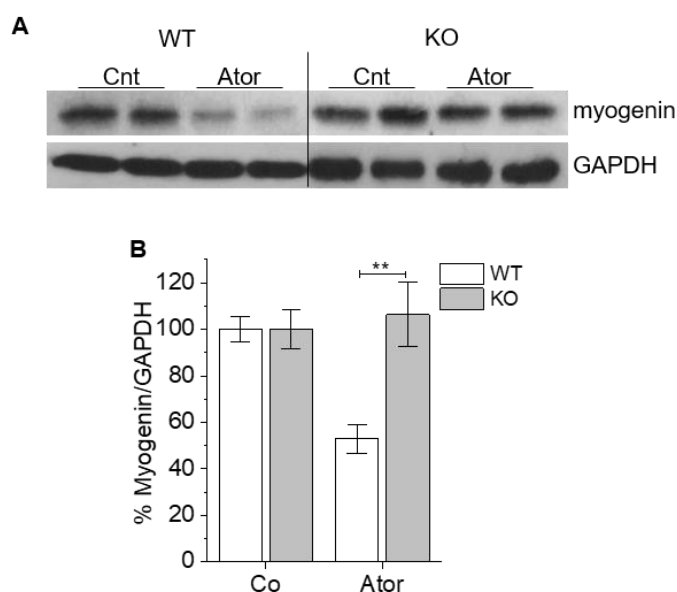


Figure 3.9. Effect of *GILZ* knockout on statin-induced anti-myogenic effects. Primary murine myoblasts from WT and *GILZ* KO animals were induced to differentiate for 72 hours in the absence or presence of atorvastatin (5 μ M). Myogenin levels were measured *via* western blot, one representative blot is shown (A). Densitometric analysis (B). Data show the mean of 3 independent experiments \pm SEM. ** $P < 0.01$ relative to the control.

To further analyse the role of *GILZ* in these effects, we generated C2C12 cell lines stably expressing scrambled or *GILZ* shRNA constructs by lentiviral transduction. The C2C12^{shGilz1} and C2C12^{shGilz2} cell lines showed a degree of gene knockdown of approximately 70% and 60%, respectively, whereas in the scrambled control cell line, C2C12^{scr}, *Gilz* expression was unaffected (Figure 3.10).

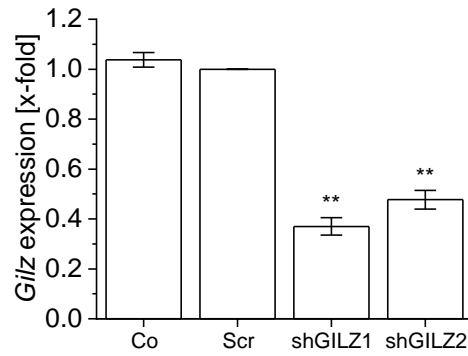


Figure 3.10. *Gilz* expression in stable C2C12^{shGilz} cell lines. Scrambled and shGILZ-silenced C2C12 cell lines were generated by lentiviral transduction, *Gilz* mRNA expression was normalised against the housekeeping gene (*Csnk2a2*) and is presented as fold change of the control. Data show the mean of 3 independent experiments \pm SEM. **P<0.01 relative to scrambled cells.

We hypothesised that, as a result of restored myogenin expression, *Gilz* silencing should reinstate the ability of the myoblasts to differentiate in the presence of statins. Importantly, we found that C2C12^{shGilz1} and C2C12^{shGilz2} cells displayed terminally differentiated myotubes already after 4 days in DM, whereas C2C12^{scr} cells were not fully differentiated yet (Figures 3.11 A and 3.12 A, upper panels). GILZ knockdown, however, could only partially reverse the impairment in differentiation caused by statins: although Jenner-Giemsa staining showed myotube formation in the C2C12^{shGilz} lines (Figure 3.12, lower panels), these cells were not differentiated to the same extent as their controls. Nevertheless, fusion index analysis of MHC-stained cells showed an improvement in myotube formation from C2C12^{shGilz} cells compared with the C2C12^{scr} line (Figure 3.11 B).

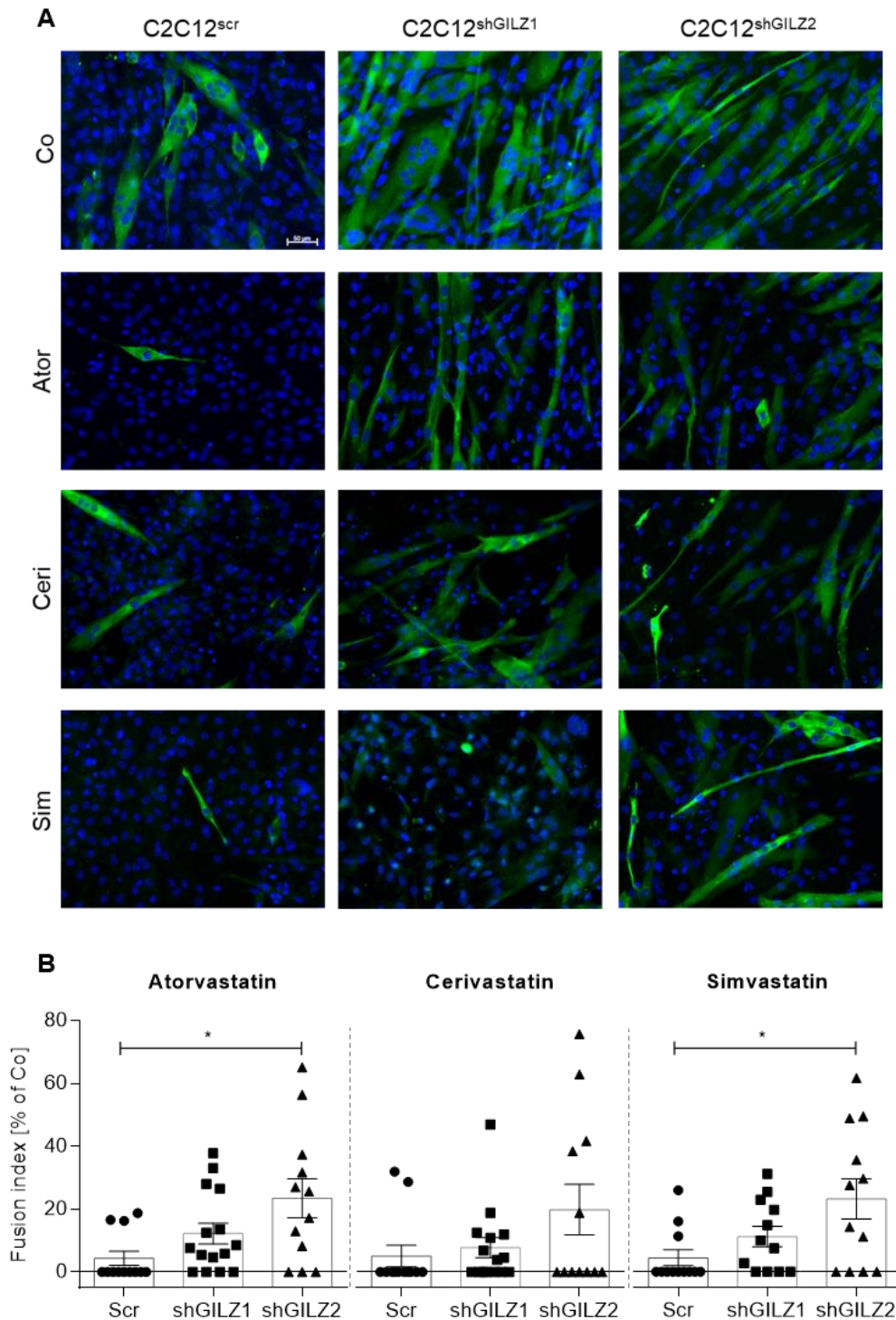


Figure 3.11. Effect of GILZ absence on statin-induced anti-myogenic effects, as measured by MHC IF. Scrambled (Scr)- and shGILZ-C2C12 cell lines were induced to differentiate for 4 days in the absence or presence of atorvastatin (5 μ M), cerivastatin (0.1 μ M), or simvastatin (1 μ M), and subjected to MHC IF, representative images are shown (A). Scale bar, 50 μ m. The degree of differentiation was quantified by measuring the fusion index (B) and is presented relative to the controls. Bars show the mean of at least 3 independent experiments performed in replicates \pm SEM, data points correspond to each quantified field. Comparison was performed using Kruskal-Wallis test followed by Dunn's post-hoc analysis. * $P < 0.05$.

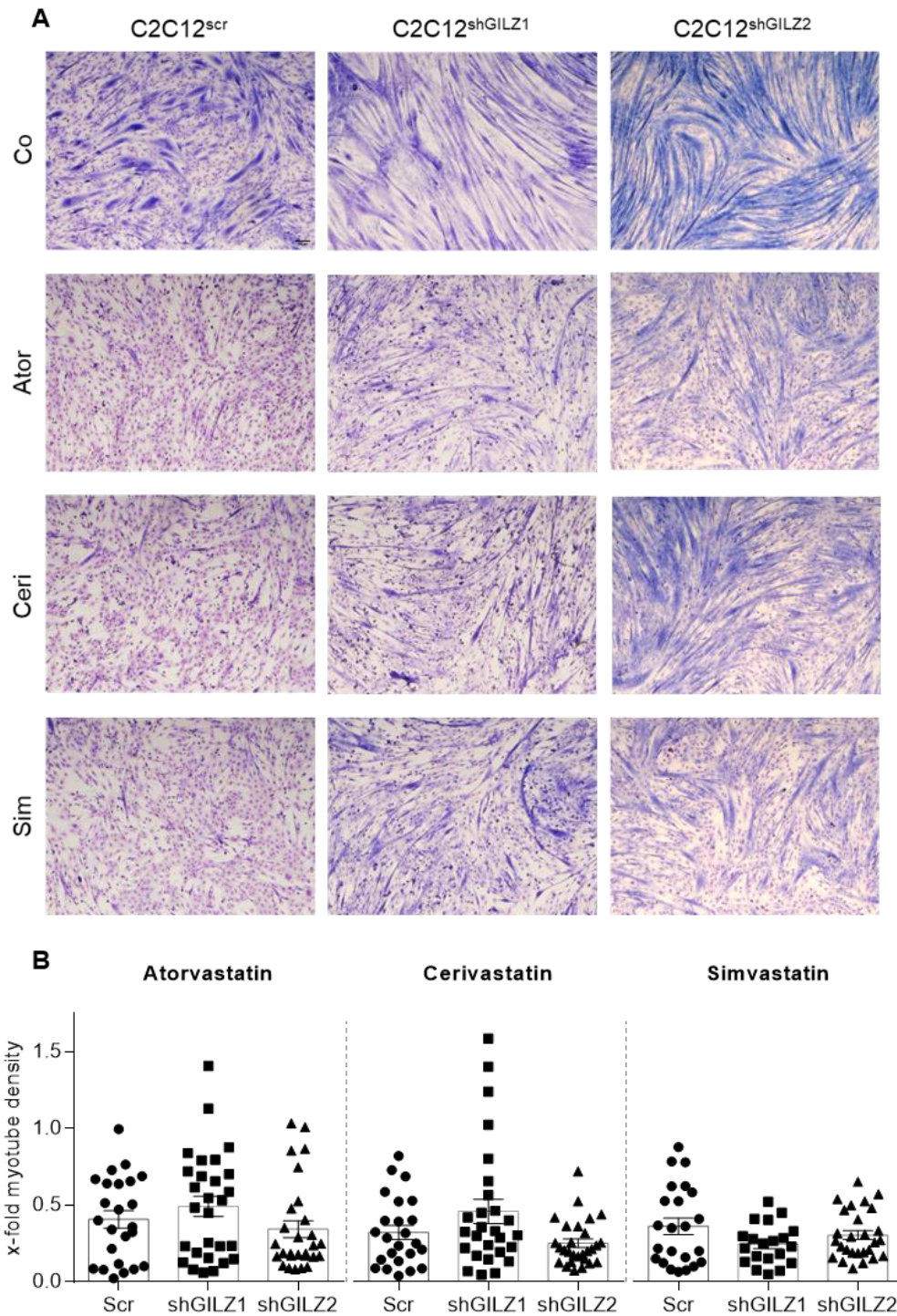


Figure 3.12. Effect of GILZ absence on statin-induced anti-myogenic effects, as measured by Jenner-Giemsa staining. Scrambled (Scr)- and shGILZ-C2C12 cell lines were induced to differentiate for 4 days in the absence or presence of atorvastatin (5 μ M), cerivastatin (0.1 μ M), or simvastatin (1 μ M), and subjected to Jenner-Giemsa staining, representative images are shown (A). Scale bar, 100 μ m. The degree of differentiation was quantified by measuring the myotube density and is presented as fold of the corresponding controls (B). Bars show the mean of at least 3 independent experiments performed in replicates \pm SEM, data points correspond to each quantified field.

3.2.8 *FoxO3 mediates GILZ induction by statins in muscle*

In the search for potential upstream regulators of GILZ expression after statin treatment in muscle, we focused on the Forkhead Box O3 (FoxO3) protein. FoxO3 is a direct phosphorylation target of Akt, and our observations in skeletal muscle tissue from FoxO3 KO mice, where *Gilz* expression levels were significantly lower than in WT animals, hinted towards FoxO3 as a transcriptional regulator of GILZ in this tissue (Figure 3.13 A). Like in primary myoblasts, we observed that treatment of C2C12 myoblasts with statins led to Akt dephosphorylation and, in line with this, to reduced levels of phosphorylated FoxO3 protein, in parallel to GILZ induction (Figure 3.13 B–D). Hence, we performed chromatin immunoprecipitation to evaluate whether FoxO3 activated *Gilz* transcription in myoblasts by binding to the forkhead responsive elements (FHRE) in its promoter following statin treatment. Indeed, we found sequences corresponding to three of the four FHRE present in the *Gilz* promoter in immunoprecipitates from atorvastatin-treated myoblasts, indicating that GILZ induction in muscle follows dephosphorylation, nuclear translocation, and activation of FoxO3 (Figure 3.13 E).

3.2.9 *Statins induce Gilz in zebrafish embryos, and deregulation of Gilz expression impairs somitogenesis*

The zebrafish is a powerful and versatile *in vivo* model for the study of developmental and physiological processes that has been used for the elucidation of statin effects on muscle development (Campos et al., 2016) and homeostasis (Hanai et al., 2007; Huang et al., 2011; Pasha and Moon, 2017). Given that the zebrafish expresses a GILZ orthologue (Tse et al., 2013), we chose it as an *in vivo* model to study the effects of statins on GILZ expression.

In line with our *in vitro* findings, treatment of zebrafish embryos at 20 hpf with statins at concentrations that have been described to cause major muscle damage, led to an up-regulation of *gilz* mRNA (Figure 3.14 A). To characterise the effects of increased Gilz expression in zebrafish muscle development, we performed myosin IF in *Gilz* overexpressing embryos. Compared with control animals, we found a diffuse MHC staining with loss of septa, a clear sign that *Gilz* impairs embryonic muscle development. To causally link *Gilz* expression with statin-induced muscle damage, we considered performing gene silencing *via* MO injection to evaluate the effects of statin treatment in WT *vs* morphant embryos. *gilz* morphants, however, showed similar features to that of the overexpressing embryos in muscle, as observed by myosin staining (Figure 3.14 B), indicating that *Gilz* plays an important role in the regulation of somitogenesis.

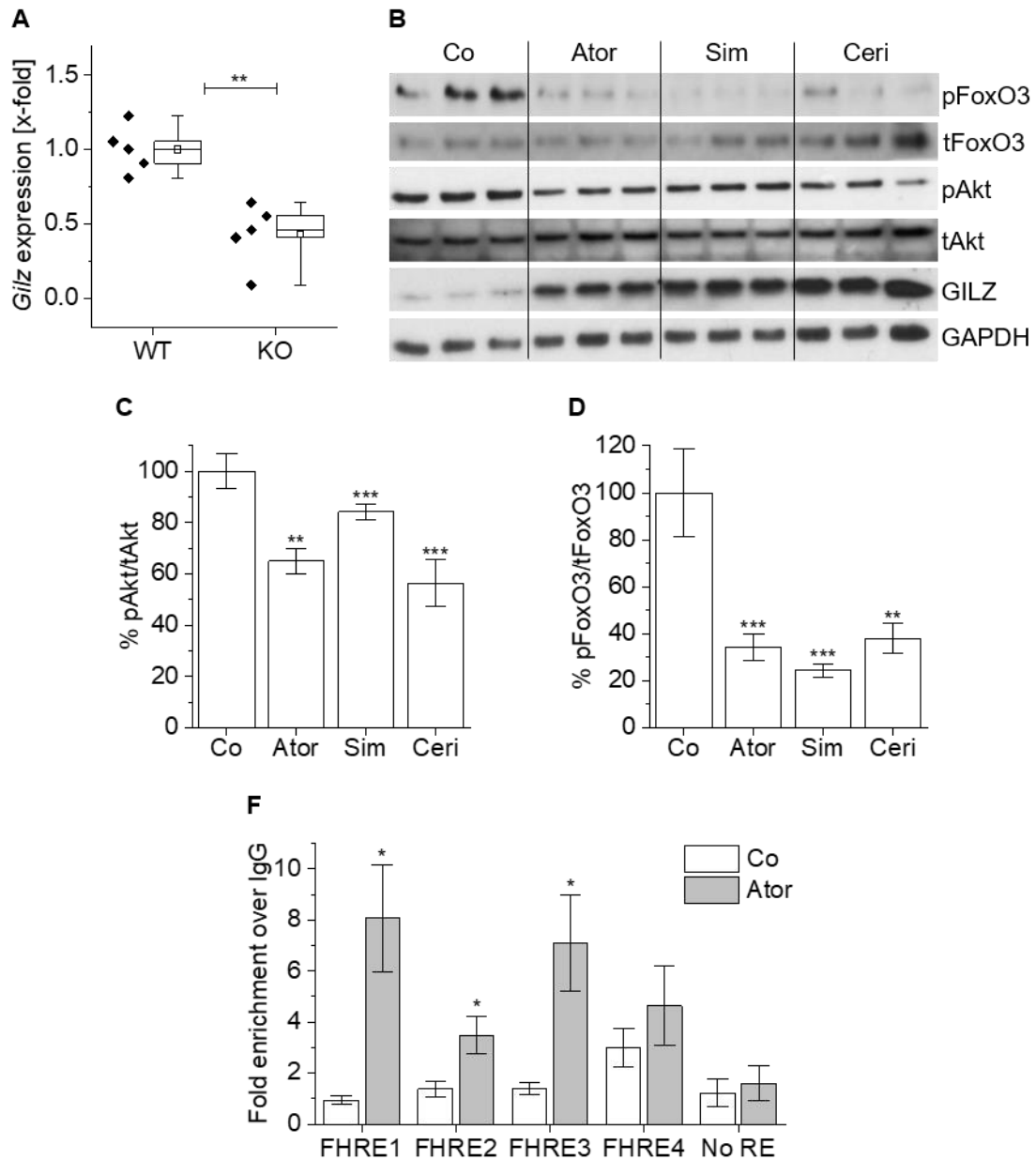


Figure 3.13. Involvement of FoxO3 in statin-induced GILZ expression. *Gilz* expression on skeletal muscle from FoxO3 KO mice (A). mRNA expression data was obtained from WT and KO mice (n=5), normalised against the housekeeping gene (*Csnk2a2*), and is presented as fold change of WT in box-plots showing the 25–75th percentiles, mean (square), median (line) and range (whiskers). Western blot analysis C2C12 myoblasts treated with 50 μ M statin for 6 hours, a representative blot is shown (B). Densitometric analysis of ratio of phosphorylated to total FoxO3 (C). ChIP analysis was used to detect the binding of FoxO3 to the *Gilz* promoter region (D). Expression data is presented as fold enrichment over IgG. Data show the mean of 3 independent experiments \pm SEM. *P<0.05; **P<0.01, ***P<0.001 relative to the control.

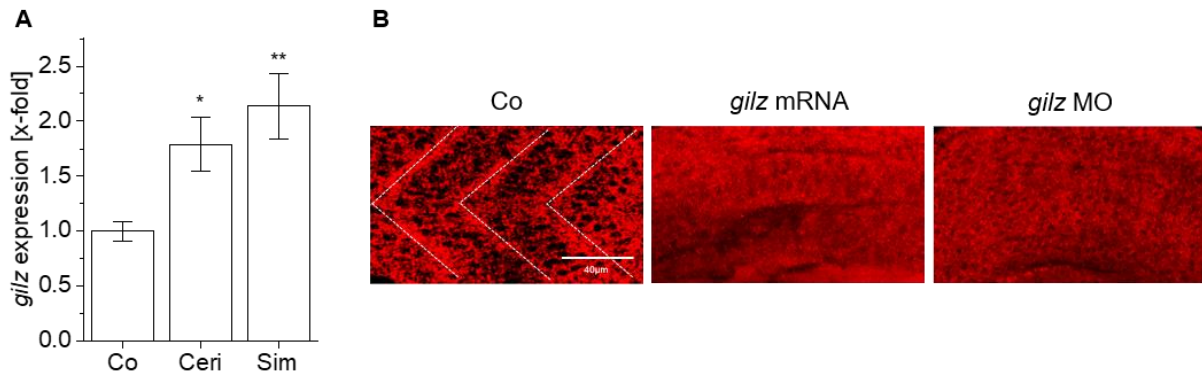


Figure 3.14. Effect of statins on gene expression in zebrafish, and effect of *gilz* deregulation in zebrafish muscle development. Zebrafish embryos at 20 hpf were treated with cerivastatin or simvastatin lactone (1 μ M) for 12 hours (A). mRNA expression was normalised against the housekeeping gene (*actb2*) and is presented as fold change of control. MHC IF of *gilz*-overexpressing and *gilz*-morphant zebrafish embryos at 24 hpf, representative pictures are shown (B). Panels are side views, anterior, left. White dotted lines in Co outline the V-shape pattern of somites. Bar, 40 μ m. Data show the mean of 3 independent experiments performed in replicates \pm SEM. * $P < 0.05$, ** $P < 0.01$, relative to the control.

3.3 Discussion

More than 30 years after their introduction to the market, statins remain the cornerstone of the pharmacological management of hyperlipidaemia and CVD prevention. In light of their importance and extended use, the understanding of the mechanisms underlying the onset of SAMS is of highest relevance (Stroes et al., 2015). In the present study, we report a role for GILZ as a pivotal mediator of the myotoxic and anti-myogenic effects of statins. We first demonstrate that treatment of murine myoblasts with different statins, at concentrations typical for *in vitro* studies on SAMS (Bouitbir et al., 2012; Hanai et al., 2007; Schirris et al., 2015), induces GILZ expression. Since SAMS are a class effect, and several of the mechanisms underlying muscle toxicity are directly related to the inhibition of HMG-CoA (Osaki et al., 2015; Trapani et al., 2012), we evaluated whether GILZ expression depended on this pathway as well. Indeed, we found GILZ induction to be mevalonate-dependent, more specifically, on geranylgeranylation.

The significantly lower myotoxicity of the hydrophilic statin pravastatin (Gadbut et al., 1995; Kaufmann et al., 2006; Kobayashi et al., 2008; Schirris et al., 2015), might be the result of reduced cellular uptake in our *in vitro* setting, that also accounts for the rather modest levels of *Gilz* induction observed in comparison to the other statins. The hydrophilicity of the molecules is also of relevance when comparing the cytotoxic effects of the lactone vs hydroxy acid forms of statins towards muscle, given that the former are significantly more lipophilic than the latter (Skottheim et al., 2008). It has been reported that patients with atorvastatin-induced myopathy have increased levels of the lactone form of the drug in plasma (Hermann et al., 2006), and *in vitro* studies also demonstrated that physiological conditions that favour the conversion of statins to their lactone form, such as acidosis, increase statin myotoxicity (Taha et al., 2016).

Several molecular mechanisms of statin-induced myotoxicity have been proposed, describing their deleterious effects on mitochondrial function, calcium homeostasis, and cell survival in the myocyte (du Souich et al., 2017). In our hands, statins caused Akt dephosphorylation and activation of the apoptotic cascade in undifferentiated myoblasts. This effect agrees with previous findings in cultured myotubes (Bonifacio et al., 2015; Johnson et al., 2004). Our observations suggest a crucial role for GILZ in mediating this action. First described in thymocytes as an anti-apoptotic protein (D'Adamio et al., 1997), GILZ can exert anti- or pro-apoptotic effects depending on the cell type: for instance, GILZ has been shown to promote apoptosis through Mcl-1 downregulation in neutrophils (Espinasse et al., 2016), or by inhibition of the Akt/mTOR signalling pathway, in myeloma cells (Joha et al., 2012).

There are discrepancies, however, in the mechanism by which statins induce cell death in cultured myoblasts/myotubes vs mature fibres. For instance, statins trigger apoptosis in cultured

cells, whereas mature skeletal muscles show necrotic features (Sakamoto and Kimura, 2013). Hence, instead of using terminally differentiated cultured myotubes, we chose isolated FDB myofibers as an *ex vivo* model to evaluate the effects of the absence of GILZ in statin toxicity towards mature muscle. We noticed that treatment of murine FDB fibres with atorvastatin, simvastatin, and cerivastatin caused cell death with similar features as those previously described for fluvastatin-treated rat FDB fibres (Sakamoto et al., 2011). Furthermore, in accordance with our observations in proliferating myoblasts, GILZ was of crucial importance in mediating statin-induced fibre breakdown.

FoxO3 is a transcription factor involved in different aspects of muscle homeostasis, like regulation of mitochondrial metabolism, activation of protein breakdown *via* the ubiquitin-proteasome and autophagy pathways, and inhibition of muscle precursor cell proliferation (Sanchez et al., 2014). In statin-induced myopathy, reports have shown that FoxO3 activation results in expression of the muscle atrophy-related protein MAFbx/atrogen-1 and other genes implicated in muscle proteolysis *in vitro* and *in vivo* (Hanai et al., 2007; Mallinson et al., 2009). Moreover, FoxO3 has been reported as a transcriptional regulator of GILZ in T cells, where it drives IL-2 withdrawal-induced GILZ expression (Asselin-Labat et al., 2005). We found statin-induced GILZ expression in muscle to be FoxO3-dependent and, as mentioned above, GGPP dependent. These results are in accordance with previous studies that linked SAMS to reduced geranylgeranylation, but not farnesylation, of different small GTPases like Rac1, Rap1, and Rab1 (Baba et al., 2008; Cao et al., 2009; Johnson et al., 2004; Sakamoto et al., 2007). Our findings suggest that the inhibition of protein geranylgeranylation by statins downregulates the Akt signalling pathway, leading to FoxO3-driven GILZ induction, which in turn further decreases Akt phosphorylation and promotes apoptosis.

The fact that GILZ is expressed in skeletal muscle, as observed by us and reported in earlier studies (Cannarile et al., 2001), might denote a role in muscle tissue homeostasis. Indeed, an earlier study showed that GILZ and its longer isoform, L-GILZ, modulate myogenesis in the absence of pharmacological intervention, and mediate glucocorticoid-induced inhibition of myogenesis by decreasing MyoD-mediated myogenin transcription, thus impairing myoblast fusion (Bruscoli et al., 2010). For this reason, we investigated the role of GILZ in the anti-myogenic effects of statins. We found that all statins were able to induce GILZ transcription, an effect that seemed to correlate with the anti-myogenic effect of the statin used. A previous study reported no differences in myogenin mRNA levels in simvastatin-treated C2C12 (Baba et al., 2008). We, however, found myogenin protein expression to be impaired in primary differentiating myoblasts treated with atorvastatin. Moreover, our results in GILZ KO myoblasts indicate that statin-induced GILZ expression, and the consequent myogenin transcriptional repression, is a mechanism by which this class of drugs impairs myogenesis.

GILZ silencing by shRNA caused the resulting C2C12^{shGilz} cell lines to differentiate considerably faster than the C2C12^{scr} control, even to a higher degree than observed for WT cells after terminal differentiation. This supports the importance of GILZ itself as a modulator of myogenesis and corresponds to our observations in zebrafish embryos, where Gilz overexpression severely impaired somitogenesis. Importantly, zebrafish embryos represent a frequently used *in vivo* model for the mechanistic study of SAMS (Campos et al., 2016, 2015; Huang et al., 2011; Pasha and Moon, 2017). The regulatory role played by Gilz in zebrafish embryonic development is rather complex: the study that first described the presence of a GILZ orthologue in zebrafish, showed that manipulation of Gilz expression in this model, either *via* MO silencing or mRNA overexpression, causes significant defects in embryonic development, altering the dorsoventral patterning, segmentation, and brain development processes (Tse et al., 2013). In rodents, however, GILZ-independent regulatory pathways are most likely involved in the modulation of skeletal muscle development, since GILZ KO mice do not exhibit altered muscle features (unpublished observations).

Even though myogenin expression was rescued in the absence of GILZ, we could not observe a complete recovery in myotube formation after statin treatment in C2C12^{shGilz} cells. This might be related to residual GILZ expression in the silenced cells, or to additional pathways that mediate the anti-myogenic effects observed, such as the IGF-1/PI3K/Akt pathway (Ogura et al., 2007). Our observations indicate that GILZ is critical for statin-induced inhibition of myogenin, an MRF crucial for myoblast fusion and terminal differentiation (Asfour et al., 2018). Additional factors, however, may also contribute to the inhibition of muscle regeneration by statins.

Taken together, our data point towards GILZ as an essential mediator of the molecular mechanisms leading to statin-induced muscle damage and impairment of muscle regeneration. This study contributes to a better understanding of the molecular mechanisms underlying statin-induced myopathy, a necessary step towards the development of prevention strategies and safer therapy approaches for a class of drugs that remains a pillar in the treatment of cardiovascular disease.

The contents of this chapter have been submitted for publication as:

The Glucocorticoid-Induced Leucine Zipper (GILZ) Mediates Statin-Induced Muscle Damage

J. Vanessa Valbuena Perez; Jessica Hoppstädter, Ph.D.; Rebecca Linnenberger; William K. F. Tse, Ph.D.; Sara Flamini; Anastasia Andreas; Jennifer Herrmann, Ph.D.; Christian Herr, Ph.D.; Rolf Müller, Ph.D.; Robert Bals, Ph.D.; Carlo Riccardi, Ph.D.; Stefano Bruscoli, Ph.D.; and Alexandra K. Kiemer, Ph.D.

4. Chapter II

A potential role for GILZ in the pleiotropic effects of statins

4.1 Introduction

Statin therapy improves adverse outcomes in CVD patients (Almeida and Budoff, 2019), and is beneficial in primary prevention of CVD (Taylor et al., 2013). It has been suggested that the overall benefit of statin use is attributable not only to reduction of LDL-cholesterol but also to a plethora of pleiotropic effects, exerted on different cell types involved in cardiovascular homeostasis (Oesterle et al., 2017). Although the clinical significance of these effects is still debated (Labos et al., 2018), it is clear that statins reduce systemic inflammation, as demonstrated by different trials where reductions in high-sensitivity CRP are observed in patients with or without concomitant hyperlipidaemia (Ridker et al., 2008).

Atherosclerosis, the main pathophysiological condition driving CVD, is considered a chronic inflammatory disease (Mendis et al., 2011; Tousoulis et al., 2014). Indeed, the key role of inflammation in this pathology could be confirmed with the results from the CANTOS trial, where therapeutic targeting of the pro-inflammatory cytokine IL-1 β with canakinumab led to a significantly lower rate of recurrent cardiovascular events (Ridker et al., 2017). Development of the atherosclerotic plaque involves endothelial dysfunction, monocyte and T-cell recruitment and activation, lipid accumulation, and smooth muscle cell proliferation (Novikova et al., 2018; Ross, 1999). Statins have shown different beneficial, anti-inflammatory effects in these cell types: for example, reduction in expression of adhesion molecules in endothelial and smooth muscle cells (Chung et al., 2002), in matrix metalloproteinase (MMPs) secretion in macrophages and smooth muscle cells (Luan et al., 2003), or reduced inflammasome activation in endothelial cells (Wang et al., 2017). These effects are attributed to inhibition of Rho GTPase-mediated pro-inflammatory activity, of oxidative stress, and the activity of pro-inflammatory transcription factors, like NF- κ B (Huacuja Álvarez et al., 2006; Oesterle et al., 2017; Tousoulis et al., 2014).

GILZ is an immunomodulatory, anti-inflammatory protein (Ronchetti et al., 2015). Altered endogenous GILZ expression has been reported in different inflammation-related conditions, like obesity (Lee et al., 2016; Robert et al., 2016), rheumatoid arthritis (Beaulieu et al., 2010), endotoxin tolerance (Hoppstädter et al., 2015) and, interestingly, vascular inflammation (Hahn et al., 2014). Studies in different cell types indicate that GILZ exerts its anti-inflammatory activity *via* inhibition of NF- κ B transcriptional activity (Ayroldi et al., 2001; Cheng et al., 2013; Yang et al., 2008). Of notice, apart from glucocorticoids, GILZ can be induced in response to other anti-inflammatory compounds like curcumin in macrophages (Hoppstädter et al., 2016), as well as by vascular protective conditions, such as laminar shear stress in endothelial cells (Hahn et al., 2014). We aimed at evaluating the hypothesis that statins can induce GILZ in two cell types involved in vascular inflammation, *i.e.* endothelial cells and macrophages, and that this protein plays a role in the anti-inflammatory, pleiotropic effects of statins.

4.2 Results

4.2.1 Statin cytotoxicity towards endothelial cells and macrophages

Evaluation of statin toxicity towards endothelial cells and macrophages was performed by treatment of HUVECs and BMMs with increasing concentrations of atorvastatin, cerivastatin, simvastatin in lactone and acid form, and pravastatin. The effects on cell viability were measured *via* MTT assay. Similar to the findings in skeletal muscle (Chapter I), pravastatin was the least toxic of statins, while the other statins were toxic already at low concentrations (Figure 4.1). For this reason, concentrations in the nanomolar–low micromolar range were used for further experiments. The viability of BMMs was not affected by statin treatment at the evaluated concentrations (data not shown).

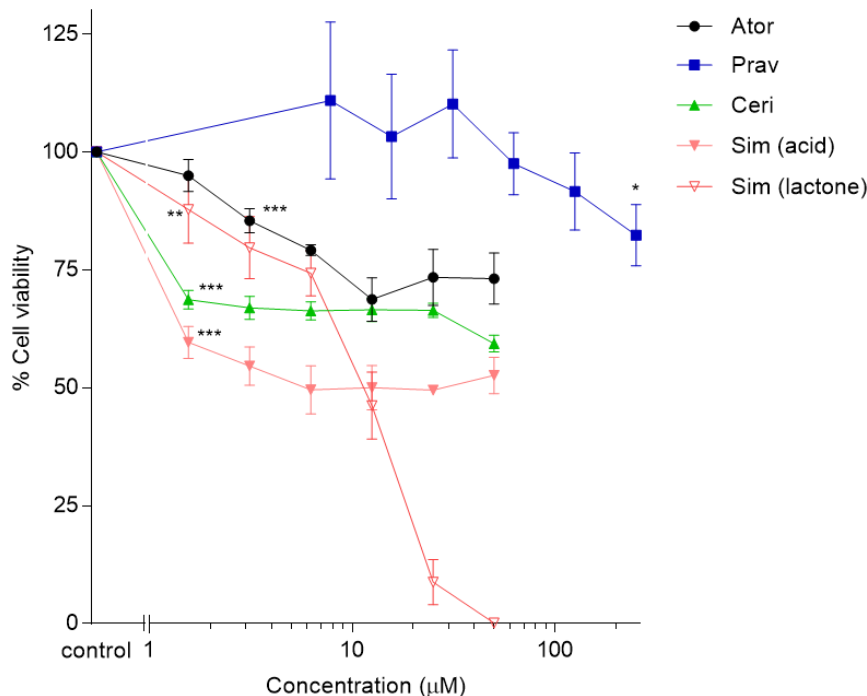


Figure 4.1. Statin cytotoxicity towards endothelial cells. HUVEC were treated with atorvastatin, cerivastatin, pravastatin, simvastatin lactone or simvastatin sodium salt in increasing concentrations for 24 hours. The cell viability was measured via MTT assay. Data show the mean of three independent experiments \pm SEM. * $P < 0.05$, ** $P < 0.01$, *** $P < 0.001$ for the lowest concentration that caused a significant decrease in viability relative to the control.

4.2.2 Atorvastatin induces *GILZ* expression in endothelial cells and macrophages

To assess the effects of statin treatment on *GILZ* expression in endothelial cells and macrophages, HUVECs and BMMs were treated with a non-toxic concentration of atorvastatin (3 μ M) for up to 24 hours, to measure the levels of *GILZ* mRNA at different time points. Atorvastatin induced *GILZ* expression in endothelial cells already at 2 hours of treatment, the induction was significant at 8 hours and continued to increase until the end of treatment (Figure

4.2 A). Furthermore, a moderate increase in *Gilz* expression was observed in BMMs, statistically significant at 16 hours (Figure 4.2 D). The shear stress-inducible, atheroprotective transcription factor *KLF2*, is known to be upregulated by statins (Parmar et al., 2005; Tuomisto et al., 2008), and endothelial nitric oxide synthase (*eNOS*) is one of the key targets of statins in vascular endothelium (Margaritis et al., 2014); both mRNAs were also measured as positive controls. As expected, atorvastatin treatment induced *KLF2* and *eNOS* expression in a time-dependent manner (Figure 4.2 B–C, E).

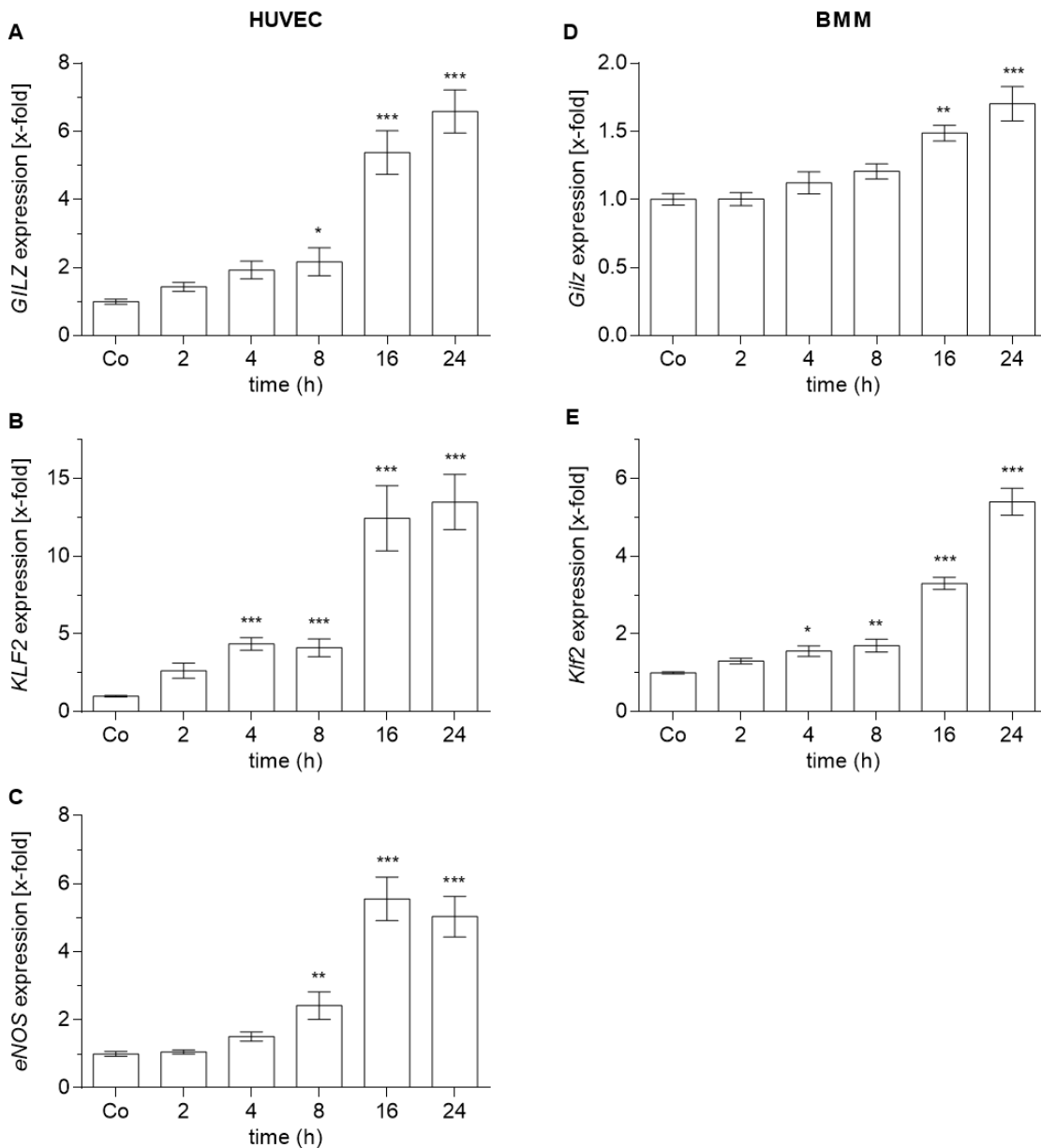


Figure 4.2. Effect of statin treatment on mRNA expression in endothelial cells and macrophages. HUVECs (A–C) and BMMs (D–E) were treated with atorvastatin (3 μ M) for up to 24 hours, mRNA expression levels were measured. Gene expression was normalised against the housekeeping gene (A–C *ACTB*; D–E *Rn18s*) and is presented as fold change of control. Data show the mean of 3 independent experiments performed in replicates with cells derived from different donors \pm SEM. * $P < 0.05$, ** $P < 0.01$, *** $P < 0.001$ relative to the control.

4.2.3 Statin-induced *GILZ* expression in HUVECs is mevalonate-dependent

To evaluate the dependence of *GILZ* induction on HMG-CoA inhibition, HUVECs were treated with non-toxic concentrations of statins in the absence or presence of mevalonate. As shown in Figure 4.3, all statins induced *GILZ* expression after 24 hours of treatment. The effect was reversed by coincubation with mevalonate.

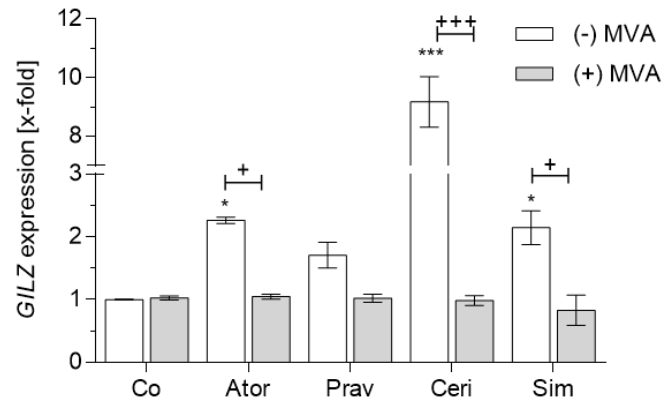


Figure 4.3. Effect of mevalonate on statin-induced *GILZ* expression in endothelial cells. HUVECs were treated with atorvastatin (1 μ M), pravastatin (50 μ M), cerivastatin (100 nM), or simvastatin (200 nM) in the absence or presence of mevalonate (100 μ M) for 24 hours. *GILZ* expression was normalised against the housekeeping gene (*ACTB*) and is presented as fold change of control. Data show the mean of 2 independent experiments performed in replicates with cells derived from different donors \pm SEM. * $P < 0.05$, ** $P < 0.01$, *** $P < 0.001$ relative to the control. + $P < 0.05$ +++ $P < 0.001$ relative to the non-MVA condition

4.2.4 *KLF2* is not involved in the regulation of *GILZ* expression in endothelial cells

Given the main role played by *KLF2* as mediator of the cardiovascular beneficial effects of statins, and the parallel upregulation of both genes observed upon atorvastatin treatment, it was of interest to evaluate whether regulation of *KLF2* expression influenced *GILZ* expression in endothelial cells. The notion of *KLF2* as transcriptional activator of *GILZ* expression was supported by *in silico* analysis of the murine *Gilz* promoter, where *KLF2*-binding sites were found (data not shown). Knockdown of the *KLF2* gene in HUVECs was performed using an siRNA approach. In addition, overexpression was achieved by means of a doxycycline-inducible lentiviral expression system. siRNA knockdown resulted in a 50% decrease in gene expression (Figure 4.4 A) but had no effects on baseline expression of *GILZ* in transfected HUVECs, compared with the scramble controls (Figure 4.4 B). Similarly, lentiviral overexpression at two different MOIs resulted in a 10–15-fold induction of *KLF2* expression but had no effects on *GILZ* (Figure 4.4 C).

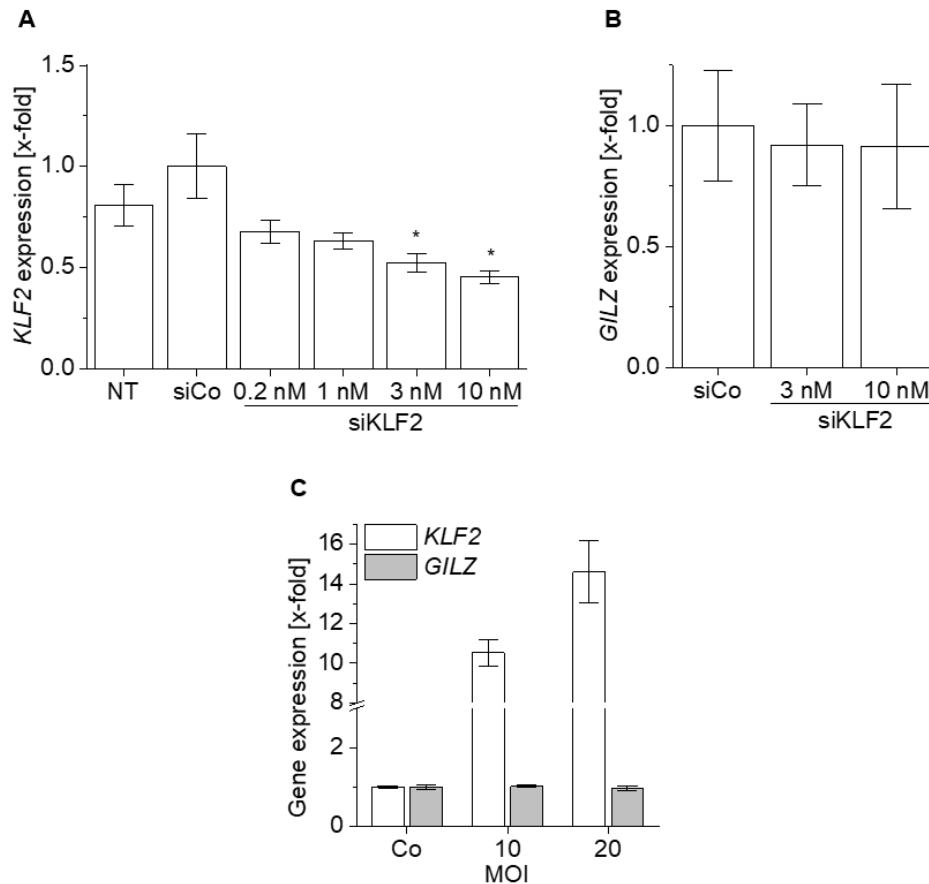


Figure 4.4. Effect of KLF2 knockdown and overexpression on GILZ expression in endothelial cells. HUVECs were transfected with siRNA targeting *KLF2* at different concentrations for 24 hours, *KLF2* levels were determined (A). *GILZ* levels were measured at the concentrations where significant KD was found (B). HUVECs were transduced with hKLF2 lentivirus and allowed to overexpress KLF2 for 72 hours before harvesting for mRNA analysis (C). mRNA expression was normalised against the housekeeping gene (*ACTB*) and is presented as fold change of control. Data show the mean of 3 independent experiments performed in replicates with cells derived from different donors (A–B) or a single experiment performed in duplicate (C) \pm SEM. * $P < 0.05$ relative to the control.

4.2.5 Development of a *GILZ-KO* endothelial cell line model via CRISPR/Cas9 editing

For analysis of the functional implications of *GILZ* induction by statins in vascular endothelium, a cell model with *GILZ* loss of function would be of interest. To this end, CRISPR/Cas9 technology, a highly versatile and efficient tool for gene editing (Boettcher and McManus, 2015), was used for the establishment of an endothelial *GILZ-KO* cell line. HUVECs are primary cells, hence not suitable for stable cell line generation. Therefore, the human dermal microvascular endothelium cell line HMEC-1 was chosen for CRISPR/Cas9 mediated *GILZ* deletion. Statin treatment significantly induced *GILZ* expression in these cells to a similar extent as in primary cells (Figure 4.5). To avoid the caveats of plasmid cloning, transfection/transduction, and expression of the CRISPR components in the cells, a system that involved direct delivery of Cas9 recombinant protein and the synthetic sgRNA was chosen. The

gene editing experiment was also performed in C2C12 myoblasts and murine RAW 264.7 macrophages, in parallel to HMEC-1 cells.

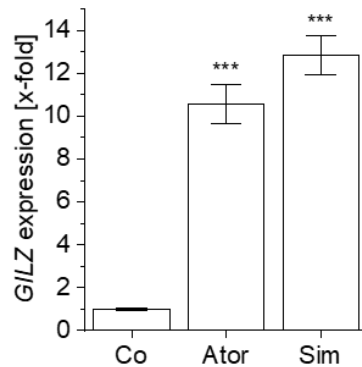


Figure 4.5. Effect of statin treatment on GILZ expression in an endothelial cell line. HMEC-1 cells were treated with simvastatin or atorvastatin at 1 μ M for 24 hours, *GILZ* mRNA expression was normalised against the housekeeping gene (*ACTB*) and is presented as fold change of control. Data show the mean of 2 independent experiments performed in replicates \pm SEM. *** $P < 0.001$ relative to the control.

The *GILZ* gene is located on the X chromosome. For HMEC-1 and RAW264.7 cells, lines of male origin, this means only one allele needs to be edited by non-homologous end joining (NHEJ). C2C12, on the other side, is a female cell line with a hypo tetraploid karyotype — including 4 copies of the X chromosome— (Casas-Delucchi et al., 2011), which makes it difficult to obtain a clone with complete knockout. The validated murine and human sgRNA sequences were located in the last exon of their corresponding gene (Figure 4.6 A-B). Off-target analysis performed with the GT-scan software tool (O'Brien and Bailey, 2014) showed no predicted off-target effects in exonic regions of the genomes, thus, specific editing could be expected. The T7E1 mismatch assay performed in the bulked cell population after transfection indicated cutting by Cas9 in C2C12 and HMEC-1, but not in RAW 264.7 (Figure 4.6 C). After clonal expansion, none of the 20 C2C12 clones screened had indels in all alleles, while the 3 HMEC-1 clones that survived showed successful genomic 1 and 34-bp deletions (Figure 4.7). The growth of these clones, however, was impaired. For this reason, the cells could not be further expanded for characterization. As for the RAW264.7 macrophage model, the lack of editing could be due to poor transfection efficiency, common for this cell line. Hence, to facilitate the screening for functional sgRNAs and the generation of KO cell lines, a Cas9-expressing cell line was developed by a lentiviral approach (data not shown).

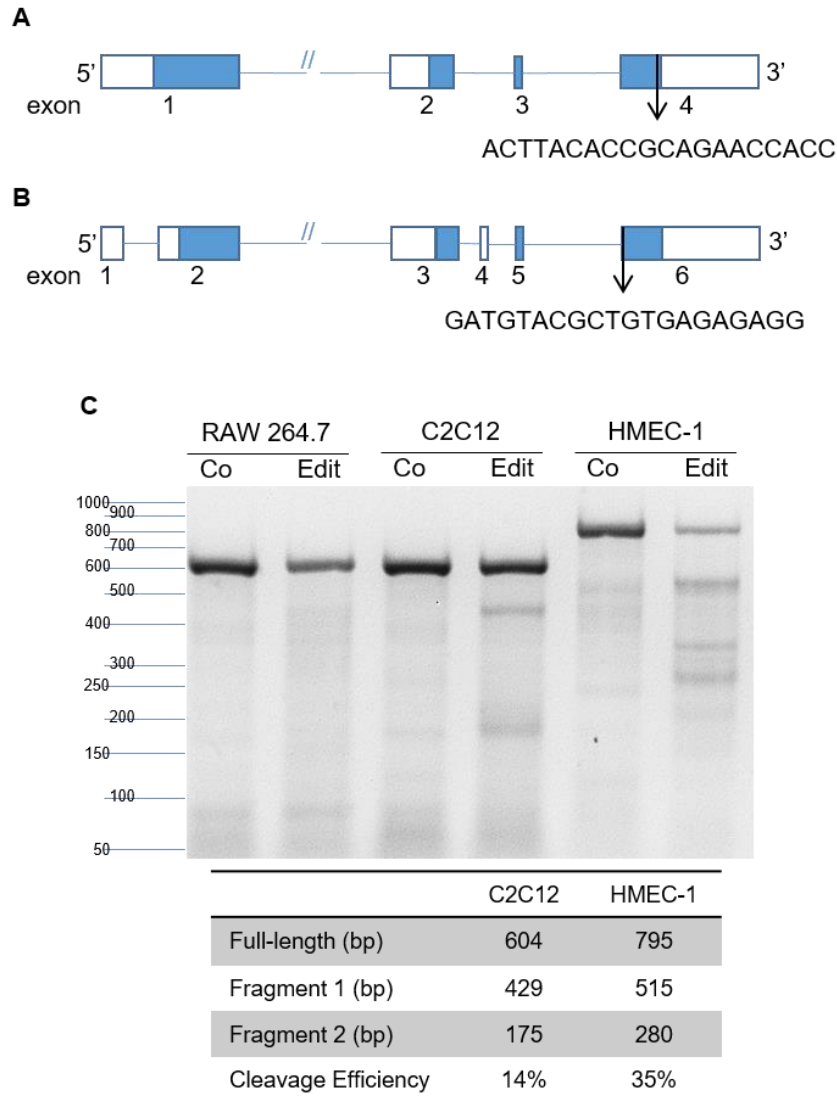


Figure 4.6. CRISPR/Cas9 – mediated GILZ knockout in cell lines. Schematic representation of the human (A) and murine (B) GILZ genes, black arrows indicate the approximate position of the sgRNAs. Genome editing efficiency in bulked population of edited RAW 264.7, C2C12, and HMEC-1 cells (C). The target genomic region from control and transfected cells was amplified by PCR and subjected to mismatch T7E1 assay, products were separated on an agarose gel for analysis. Cleavage efficiency was estimated from the intensities of the parental and cleaved bands.

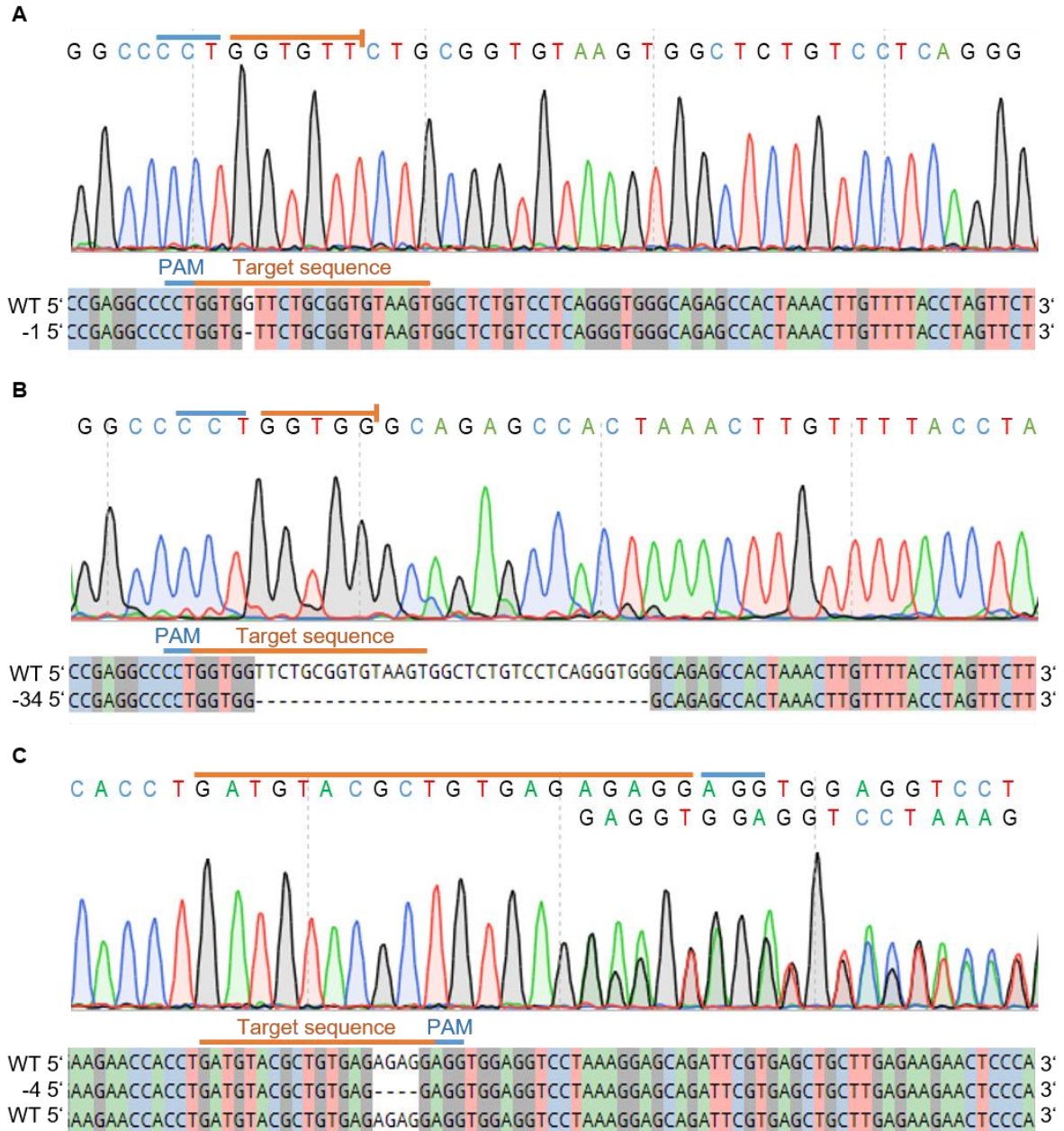


Figure 4.7. Validation of CRISPR/Cas9-mediated genome editing in HMEC-1 and C2C12 clones *via* Sanger sequencing. Sequence of three edited HMEC-1 clones was obtained, chromatogram analysis shows a single allele sequence. Clones 1 and 5 have the same 1 bp deletion (**A**) clone 2 has a 34 bp deletion (**B**). Example sequence of a non-pan-allelic edit obtained in C2C12 clone 17, two sequences are observed in the chromatogram, one corresponding to the WT sequence, and one with a 4 bp deletion (**C**). Sequences were deconvoluted using the CRISP-ID web application, first rows correspond to the reference, WT cells, and bottom rows to the observed sequencing results.

4.3 Discussion

The benefits of statin treatment on CVD are indisputable. Nevertheless, further study of the molecular mechanisms underlying the actions of statins in vascular inflammation are still needed (Almeida and Budoff, 2019). Here it is demonstrated that statins induce the anti-inflammatory protein GILZ in two cell types of critical importance in atherogenesis (Novikova et al., 2018), *i.e.* endothelial cells and macrophages. The induction was mevalonate-dependent, that is, specific to their mechanism of action. Based on the results in muscle cells (chapter I), it might be possible that statin-induced GILZ expression occurs *via* inhibition of protein prenylation in these cell types as well. The role of GILZ in inflammation has been characterised in different tissues and cell types, and more recently it has been shown that GILZ peptide analogues have therapeutic potential for treatment of chronic inflammatory diseases in the central nervous system (Gu et al., 2018; Srinivasan et al., 2016). Therefore, one might expect GILZ induction to be at least partially responsible for the pharmacological effects of statins in vascular inflammation.

A well-recognised mediator of the pleiotropic effects of statins is KLF2 (Parmar *et al.*, 2005; Sen-Banerjee *et al.*, 2005; Tuomisto *et al.*, 2008), a transcription factor that can also be induced by glucocorticoid receptor activation in macrophages, in what has been proposed to be an important cooperation for the control of inflammatory processes (Chinenov et al., 2014). Although the induction patterns of *KLF2* and *GILZ* after atorvastatin treatment were very similar in HUVECs, the exploratory findings presented here do not support the hypothesis that KLF2 acts as an upstream regulator of GILZ expression in endothelium. Whether GILZ might act as an upstream regulator of KLF-2 expression remains to be investigated.

It was possible to successfully introduce genomic edits in the *GILZ* gene in HMEC-1 cells by using CRISPR/Cas9 technology, establishing a protocol for generation of knockouts in our laboratory that can be of use to evaluate the functional aspects of GILZ induction by statins. The three HMEC-1 clones with validated deletions exhibited impaired growth, which might be indicative of a role for GILZ in endothelial cell proliferation. Since the validated target sgRNA sequence was in the last exon of the gene, constitutive to all transcript variants but at the C-terminal portion of the protein, it is likely that the clones did not have abolished expression of GILZ. For CRISPR/Cas9 mediated KO generation it is recommended targeting portions near the N-terminus of the protein, or 5' constitutive exons, to increase the probability of a frameshift mutation that leads to nonsense-mediated mRNA decay or a non-functional protein product (Doench et al., 2014; Joung et al., 2017). The deletions obtained here, however, may cause alterations in the C-terminal portion of GILZ, responsible for interaction with NF- κ B (Di Marco et al., 2007). Further work in generation of GILZ KO HMEC-1 cells might clarify this issue.

Although still a matter of discussion, a body of evidence points towards pleiotropic effects of statins as major contributors to their beneficial effects on the cardiovascular system. The findings presented in this study open the opportunity to investigate the potential role of GILZ as mediator of the anti-inflammatory actions of statins in the cardiovascular system.

5. Chapter III

Macroph-aging: role of glucocorticoid metabolism

5.1 Introduction

Aging is characterised by a gradual decline of the immune function that results in a chronic, low-grade systemic inflammatory state, termed “Inflammaging” (Franceschi et al., 2000). This chronic inflammation, fuelled by continuous exposure to a number of exogenous and endogenous antigens during lifespan, is considered by geroscience one of the seven pillars of aging, and largely determines the onset of age-related diseases (Franceschi et al., 2018).

Different factors, like cell senescence, endocrine, and metabolic alterations, contribute to sustain inflammaging (Bandaranayake and Shaw, 2016). Among these, the macrophage is considered a key cell type driving age-related inflammation. Indeed, since its origins, the theory of inflammaging has been intertwined with “macroph-aging”, that is, the chronic activation of macrophages with age (Franceschi et al., 2000; Prattichizzo et al., 2016). Macrophages are a widely distributed, heterogeneous, plastic cell population, with central roles as effector and mediator of the innate and adaptive immune response (Janeway et al., 2001; Wynn et al., 2013). Several studies in humans and animals have reported age-related alterations in different macrophage functions, such as phagocytic activity, pro-inflammatory cytokine secretion, and antigen presentation (Jackaman et al., 2017; Sebastián et al., 2005). Furthermore, loss of macrophages has been associated with improved inflammatory-induced pathology and survival after systemic immunostimulation (Bouchlaka et al., 2013), and with reduced neurodegeneration (Yuan et al., 2018) in murine models of aging.

Endogenous GCs are main regulators of the immune function (Cain and Cidlowski, 2017). GC secretion is regulated in a circadian manner, and in response to stress, by the HPA axis, the function of which is dysregulated with advancing age (Gupta and Morley, 2014). Although sometimes contradictory, literature reports regarding altered cortisol secretory profiles in humans often describe elevations in cortisol levels in aged subjects that correlate with negative health outcomes (Gaffey et al., 2016). Noticeably, increased cortisol levels seem to be a phenotypic feature of centenarians, subjects who are able to cope with inflammation and have achieved longevity by mounting an effective anti-inflammaging response (Franceschi et al., 2007; Genedani et al., 2008; Sergio, 2008). Thus, the balance between pro- and anti-inflammatory mediators is what ultimately determines successful aging. Because of their role in modulation of the inflammatory response (Busillo and Cidlowski, 2013), one might hypothesise that alterations in GC metabolism affect the function of immune cells, including macrophages, during aging.

Previous work in our group found a pro-inflammatory phenotype in aged (85 weeks) C57BL/6 mice compared with their young (10 weeks) counterparts. This phenotype was characterised by higher levels of circulating pro-inflammatory cytokines, like TNF- α , and lower levels of total

corticosteroids in serum (Figure 5.1 A–B). Likewise, flow cytometry analysis showed decreased expression of the GC-inducible, anti-inflammatory protein GILZ in the myeloid compartment of different organs, in PBLs, and in PMs from aged animals (Data not shown and figure 5. C). Given the importance of macrophage activation and GC response in the aged immune system, we aimed to further evaluate the age-associated changes in gene expression and GC metabolism across tissues, as well as in the myeloid compartment of mice, to improve the current understanding of “macroph-aging”.

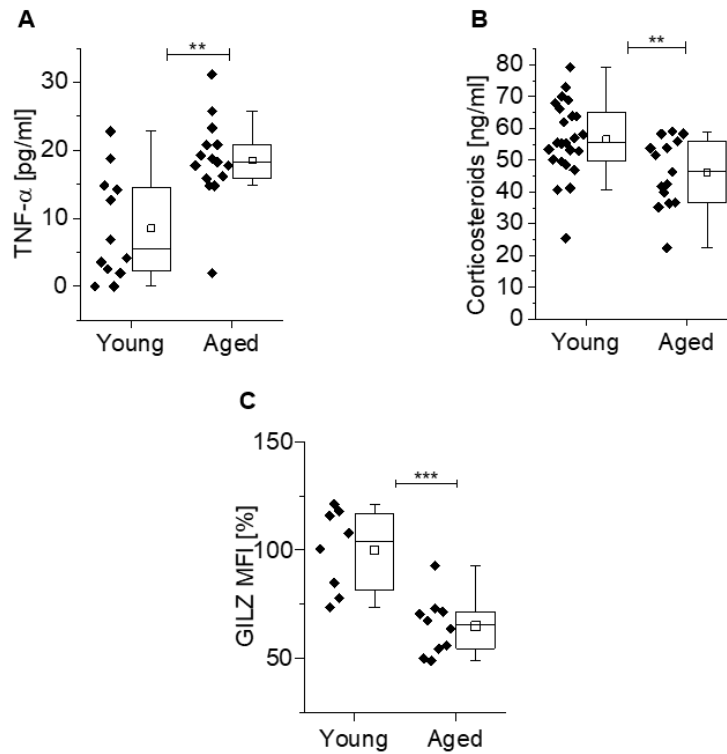


Figure 5.1. Aged mice show a pro-inflammatory phenotype. Levels of TNF- α (A) and total corticosteroids (B) in serum from young (10 weeks) and aged (85 weeks) C57BL/6 mice (n=12–15), as determined by ELISA. Flow cytometry analysis of GILZ levels in PMs isolated from young and aged mice (C, n=8–10). Box-plots show the 25–75th percentiles (Box), mean (square), median (line) and range within 1.5 IQR (whiskers). **P<0.01, ***P<0.001 relative to young mice.

5.2 Results

5.2.1 Lipid peroxidation and clinical chemistry analysis

To further characterise the aged-related changes of C57BL/6 mice, TBARS assay was performed to measure the oxidative stress levels of young and aged animals in liver tissue. Contrary to what could be expected, there were lower levels of malondialdehyde in livers from aged mice, compared with the young controls (Figure 5.2). Serum analysis of aspartate and alanine transaminases, triglycerides, cholesterol, albumin, and uric acid levels did not reveal age-related significant differences among groups (Table 5.1).

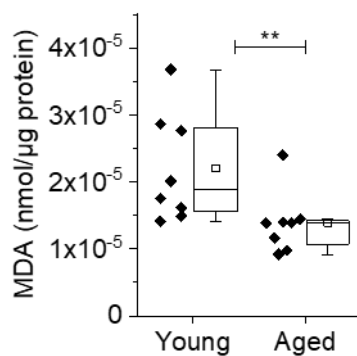


Figure 5.2. Oxidative stress levels in livers from young and aged mice. TBARS assay was performed in liver tissues from young (10 weeks) and aged (85 weeks) C57BL/6 mice (n=8). MDA concentrations were normalised to total protein content in the sample and are presented in Box-plots showing the 25–75th percentiles (Box), mean (square), median (line) and range within 1.5 IQR (whiskers). **P<0.01 relative to young mice.

Table 5.1. Clinical chemistry analysis in serum from young and aged C57BL/6 mice.

	Female		Male	
	Young (n=3)	Aged (n=6)	Young (n=9)	Aged (n=6)
AST (U/l)	1005 (420-1450)	555 (390-800)	1015 (450-1205)	592.5 (515-890)
ALT (U/l)	95 (50-135)	107.5 (60-190)	175 (70-425)	132.5 (75-320)
Triglycerides (mg/dl)	105 (90-110)	82.5 (65-110)	140 (135-175)	102.5 (95-135)
Cholesterol (mg/dl)	60 (60-65)	60 (-)	75 (65-80)	65 (60-70)
Albumin (g/l)	35 (-)	37.5 (35-40)	30 (30-35)	35 (30-35)
Uric acid (mg/dl)	7.5 (5-8)	8 (7-8)	7 (6-9.5)	7.5 (7-8)

Data are presented as median (IQR). Comparison was performed with Mann Whitney U Test. No significant differences were detected.

5.2.2 Cytokine expression in tissues from aged mice

Measurement of mRNA expression of three pro-inflammatory mediators, namely *Tnf*, *Il1b*, and *Il6*, was performed at baseline and after treatment with 5 mg/kg LPS, in different tissues from young and aged mice. There were no consistent differences in the expression of these mediators in tissue that correlated with the elevated serum cytokine levels observed by ELISA in previous experiments. At baseline, *Tnf* levels were significantly elevated in lung but decreased in lymph nodes of aged mice, while *Il1b* expression was increased in both, liver and lymph nodes (Figure 5.3 A,C). After LPS stimulation, significant differences between groups were only found for *Tnf* expression in liver and spleen (Figure 5.3 B,D). *Il6* expression was very low in all tissues, what impedes to draw significant conclusions from the data obtained (Appendix).

5.2.3 Altered glucocorticoid homeostasis in myeloid cells from aged mice

Further analysis focused on changes in gene expression of PMs and PBLs isolated from young and aged mice, given that no major differences between groups could be detected in whole tissues. The expression of GC-responsive genes other than GILZ was evaluated in these cells, finding significantly decreased levels of the dual specificity phosphatase 1 (*Dusp1*) gene, but not of *Anxa1* or *Sgk1* (Figure 5.4). The reduced levels of GILZ protein and *Dusp1* gene expression might be indicative of a decreased ability of myeloid cells to respond to GC stimulation. Since altered regulation of genes responsible for GC homeostasis within cells could account for dysregulated GC-responsiveness in aging, the expression of such genes was investigated.

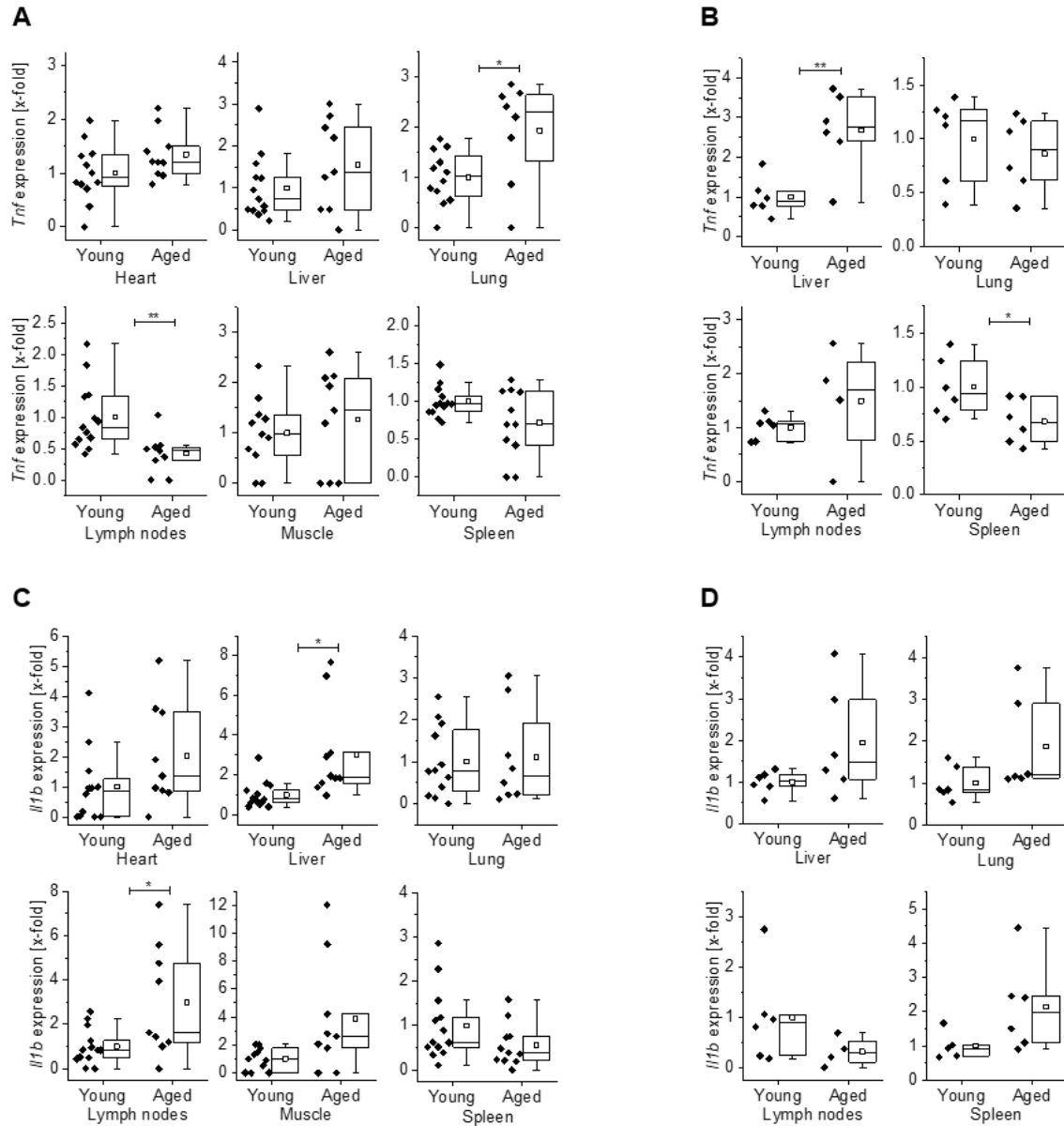


Figure 5.3. Expression of pro-inflammatory cytokines in tissues from young and aged mice. mRNA expression of *Tnf* and *Il1b* was measured in heart, liver, lung, lymph nodes, skeletal muscle, and spleen tissues from young (10 weeks) and aged (80–100 weeks) C57BL/6 mice at baseline (A,C, n=9–13), or in liver, lung, lymph nodes, and spleen after treatment with 5 mg/kg LPS for 4 hours (B,D, n=4–6). mRNA expression was normalised against the housekeeping gene (*Ppia*) and is presented as fold change of young. Box-plots show the 25–75th percentiles (Box), mean (square), median (line) and range within 1.5 IQR (whiskers). *P<0.05, **P<0.01 relative to equally treated young mice.

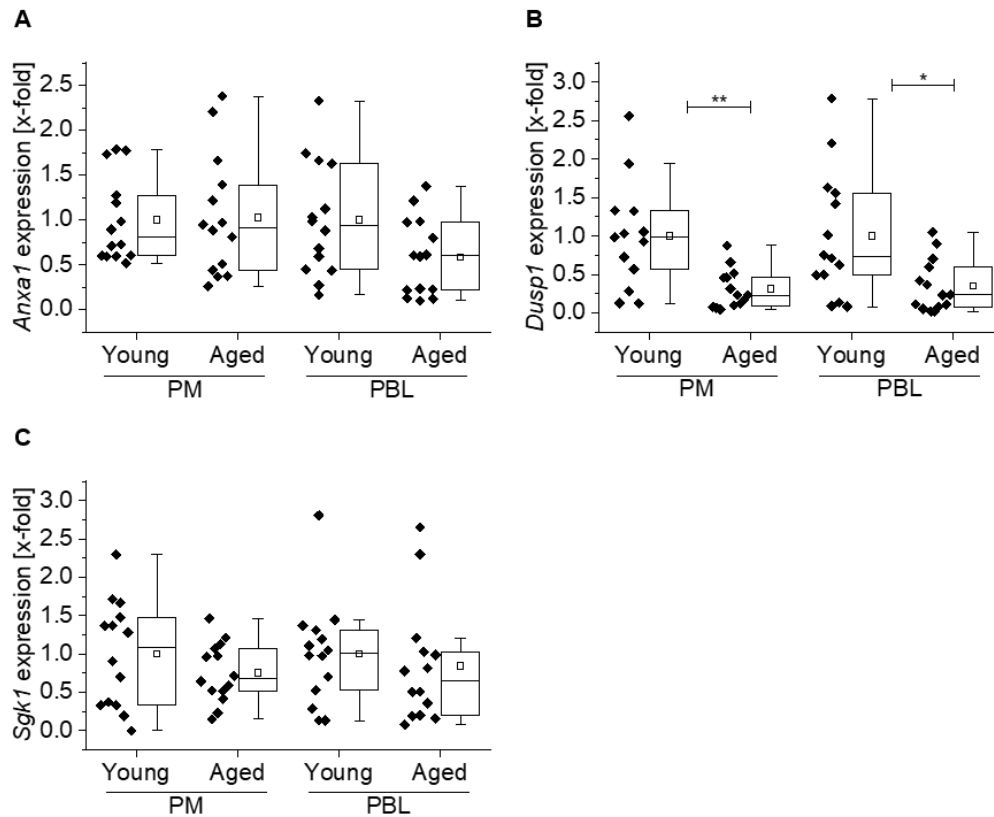


Figure 5.4. Expression of GC-responsive genes in PM/PBL from young and aged mice. mRNA expression of *Anxa1*, *Sgk1* and *Dusp1* was measured in PMs and PBLs from young (10 weeks) and aged (80–100 weeks) C57BL/6 mice (n=13–14). Gene expression was normalised against the housekeeping gene (*Ppia*) and is presented as fold change of young. Box-plots show the 25–75th percentiles (Box), mean (square), median (line) and range within 1.5 IQR (whiskers). *P<0.05, **P<0.01 relative to young mice.

GCs exert their action through binding to the ubiquitously expressed glucocorticoid receptor (GR). Therefore, changes in cellular GR expression determine GC-responsiveness (Oakley and Cidlowski, 2013; Ramamoorthy and Cidlowski, 2013). mRNA expression analysis, however, indicated that GR levels remained unchanged with aging in PMs and PBLs (Figure 5.5 A). At pre-receptor level, the intracellular action of GCs is largely determined by the activity of the two isozymes 11 β -HSD1 and 11 β -HSD2, that catalyse the interconversion of active cortisol/corticosterone and inactive cortisone/11-dehydrocorticosterone (11-DHC), thereby modulating GC availability (Tomlinson et al., 2004). *Hsd11b1* expression was significantly decreased in aged mice compared with young controls, not only in PMs and PBLs, but also in liver, where the enzyme is most abundant (Figure 5.5 B–C). The findings at mRNA level were confirmed at protein level in PMs and bone-marrow derived macrophages (BMM, Figure 5.5 D–F). Expression of the hexose-6-phosphate dehydrogenase gene (*H6pd*) was upregulated in aged PMs and PBLs. In the cell, H6PDH is the source of NADPH, needed as cofactor for 11 β -HSD1 reductase (cortisone to cortisol) activity (Atanasov et al., 2004). On the other hand, the gene expression of *Hsd11b2*, the isozyme that exerts dehydrogenase (cortisone to cortisol) activity, remained unchanged in PMs and PBLs from aged mice, compared with young controls

(Figure 5.5 G–H). These findings are indicative of alterations in intracellular GC metabolism in the macrophages of aged mice.

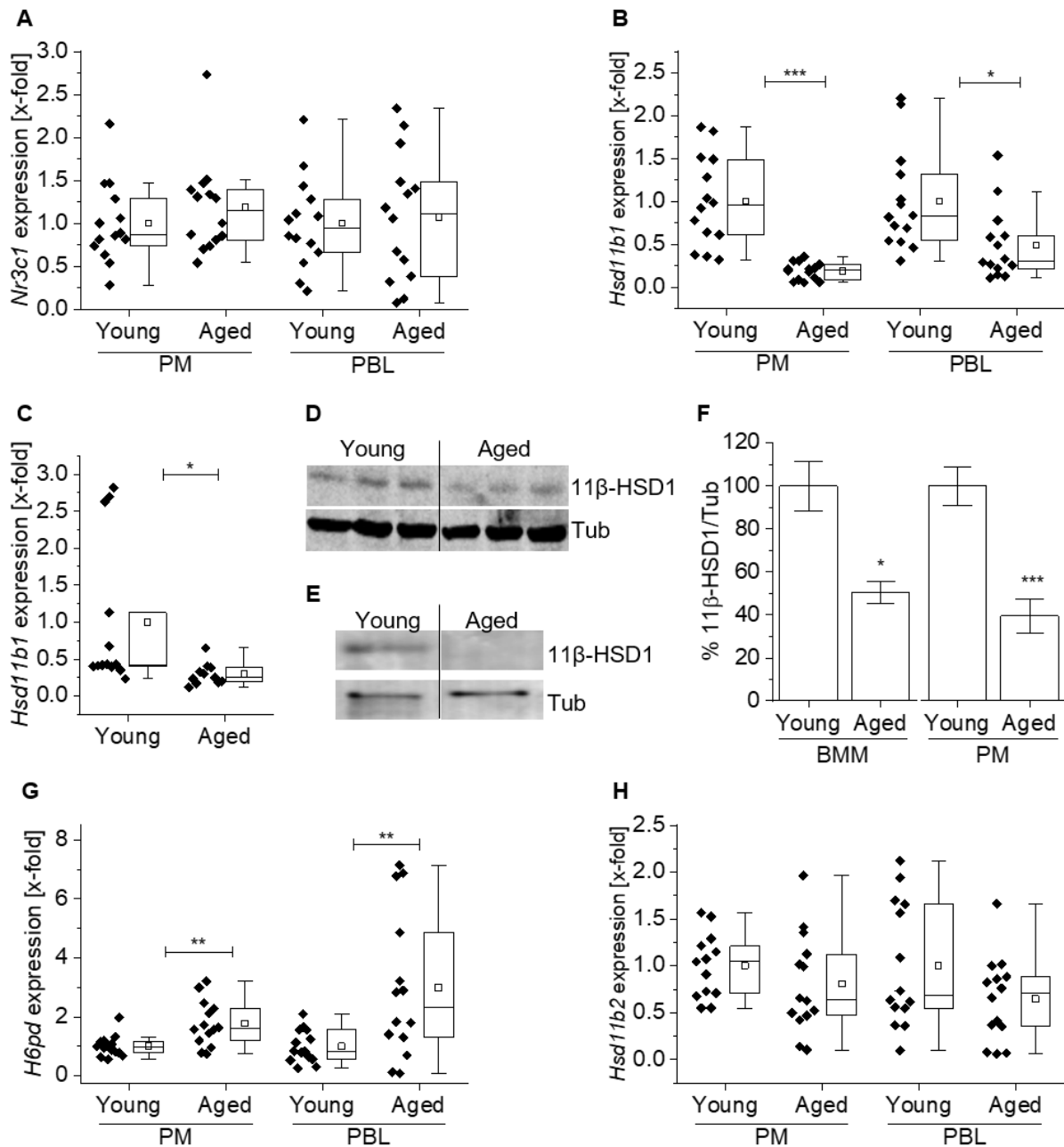


Figure 5.5. Alterations in glucocorticoid metabolism in aged mice. Expression of GR mRNA (*Nr3c1*) in PMs and PBLs from young (10 weeks) and aged (80–100 weeks) C57BL/6 mice (n=13–14, **A**). *Hsd11b1* expression in PMs, PBLs, and liver tissue from young and aged mice (**B–C**). 11β-HSD1 protein expression was measured in BMMs (**D**, n=4) and PMs (**E**, n=11–12). Representative blots are shown. Densitometric analysis, normalised to the housekeeping protein (α -Tubulin, **E**). mRNA levels of *H6pd* and *Hsd11b2* were also measured in PMs and PBLs (**G–H**). Gene expression was normalised against the housekeeping gene (*Ppia*) and is presented as fold change of young. Box-plots show the 25–75th percentiles (Box), mean (square), median (line) and range within 1.5 IQR (whiskers). Bars show the mean \pm SEM. *P<0.05, **P<0.01, ***P<0.001 relative to young mice.

5.2.4 Reduced corticosterone levels and 11 β -HSD1 activity in aged mice

Analysis of the functional implications of reduced 11 β -HSD1 expression was first performed by measurement of the levels of corticosterone and 11-DHC, the main GCs in rodents (Gong et al., 2015), in serum from young and aged mice. In line with the previous ELISA findings, aged mice displayed reduced levels of both corticosteroids in serum (Figure 5.6 A–B). The ratio of active corticosterone to inactive 11-DHC, however, remained unchanged in both groups (data not shown).

Since 11 β -HSD1 regulates the intracellular availability of active GCs, alterations in 11 β -HSD1 reductase activity were evaluated by measuring the conversion rate of deuterated cortisone to cortisol in isolated young and aged PMs. As could be expected, the downregulation of the enzyme resulted in less intracellular conversion to cortisol (Figure 5.6 C). Hence, one might hypothesise, in the *in vivo* setting reduced 11 β -HSD1 expression translates into less corticosterone available to activate the GR in aging macrophages.

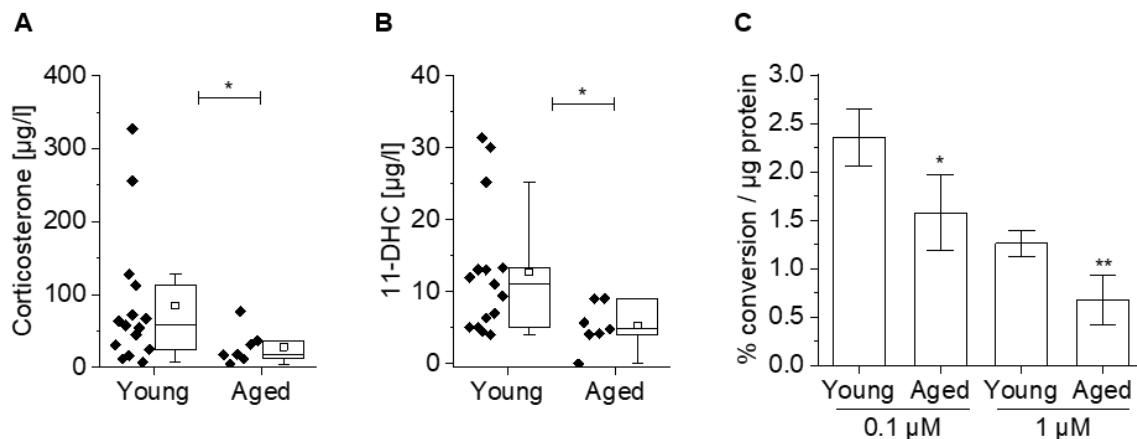


Figure 5.6. Differences in serum glucocorticoids and 11 β -HSD1 activity in young and aged mice. Serum levels of corticosterone and 11-DHC from young (10 weeks, n=15) and aged (80–100 weeks, n=7) male C57BL/6 mice were measured by LC-HRMS/MS (A,B). PMs isolated from young and aged animals (n=10) were incubated for 24 hours with 0.1 μ M and 1 μ M cortisone-D₈, the conversion to cortisol-D₈ was measured in supernatants by LC-HRMS/MS (C). Conversion percentages were normalised to total protein content in the sample. Box-plots show the 25–75th percentiles (Box), mean (square), median (line) and range within 1.5 IQR (whiskers). Bars show the mean \pm SEM. *P<0.05, **P<0.01, relative to young mice.

5.2.5 Upstream regulators of 11 β -HSD1 are downregulated in aged macrophages

Transcription of *Hsd11b1* is regulated by members of the CCAAT/enhancer binding protein (C/EBP) family of transcription factors (Chapman et al., 2013). As a first insight into the mechanisms leading to 11 β -HSD1 downregulation in aged PM and PBL, mRNA levels of C/EBP α and C/EBP β were measured. Both genes were significantly downregulated in PMs

from aged animals. In PBLs, a similar tendency for *Cebpa* expression was observed, while the expression of *Cebpb* remained unchanged (Figure 5.7).

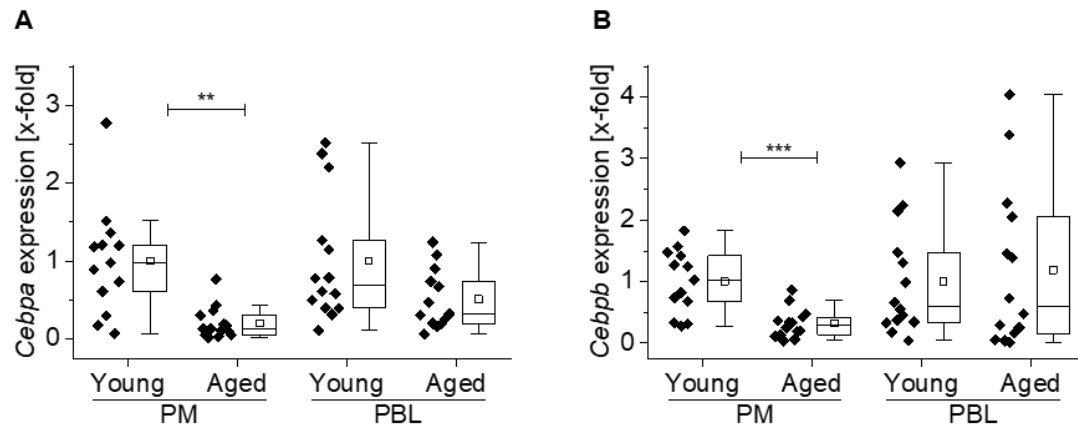


Figure 5.7. Gene expression of upstream regulators of 11 β -HSD1. *Cebpa* (A) and *Cebpb* (B) mRNA levels were measured in PMs and PBLs from young (10 weeks) and aged (80–100 weeks) C57BL/6 mice (n=13–14). Gene expression was normalised against the housekeeping gene (*Ppia*) and is presented as fold change of young. Box-plots show the 25–75th percentiles (Box), mean (square), median (line) and range within 1.5 IQR (whiskers). **P<0.01, ***P<0.001 relative to young mice.

5.3 Discussion

The aging process represents a gradual deterioration of the function and homeostasis of different systems that are closely linked with the onset of chronic diseases, and ultimately determine survival. The present work shows evaluation of the phenotype of aging C57BL/6 mice, and reports alterations in the intracellular GC homeostasis of macrophages and PBLs from these mice.

Oxidative stress has been signalled as a determinant factor that contributes to age-related inflammation (De la Fuente and Miquel, 2009). In serum (Balkan et al., 2002) and erythrocytes (Kawamoto et al., 2005) of aged subjects, increased levels of endogenous lipid peroxidation, indicative of oxidative stress, have been reported. On the other hand, the literature about lipid peroxidation on mammal tissues is conflicting, and the results are species-, sex-, and tissue-dependent (Khansari et al., 2009). In this setting, age was associated with reduced hepatic lipid peroxidation—and thus oxidative stress—similar to previous reports in 22-month C57BL/6 mice (Selman et al., 2008). The reduced MDA levels found in aged mice may be explained by conserved or improved antioxidant capacity in the liver, as previously shown for old female Fischer 344 rats (Rikans et al., 1991). This aspect, however, was not evaluated in the present study.

The involvement of GC signalling and metabolism in chronic inflammation and stress-related disorders, two phenomena that occur with aging, has been a topic of interest for the last decades (Herriot et al., 2017). Literature reports indicate associations between both, higher and lower GC levels, and negative health outcomes (Gaffey et al., 2016; Raison and Miller, 2003). In rodents, increase (Kizaki et al. 2002), no differences (Morano et al., 1994) and, more recently, decrease (Zambrano et al., 2015) of serum corticosterone with age has been reported. Given that GCs have an anti-inflammatory and immunosuppressive function, it is logical to think that the reduced total circulating GCs, and particularly corticosterone, found in our study might contribute to the pro-inflammatory phenotype observed in aged mice. Nevertheless, cellular GC-responsiveness is ultimately determined by the intracellular availability of active GCs, as well as the expression of GRs. Aged PMs and PBLs, indeed, showed reduced levels of two GC-inducible genes with important roles in the regulation of the inflammatory response: GILZ downregulation has been associated with increased pro-inflammatory activation of macrophages (Hopstädter et al., 2015), and DUSP-1 has been shown to reduce their pro-inflammatory cytokine expression upon LPS-activation (Abraham et al., 2006; Chen et al., 2002).

Although a previous study reported elevated GR mRNA expression in peritoneal exudate cells from aged mice (Kizaki et al., 1998), our findings suggest that alterations in GC-homeostasis

from PMs are not associated with altered GR expression but with reduced intracellular activation of 11-DHC by 11 β -HSD1. There might be different functional implications of blunted 11 β -HSD1 signalling in aged macrophages: it has been shown that 11 β -HSD1-deficient mice are more susceptible to endotoxemia, and macrophages derived from these mice are hyperresponsive to LPS stimulation (Zhang and Daynes, 2007). Loss of 11 β -HSD1 in macrophages has also been associated with delayed phagocytic capacity (Gilmour et al., 2006).

Various studies have addressed the changes in 11 β -HSD1 expression and activity in different tissues and cell types with aging. For example, elevated expression in hippocampus from aged C57BL/6J mice was related to impaired cognitive function (Holmes et al., 2010). Similarly, protein expression was elevated in skeletal muscle from aged female volunteers, and correlated with reduced grip strength and insulin resistance (Hassan-Smith et al., 2015). Age-related elevations in 11 β -HSD1 have also been reported for brown adipose tissue (Doig et al., 2017), skin (Tiganescu et al., 2013), and CD4⁺ T lymphocytes (Zhang et al., 2005). Interestingly, 11 β -HSD1 was regulated in the opposite fashion not only in PMs, but also in PBLs, a mixed population of granulocytes, lymphocytes, and monocytes. To our knowledge, this is the first report on age-induced changes in 11 β -HSD1 expression in macrophages.

In summary, the present data provide insight into the alterations in GC metabolism in macrophages during aging. The reduced circulating corticosterone levels, together with a decreased availability of active GC within cells as a consequence of reduced 11 β -HSD1, might contribute to the imbalance between pro- and anti-inflammatory signalling in macrophages from aged mice, thus promoting the inflammaging phenotype.

The results presented in this chapter are part of the following manuscript, in preparation:

Macroph-aging: Role of glucocorticoid metabolism

J. Vanessa Valbuena Perez; Anna Dembek; Rebecca Linnenberger; Carlo Riccardi, Ph.D.; Stefano Bruscoli, Ph.D.; Markus R. Meyer, Ph.D.; Alexandra K. Kiemer Ph.D.; and Jessica Hoppstädter. Ph.D.

6. Summary and Conclusions

Statins are essential in the pharmacotherapy for prevention of the most important cause of death globally, *i.e.* cardiovascular disease. These drugs are generally considered safe and exert a plethora of beneficial effects in the vasculature. SAMS, however, still represent an important reason for non-adherence to treatment. Because of their widespread use, even a low incidence in SAMS would represent a substantial number of patients affected. In the present study, GILZ was identified as an essential mediator of the molecular mechanisms underlying statin-induced muscle damage and impairment of muscle regeneration. We confirmed the importance of impaired protein geranylgeranylation, Akt signalling, and FoxO3 activation in statin-induced myotoxicity, and demonstrated that loss of GILZ can prevent statin-induced cell death.

The effects of statins in muscle differentiation have been less investigated than their myotoxicity. This work demonstrated that GILZ induction by statins is also involved in their deleterious effects on myoblast differentiation, since GILZ depletion was able to partially rescue myogenesis in the presence of statins. Moreover, the involvement of endogenous GILZ in the regulation of skeletal muscle development and regeneration appears as an interesting topic for further research.

The functional implications of GILZ induction by statins are, nonetheless, not only negative, since GILZ is also induced in vascular endothelial cells and macrophages, two cell types in which the anti-inflammatory function of this protein is well characterised. To which extent GILZ contributes to the pleiotropic, anti-inflammatory actions of statins, remains to be investigated.

In conclusion, the first part of this study contributes to a better understanding of the molecular mechanisms underlying statin-induced myopathy, a valuable step towards the development of prevention strategies and safer therapy approaches for this class of drugs. Furthermore, the findings presented here open the opportunity to investigate the potential role of GILZ as a mediator of the anti-inflammatory actions of statins in the cardiovascular system.

The onset of CVD and other chronic inflammatory diseases is largely predicted by age. Indeed, the field of geroscience considers that aging and age-related diseases share a molecular basis, in which inflammation plays a key role. The comprehensive investigation of the mechanisms that fuel, maintain, and modulate inflammaging is therefore necessary to understand its potential role in age-related pathogenesis and identify points for intervention. Macrophages are the central cell type driving the inflammatory response, and maladaptive function of aged macrophages largely contributes to inflammaging. The second part of this work investigated whether GC regulation was altered with age in this cell type, given that GCs are main modulators of the immune function and stress response. The data obtained provide insight into the alterations in GC metabolism in macrophages during aging. Reduced circulating GC levels,

together with a decreased availability of active GC within cells as a consequence of reduced 11 β -HSD1, might contribute to the imbalance between pro- and anti-inflammatory signalling in macrophages from aged mice, thus promoting the inflammaging phenotype.

7. References

- Abraham SM, Lawrence T, Kleiman A, Warden P, Medghalchi M, Tuckermann J, et al. Antiinflammatory effects of dexamethasone are partly dependent on induction of dual specificity phosphatase 1. *J Exp Med* 2006;203:1883–9. doi:10.1084/jem.20060336.
- Addgene. Addgene: pLKO.1–TRC Cloning vector protocol version 1.0 2006. <http://www.addgene.org/tools/protocols/plko/> (accessed August 12, 2018).
- Almeida SO, Budoff M. Effect of statins on atherosclerotic plaque. *Trends Cardiovasc Med* 2019. doi:10.1016/j.tcm.2019.01.001.
- Andrés V, Walsh K. Myogenin expression, cell cycle withdrawal, and phenotypic differentiation are temporally separable events that precede cell fusion upon myogenesis. *J Cell Biol* 1996;132:657–66. doi:10.1083/jcb.132.4.657.
- Arai Y, Martin-Ruiz CM, Takayama M, Abe Y, Takebayashi T, Koyasu S, et al. Inflammation, but not telomere length, predicts successful ageing at extreme old age: a longitudinal study of semi-supercentenarians. *EBioMedicine* 2015;2:1549–58. doi:10.1016/J.EBIOM.2015.07.029.
- Asfour HA, Allouh MZ, Said RS. Myogenic regulatory factors: The orchestrators of myogenesis after 30 years of discovery. *Exp Biol Med* 2018;243:118–28. doi:10.1177/1535370217749494.
- Asselin-Labat M-L, Biola-Vidamment A, Kerbrat S, Lombès M, Bertoglio J, Pallardy M. FoxO3 mediates antagonistic effects of glucocorticoids and interleukin-2 on glucocorticoid-induced leucine zipper expression. *Mol Endocrinol* 2005;19:1752–64. doi:10.1210/me.2004-0206.
- Atanasov AG, Nashev LG, Schweizer RA., Frick C, Odermatt A. Hexose-6-phosphate dehydrogenase determines the reaction direction of 11 β -hydroxysteroid dehydrogenase type 1 as an oxoreductase. vol. 571. 2004. doi:10.1016/j.febslet.2004.06.065.
- Ayroldi E, Macchiarulo A, Riccardi C. Targeting glucocorticoid side effects: selective glucocorticoid receptor modulator or glucocorticoid-induced leucine zipper? A perspective. *FASEB J* 2014;28:5055–70. doi:10.1096/fj.14-254755.
- Ayroldi E, Migliorati G, Bruscoli S, Marchetti C, Zollo O, Cannarile L, et al. Modulation of T-cell activation by the glucocorticoid-induced leucine zipper factor via inhibition of nuclear factor kappaB. *Blood* 2001;98:743–53. doi:10.1182/BLOOD.V98.3.743.
- Ayroldi E, Riccardi C. Glucocorticoid-induced leucine zipper (GILZ): a new important mediator of glucocorticoid action. *FASEB J* 2009;23:3649–58. doi:10.1096/fj.09-134684.
- Baba TT, Nemoto TK, Miyazaki T, Oida S. Simvastatin suppresses the differentiation of C2C12 myoblast cells via a Rac pathway. *J Muscle Res Cell Motil* 2008;29:127–34. doi:10.1007/s10974-008-9146-9.
- Balkan J, Kanbagli Ö, Mehmetçik G, Mutlu-Türkoglu Ü, Aykaç-Toker G, Uysal M. Increased lipid peroxidation in serum and low-density lipoproteins associated with aging in humans. *Int J Vitam Nutr Res* 2002;72:315–20. doi:10.1024/0300-9831.72.5.315.
- Bandaranayake T, Shaw AC. Host resistance and immune aging. *Clin Geriatr Med* 2016;32:415–32. doi:10.1016/j.cger.2016.02.007.
- Baylis D, Bartlett DB, Patel HP, Roberts HC. Understanding how we age: insights into inflammaging. *Longev Heal* 2013;2:8. doi:10.1186/2046-2395-2-8.

- Beaulieu E, Ngo D, Santos L, Yang YH, Smith M, Jorgensen C, et al. Glucocorticoid-induced leucine zipper is an endogenous antiinflammatory mediator in arthritis. *Arthritis Rheum* 2010;62:2651–61. doi:10.1002/art.27566.
- Bentzinger CF, Wang YX, Rudnicki MA. Building muscle: molecular regulation of myogenesis. *Cold Spring Harb Perspect Biol* 2012;4:a008342. doi:10.1101/cshperspect.a008342.
- Boettcher M, McManus MT. Choosing the right tool for the job: RNAi, TALEN, or CRISPR. *Mol Cell* 2015;58:575–85. doi:10.1016/j.molcel.2015.04.028.
- Bonifacio A, Sanvee GM, Bouitbir J, Krähenbühl S. The AKT/mTOR signaling pathway plays a key role in statin-induced myotoxicity. *Biochim Biophys Acta* 2015;1853:1841–9. doi:10.1016/j.bbamcr.2015.04.010.
- Bouchlaka MN, Sckisel GD, Chen M, Mirsoian A, Zamora AE, Maverakis E, et al. Aging predisposes to acute inflammatory induced pathology after tumor immunotherapy. *J Exp Med* 2013;210:2223–37. doi:10.1084/jem.20131219.
- Bouitbir J, Charles A-L, Echaniz-Laguna A, Kindo M, Daussin F, Auwerx J, et al. Opposite effects of statins on mitochondria of cardiac and skeletal muscles: a ‘mitohormesis’ mechanism involving reactive oxygen species and PGC-1. *Eur Heart J* 2012;33:1397–407. doi:10.1093/eurheartj/ehr224.
- Bruscoli S, Donato V, Velardi E, Di Sante M, Migliorati G, Donato R, et al. Glucocorticoid-induced leucine zipper (GILZ) and long GILZ inhibit myogenic differentiation and mediate anti-myogenic effects of glucocorticoids. *J Biol Chem* 2010;285:10385–96. doi:10.1074/jbc.M109.070136.
- Bruscoli S, Velardi E, Di Sante M, Bereshchenko O, Venanzi A, Coppo M, et al. Long glucocorticoid-induced leucine zipper (L-GILZ) protein interacts with ras protein pathway and contributes to spermatogenesis control. *J Biol Chem* 2012;287:1242–51. doi:10.1074/jbc.M111.316372.
- Busillo JM, Cidlowski JA. The five Rs of glucocorticoid action during inflammation: ready, reinforce, repress, resolve, and restore. *Trends Endocrinol Metab* 2013;24:109–19. doi:10.1016/J.TEM.2012.11.005.
- Cain DW, Cidlowski JA. Immune regulation by glucocorticoids. *Nat Rev Immunol* 2017;17:233–47. doi:10.1038/nri.2017.1.
- Campos LM, Rios EA, Guapyassu L, Midlej V, Atella GC, Herculano-Houzel S, et al. Alterations in zebrafish development induced by simvastatin: Comprehensive morphological and physiological study, focusing on muscle. *Exp Biol Med (Maywood)* 2016;241:1950–60. doi:10.1177/1535370216659944.
- Campos LM, Rios EA, Midlej V, Atella GC, Herculano-Houzel S, Benchimol M, et al. Structural analysis of alterations in zebrafish muscle differentiation induced by simvastatin and their recovery with cholesterol. *J Histochem Cytochem* 2015;63:427–37. doi:10.1369/0022155415580396.
- Cannarile L, Zollo O, D’Adamio F, Ayroldi E, Marchetti C, Tabilio A, et al. Cloning, chromosomal assignment and tissue distribution of human GILZ, a glucocorticoid hormone-induced gene. *Cell Death Differ* 2001;8:201–3. doi:10.1038/sj.cdd.4400798.
- Cao P, Hanai J-I, Tanksale P, Imamura S, Sukhatme VP, Lecker SH. Statin-induced muscle damage and atrogen-1 induction is the result of a geranylgeranylation defect. *FASEB J* 2009;23:2844–54. doi:10.1096/fj.08-128843.

- Casas-Delucchi CS, Brero A, Rahn H-P, Solovei I, Wutz A, Cremer T, et al. Histone acetylation controls the inactive X chromosome replication dynamics. *Nat Commun* 2011;2:222. doi:10.1038/ncomms1218.
- Catapano AL, Graham I, De Backer G, Wiklund O, Chapman MJ, Drexel H, et al. 2016 ESC/EAS guidelines for the management of dyslipidaemias. *Eur Heart J* 2016;37:2999–3058. doi:10.1093/eurheartj/ehw272.
- Chapman K, Holmes M, Seckl J. 11 β -hydroxysteroid dehydrogenases: intracellular gate-keepers of tissue glucocorticoid action. *Physiol Rev* 2013;93:1139–206. doi:10.1152/physrev.00020.2012.
- Chen P, Li J, Barnes J, Kokkonen GC, Lee JC, Liu Y. Restraint of proinflammatory cytokine biosynthesis by mitogen-activated protein kinase phosphatase-1 in lipopolysaccharide-stimulated macrophages. *J Immunol* 2002;169:6408–16. doi:10.4049/JIMMUNOL.169.11.6408.
- Cheng Q, Fan H, Ngo D, Beaulieu E, Leung P, Lo CY, et al. GILZ overexpression inhibits endothelial cell adhesive function through regulation of NF- κ B and MAPK activity. *J Immunol* 2013;191:424–33. doi:10.4049/jimmunol.1202662.
- Chinenov Y, Coppo M, Gupte R, Sacta MA, Rogatsky I. Glucocorticoid receptor coordinates transcription factor-dominated regulatory network in macrophages. *BMC Genomics* 2014;15:656. doi:10.1186/1471-2164-15-656.
- Chung H, Lee I, Kang H, Suh J, Kim H, Park K, et al. Statin inhibits interferon- γ -induced expression of intercellular adhesion molecule-1 (ICAM-1) in vascular endothelial and smooth muscle cells. *Exp Mol Med* 2002;34:451–61.
- Collins R, Reith C, Emberson J, Armitage J, Baigent C, Blackwell L, et al. Interpretation of the evidence for the efficacy and safety of statin therapy. *Lancet* 2016;388:2532–61. doi:10.1016/S0140-6736(16)31357-5.
- Costantino S, Paneni F, Cosentino F. Ageing, metabolism and cardiovascular disease. *J Physiol* 2016;594:2061–73. doi:10.1113/JP270538.
- D'Adamio F, Zollo O, Moraca R, Ayroldi E, Bruscoli S, Bartoli A, et al. A new dexamethasone-induced gene of the leucine zipper family protects T lymphocytes from TCR/CD3-activated cell death. *Immunity* 1997;7:803–12. doi:10.1016/S1074-7613(00)80398-2.
- Dehairs J, Talebi A, Cherifi Y, Swinnen J V. CRISP-ID: decoding CRISPR mediated indels by Sanger sequencing. *Sci Rep* 2016;6:28973. doi:10.1038/srep28973.
- Doench JG, Hartenian E, Graham DB, Tothova Z, Hegde M, Smith I, et al. Rational design of highly active sgRNAs for CRISPR-Cas9-mediated gene inactivation. *Nat Biotechnol* 2014;32:1262–7. doi:10.1038/nbt.3026.
- Doig CL, Fletcher RS, Morgan SA, McCabe EL, Larner DP, Tomlinson JW, et al. 11 β -HSD1 modulates the set point of brown adipose tissue response to glucocorticoids in male mice. *Endocrinology* 2017;158:1964–76. doi:10.1210/en.2016-1722.
- Domann R, Martinez J. Alternative to cloning cylinders for isolation of adherent cell clones. *Biotechniques* 1995;18:594–5.
- Endo A. A historical perspective on the discovery of statins. *Proc Jpn Acad Ser B Phys Biol Sci* 2010;86:484–93. doi:10.2183/PJAB.86.484.

- Espinasse M-A, Pépin A, Virault-Rocroy P, Szely N, Chollet-Martin S, Pallardy M, et al. Glucocorticoid-induced leucine zipper is expressed in human neutrophils and promotes apoptosis through Mcl-1 down-regulation. *J Innate Immun* 2016;8:81–96. doi:10.1159/000439052.
- Fan H, Morand EF. Targeting the side effects of steroid therapy in autoimmune diseases: the role of GILZ. *Discov Med* 2012;13:123–33.
- Franceschi C, Bonafè M, Valensin S, Olivieri F, De Luca M, Ottaviani E, et al. Inflamm-aging: an evolutionary perspective on immunosenescence. *Ann N Y Acad Sci* 2000;908:244–54. doi:10.1111/j.1749-6632.2000.tb06651.x.
- Franceschi C, Capri M, Monti D, Giunta S, Olivieri F, Sevini F, et al. Inflammaging and anti-inflammaging: A systemic perspective on aging and longevity emerged from studies in humans. *Mech Ageing Dev* 2007;128:92–105. doi:10.1016/j.mad.2006.11.016.
- Franceschi C, Garagnani P, Parini P, Giuliani C, Santoro A. Inflammaging: a new immune–metabolic viewpoint for age-related diseases. *Nat Rev Endocrinol* 2018;14:576–90. doi:10.1038/s41574-018-0059-4.
- Fulop T, Larbi A, Dupuis G, Le Page A, Frost EH, Cohen AA, et al. Immunosenescence and inflamm-aging as two sides of the same coin: friends or foes? *Front Immunol* 2018;8:1960. doi:10.3389/fimmu.2017.01960.
- Gadbut A, Caruso A, Galper J. Differential sensitivity of C2-C12 striated muscle cells to lovastatin and pravastatin. *J Mol Cell Cardiol* 1995;27:2397–402. doi:10.1016/S0022-2828(95)92163-X.
- Gaffey AE, Bergeman CS, Clark LA, Wirth MM. Aging and the HPA axis: Stress and resilience in older adults. *Neurosci Biobehav Rev* 2016;68:928–45. doi:10.1016/j.neubiorev.2016.05.036.
- Gazzerro P, Proto MC, Gangemi G, Malfitano AM, Ciaglia E, Pisanti S, et al. Pharmacological actions of statins: a critical appraisal in the management of cancer. *Pharmacol Rev* 2012;64:102–46. doi:10.1124/pr.111.004994.
- Gene. Information, Bethesda (MD): National Library of Medicine (US); National Center for Biotechnology; 2004. <https://www.ncbi.nlm.nih.gov/gene/>.
- Genedani S, Filaferro M, Carone C, Ostan R, Bucci L, Cevenini E, et al. Influence of f-MLP, ACTH(1-24) and CRH on in vitro chemotaxis of monocytes from centenarians. *Neuroimmunomodulation* 2008;15:285–9. doi:10.1159/000156472.
- Geraerts M, Willems S, Baekelandt V, Debyser Z, Gijssbers R. Comparison of lentiviral vector titration methods. *BMC Biotechnol* 2006;6:34. doi:10.1186/1472-6750-6-34.
- Gilmour JS, Coutinho AE, Cailhier J-F, Man TY, Clay M, Thomas G, et al. Local amplification of glucocorticoids by 11 β -hydroxysteroid dehydrogenase type 1 promotes macrophage phagocytosis of apoptotic leukocytes. *J Immunol* 2006;176:7605–11. doi:10.4049/jimmunol.176.12.7605.
- Gong S, Miao Y-L, Jiao G-Z, Sun M-J, Li H, Lin J, et al. Dynamics and correlation of serum cortisol and corticosterone under different physiological or stressful conditions in mice. *PLoS One* 2015;10:e0117503. doi:10.1371/journal.pone.0117503.
- Grundey SM, Stone NJ, Chair V, Bailey AL, Jones DW, Beam C, et al. 2018 AHA/ACC/AACVPR/AAPA/ABC/ACPM/ADA/AGS/APhA/ASPC/NLA/PCNA guideline on the management of blood cholesterol. *Circulation* 2018. doi:10.1161/CIR.0000000000000625.

- Gu R, Ding X, Tang W, Lei B, Jiang C, Xu G. A synthesized glucocorticoid- induced leucine zipper peptide inhibits retinal Müller cell gliosis. *Front Pharmacol* 2018;9:331. doi:10.3389/fphar.2018.00331.
- Gupta D, Morley JE. Hypothalamic-pituitary-adrenal (HPA) axis and aging. *Compr Physiol* 2014;4:1495–510. doi:10.1002/cphy.c130049.
- Hahn RT, Hoppstädter J, Hirschfelder K, Hachenthal N, Diesel B, Kessler SM, et al. Downregulation of the glucocorticoid-induced leucine zipper (GILZ) promotes vascular inflammation. *Atherosclerosis* 2014;234:391–400. doi:10.1016/j.atherosclerosis.2014.03.028.
- Hanai J, Cao P, Tanksale P, Imamura S, Koshimizu E, Zhao J, et al. The muscle-specific ubiquitin ligase atrogin-1/MAFbx mediates statin-induced muscle toxicity. *J Clin Invest* 2007;117:3940–51. doi:10.1172/JCI32741.
- Hassan-Smith ZK, Morgan SA, Sherlock M, Hughes B, Taylor AE, Lavery GG, et al. Gender-specific differences in skeletal muscle 11 β -HSD1 expression across healthy aging. *J Clin Endocrinol Metab* 2015;100:2673–81. doi:10.1210/jc.2015-1516.
- Heller DJ, Coxson PG, Penko J, Pletcher MJ, Goldman L, Odden MC, et al. Evaluating the impact and cost-effectiveness of statin use guidelines for primary prevention of coronary heart disease and stroke. *Circulation* 2017;136:1087–98. doi:10.1161/CIRCULATIONAHA.117.027067.
- Hermann M, Bogsrud M, Molden E, Asberg A, Mohebi B, Ose L, et al. Exposure of atorvastatin is unchanged but lactone and acid metabolites are increased several-fold in patients with atorvastatin-induced myopathy. *Clin Pharmacol Ther* 2006;79:532–9. doi:10.1016/j.clpt.2006.02.014.
- Herriot H, Wrosch C, Gouin JP, Miller GE. Intra-individual cortisol variability and low-grade inflammation over 10 years in older adults. *Psychoneuroendocrinology* 2017;77:141–9. doi:10.1016/j.psyneuen.2016.12.010.
- Holmes MC, Carter RN, Noble J, Chitnis S, Dutia A, Paterson JM, et al. 11 β -hydroxysteroid dehydrogenase type 1 expression is increased in the aged mouse hippocampus and parietal cortex and causes memory impairments. *J Neurosci* 2010;30:6916–20. doi:10.1523/JNEUROSCI.0731-10.2010.
- Hoppstädter J, Hachenthal N, Valbuena-Perez JV, Lampe S, Astanina K, Kunze MM, et al. Induction of glucocorticoid-induced leucine zipper (GILZ) contributes to anti-inflammatory effects of the natural product curcumin in macrophages. *J Biol Chem* 2016;291:22949–60. doi:10.1074/jbc.M116.733253.
- Hoppstädter J, Kessler SM, Bruscoli S, Huwer H, Riccardi C, Kiemer AK. Glucocorticoid-induced leucine zipper: a critical factor in macrophage endotoxin tolerance. *J Immunol* 2015;194:6057–67. doi:10.4049/jimmunol.1403207.
- Huacuja Álvarez F, Gómez Duque M, Ortiz Vargas JC, Soberanes Velázquez B, Arévalo Moreno V, Morales Villegas E, et al. Efecto de las estatinas más allá del colesterol. *Rev Endocrinol y Nutr* 2006;14:73–88.
- Huang S-H, Hsiao C-D, Lin D-S, Chow C-Y, Chang C-J, Liao I. Imaging of zebrafish in vivo with second-harmonic generation reveals shortened sarcomeres associated with myopathy induced by statin. *PLoS One* 2011;6:e24764. doi:10.1371/journal.pone.0024764.
- Jackaman C, Tomay F, Duong L, Abdol Razak NB, Pixley FJ, Metharom P, et al. Aging and cancer: The role of macrophages and neutrophils. *Ageing Res Rev* 2017;36:105–16. doi:10.1016/j.arr.2017.03.008.

- Janeway CJ, Travers P, Walport M, Shlomchik M. Principles of innate and adaptive immunity. Immunobiol. Immune Syst. Heal. Dis. 5th ed., New York: Garland Science; 2001.
- Joha S, Nugues A-L, Héтуin D, Berthon C, Dezitter X, Dauphin V, et al. GILZ inhibits the mTORC2/AKT pathway in BCR-ABL(+) cells. *Oncogene* 2012;31:1419–30. doi:10.1038/onc.2011.328.
- Johnson TE, Zhang X, Bleicher KB, Dysart G, Loughlin AF, Schaefer WH, et al. Statins induce apoptosis in rat and human myotube cultures by inhibiting protein geranylgeranylation but not ubiquinone. *Toxicol Appl Pharmacol* 2004;200:237–50. doi:10.1016/j.taap.2004.04.010.
- Joung J, Konermann S, Gootenberg JS, Abudayyeh OO, Platt RJ, Brigham MD, et al. Protocol: Genome-scale CRISPR-Cas9 knockout and transcriptional activation screening. *Nat Protoc* 2017;12:059626. doi:10.1101/059626.
- Kaufmann P, Török M, Zahno A, Waldhauser KM, Brecht K, Krähenbühl S. Toxicity of statins on rat skeletal muscle mitochondria. *Cell Mol Life Sci* 2006;63:2415–25. doi:10.1007/s00018-006-6235-z.
- Kawamoto EM, Munhoz CD, Glezer I, Bahia VS, Caramelli P, Nitrini R, et al. Oxidative state in platelets and erythrocytes in aging and Alzheimer's disease. *Neurobiol Aging* 2005;26:857–64. doi:10.1016/J.NEUROBIOLAGING.2004.08.011.
- Keire P, Shearer A, Shefer G, Yablonka-Reuveni Z. Isolation and culture of skeletal muscle myofibers as a means to analyze satellite cells. *Methods Mol Biol* 2013;946:431–68. doi:10.1007/978-1-62703-128-8_28.
- Kennedy BK, Berger SL, Brunet A, Campisi J, Cuervo AM, Epel ES, et al. Geroscience: linking aging to chronic disease. *Cell* 2014;159:709–13. doi:10.1016/j.cell.2014.10.039.
- Khansari N, Shakiba Y, Mahmoudi M. Chronic inflammation and oxidative stress as a major cause of age-related diseases and cancer. *Recent Pat Inflamm Allergy Drug Discov* 2009;3:73–80.
- Kharwanlang B, Sharma R. Glucocorticoid hormones in aging. In: Rattan S, Sharma R, editors. *Horm. Ageing Longev.*, vol. 6, Cham: Springer International Publishing; 2017, p. 37–55. doi:10.1007/978-3-319-63001-4_3.
- Kimmel CB, Ballard WW, Kimmel SR, Ullmann B, Schilling TF. Stages of embryonic development of the zebrafish. *Dev Dyn* 1995;203:253–310. doi:10.1002/aja.1002030302.
- Kizaki T, Ookawara T, Oh-Ishi S, Ito Y, Iwabuchi K, Onoé K, et al. An increase in basal glucocorticoid concentration with age induces suppressor macrophages with high-density FcγRII/III. *Immunology* 1998;93:409–14. doi:10.1046/j.1365-2567.1998.00433.x.
- Kizaki T, Suzuki K, Ookawara T, Izawa T, Saitoh D, Oh-Ishi S, et al. Stress- and aging-associated modulation of macrophage functions. *Environ Health Prev Med* 2002;6:218–28. doi:10.1007/BF02897973.
- Kobayashi M, Chisaki I, Narumi K, Hidaka K, Kagawa T, Itagaki S, et al. Association between risk of myopathy and cholesterol-lowering effect: a comparison of all statins. *Life Sci* 2008;82:969–75. doi:10.1016/j.lfs.2008.02.019.
- Köberle M, Göppel D, Grandl T, Gaentzsch P, Manncke B, Berchtold S, et al. *Yersinia enterocolitica* YopT and *Clostridium difficile* toxin B induce expression of GILZ in epithelial cells. *PLoS One* 2012;7:e40730. doi:10.1371/journal.pone.0040730.

- De la Fuente M, Miquel J. An update of the oxidation-inflammation theory of aging: the involvement of the immune system in oxi-inflamm-aging. *Curr Pharm Des* 2009;15:3003–26. doi:10.2174/138161209789058110.
- Laaksonen R, Katajamaa M, Päivä H, Sysi-Aho M, Saarinen L, Junni P, et al. A systems biology strategy reveals biological pathways and plasma biomarker candidates for potentially toxic statin-induced changes in muscle. *PLoS One* 2006;1:e97. doi:10.1371/journal.pone.0000097.
- Labos C, Brophy JM, Smith GD, Sniderman AD, Thanassoulis G. Evaluation of the pleiotropic effects of statins. *Arterioscler Thromb Vasc Biol* 2018;38:262–5. doi:10.1161/ATVBAHA.117.310052.
- Laufs U, Filipiak KJ, Gouni-Berthold I, Catapano AL, Mandraffino G, Benlian P. Practical aspects in the management of statin-associated muscle symptoms (SAMS). *Atheroscler Suppl* 2017;26:45–55. doi:10.1016/S1567-5688(17)30024-7.
- Lee M-J, Yang R-Z, Karastergiou K, Smith SR, Chang JR, Gong D-W, et al. Low expression of the GILZ may contribute to adipose inflammation and altered adipokine production in human obesity. *J Lipid Res* 2016;57:1256–63. doi:10.1194/jlr.M067728.
- López-Otín C, Blasco MA, Partridge L, Serrano M, Kroemer G. The hallmarks of aging. *Cell* 2013;153:1194–217. doi:10.1016/j.cell.2013.05.039.
- Luan Z, Chase AJ, Newby AC. Statins inhibit secretion of metalloproteinases-1, -2, -3, and -9 from vascular smooth muscle cells and macrophages. *Arterioscler Thromb Vasc Biol* 2003;23:769–75. doi:10.1161/01.ATV.0000068646.76823.AE.
- Mallinson JE, Constantin-Teodosiu D, Sidaway J, Westwood FR, Greenhaff PL. Blunted Akt/FOXO signalling and activation of genes controlling atrophy and fuel use in statin myopathy. *J Physiol* 2009;587:219–30. doi:10.1113/jphysiol.2008.164699.
- Di Marco B, Massetti M, Bruscoli S, Macchiarulo A, Di Virgilio R, Velardi E, et al. Glucocorticoid-induced leucine zipper (GILZ)/NF-kappaB interaction: role of GILZ homo-dimerization and C-terminal domain. *Nucleic Acids Res* 2007;35:517–28. doi:10.1093/nar/gkl1080.
- Margaritis M, Channon KM, Antoniades C. Statins as regulators of redox state in the vascular endothelium: beyond lipid lowering. *Antioxid Redox Signal* 2014;20:1198–215. doi:10.1089/ars.2013.5430.
- Mendis S, Puska P, Norrving B, editors. *Global Atlas on Cardiovascular Disease Prevention and Control*. Geneva: World Health Organization; 2011.
- Minciullo PL, Catalano A, Mandraffino G, Casciaro M, Crucitti A, Maltese G, et al. Inflammaging and anti-inflammaging: the role of cytokines in extreme longevity. *Arch Immunol Ther Exp (Warsz)* 2016;64:111–26. doi:10.1007/s00005-015-0377-3.
- Moffat J, Grueneberg DA, Yang X, Kim SY, Kloepfer AM, Hinkle G, et al. A lentiviral RNAi library for human and mouse genes applied to an arrayed viral high-content screen. *Cell* 2006;124:1283–98. doi:10.1016/j.cell.2006.01.040.
- Morano MI, Vázquez DM, Akil H. The role of the hippocampal mineralocorticoid and glucocorticoid receptors in the hypothalamo-pituitary-adrenal axis of the aged fisher rat. *Mol Cell Neurosci* 1994;5:400–12. doi:10.1006/MCNE.1994.1050.
- Moßhammer D, Schaeffeler E, Schwab M, Mörike K. Mechanisms and assessment of statin-related muscular adverse effects. *Br J Clin Pharmacol* 2014;78:454–66. doi:10.1111/bcp.12360.

- Muntean DM, Thompson PD, Catapano AL, Stasiolek M, Fabis J, Muntner P, et al. Statin-associated myopathy and the quest for biomarkers: can we effectively predict statin-associated muscle symptoms? *Drug Discov Today* 2017;22:85–96. doi:10.1016/J.DRUDIS.2016.09.001.
- Needham M, Mastaglia FL. Statin myotoxicity: a review of genetic susceptibility factors. *Neuromuscul Disord* 2014;24:4–15. doi:10.1016/j.nmd.2013.09.011.
- Newman CB, Preiss D, Tobert JA, Jacobson TA, Page RL, Goldstein LB, et al. Statin safety and associated adverse events: a scientific statement from the American Heart Association. *Arterioscler Thromb Vasc Biol* 2019;39. doi:10.1161/ATV.0000000000000073.
- Nolte E, Newbould J, Conklin A. International variation in the usage of medicines: a review of the literature. *Rand* 2010:xi+43.
- Novikova OA, Laktionov PP, Karpenko AA. Mechanisms underlying atheroma induction: The roles of mechanotransduction, vascular wall cells, and blood cells. *Ann Vasc Surg* 2018;53:224–33. doi:10.1016/j.avsg.2018.04.030.
- O'Brien A, Bailey TL. GT-Scan: identifying unique genomic targets. *Bioinformatics* 2014;30:2673–5. doi:10.1093/bioinformatics/btu354.
- Oakley RH, Cidlowski JA. The biology of the glucocorticoid receptor: new signaling mechanisms in health and disease. *J Allergy Clin Immunol* 2013;132:1033–44. doi:10.1016/j.jaci.2013.09.007.
- Oesterle A, Laufs U, Liao JK. Pleiotropic effects of statins on the cardiovascular system. *Circ Res* 2017;120:229–43. doi:10.1161/CIRCRESAHA.116.308537.
- Ogura T, Tanaka Y, Nakata T, Namikawa T, Kataoka H, Ohtsubo Y. Simvastatin reduces insulin-like growth factor-1 signaling in differentiating C2C12 mouse myoblast cells in an HMG-CoA reductase inhibition-independent manner. *J Toxicol Sci* 2007;32:57–67. doi:10.2131/jts.32.57.
- Osaki Y, Nakagawa Y, Miyahara S, Iwasaki H, Ishii A, Matsuzaka T, et al. Skeletal muscle-specific HMG-CoA reductase knockout mice exhibit rhabdomyolysis: A model for statin-induced myopathy. *Biochem Biophys Res Commun* 2015;466:536–40. doi:10.1016/j.bbrc.2015.09.065.
- Park KH, Weisleder N, Zhou J, Gumpfer K, Zhou X, Duann P, et al. Assessment of calcium sparks in intact skeletal muscle fibers. *J Vis Exp* 2014:e50898. doi:10.3791/50898.
- Parmar KM, Nambudiri V, Dai G, Larman HB, Gimbrone MA, García-Cardena G. Statins exert endothelial atheroprotective effects via the KLF2 transcription factor. *J Biol Chem* 2005;280:26714–9. doi:10.1074/jbc.C500144200.
- Pasha R, Moon TW. Coenzyme Q10 protects against statin-induced myotoxicity in zebrafish larvae (*Danio rerio*). *Environ Toxicol Pharmacol* 2017;52:150–60. doi:10.1016/J.ETAP.2017.03.021.
- Prattichizzo F, Bonafè M, Olivieri F, Franceschi C. Senescence associated macrophages and macroph-aging: are they pieces of the same puzzle? *Aging (Albany NY)* 2016;8:3159–60. doi:10.18632/aging.101133.
- Raison CL, Miller AH. When not enough is too much: the role of insufficient glucocorticoid signaling in the pathophysiology of stress-related disorders. *Am J Psychiatry* 2003;160:1554–65. doi:10.1176/appi.ajp.160.9.1554.

- Ramamoorthy S, Cidlowski JA. Ligand-induced repression of the glucocorticoid receptor gene is mediated by an NCoR1 repression complex formed by long-range chromatin interactions with intragenic glucocorticoid response elements. *Mol Cell Biol* 2013;33:1711–22. doi:10.1128/MCB.01151-12.
- Rashmi P, Colussi G, Ng M, Wu X, Kidwai A, Pearce D. Glucocorticoid-induced leucine zipper protein regulates sodium and potassium balance in the distal nephron. *Kidney Int* 2017;91:1159–77. doi:10.1016/j.kint.2016.10.038.
- Ravenscroft G, Nowak KJ, Jackaman C, Clément S, Lyons MA, Gallagher S, et al. Dissociated flexor digitorum brevis myofiber culture system - A more mature muscle culture system. *Cell Motil Cytoskeleton* 2007;64:727–38. doi:10.1002/cm.20223.
- Ridker PM, Danielson E, Fonseca FAH, Genest J, Gotto AM, Kastelein JJP, et al. Rosuvastatin to prevent vascular events in men and women with elevated c-reactive protein. *N Engl J Med* 2008;359:2195–207. doi:10.1056/NEJMoa0807646.
- Ridker PM, Everett BM, Thuren T, MacFadyen JG, Chang WH, Ballantyne C, et al. Antiinflammatory therapy with canakinumab for atherosclerotic disease. *N Engl J Med* 2017;377:1119–31. doi:10.1056/NEJMoa1707914.
- Rikans LE, Moore DR, Snowden CD. Sex-dependent differences in the effects of aging on antioxidant defense mechanisms of rat liver. *BBA - Gen Subj* 1991;1074:195–200. doi:10.1016/0304-4165(91)90061-K.
- Robert O, Boujedidi H, Bigorgne A, Ferrere G, Voican CS, Vettorazzi S, et al. Decreased expression of the glucocorticoid receptor-GILZ pathway in Kupffer cells promotes liver inflammation in obese mice. *J Hepatol* 2016;64:916–24. doi:10.1016/j.jhep.2015.11.023.
- Ronchetti S, Migliorati G, Riccardi C. GILZ as a mediator of the anti-inflammatory effects of glucocorticoids. *Front Endocrinol (Lausanne)* 2015;6:170. doi:10.3389/fendo.2015.00170.
- Ross R. Atherosclerosis — An Inflammatory Disease. *N Engl J Med* 1999;340:115–26. doi:10.1056/NEJM199901143400207.
- Sakamoto K, Honda T, Yokoya S, Waguri S, Kimura J. Rab-small GTPases are involved in fluvastatin and pravastatin-induced vacuolation in rat skeletal myofibers. *FASEB J* 2007;21:4087–94. doi:10.1096/fj.07-8713com.
- Sakamoto K, Kimura J. Mechanism of Statin-Induced Rhabdomyolysis. *J Pharmacol Sci* 2013;123:289–94. doi:10.1254/jphs.13R06CP.
- Sakamoto K, Wada I, Kimura J. Inhibition of Rab1 GTPase and endoplasmic reticulum-to-golgi trafficking underlies statin's toxicity in rat skeletal myofibers. *J Pharmacol Exp Ther* 2011;338:62–9. doi:10.1124/jpet.111.179762.
- Salami JA, Warraich H, Valero-Elizondo J, Spatz ES, Desai NR, Rana JS, et al. National trends in statin use and expenditures in the US adult population from 2002 to 2013. *JAMA Cardiol* 2017;2:56. doi:10.1001/jamacardio.2016.4700.
- Sanchez AMJ, Candau RB, Bernardi H. FoxO transcription factors: their roles in the maintenance of skeletal muscle homeostasis. *Cell Mol Life Sci* 2014;71:1657–71. doi:10.1007/s00018-013-1513-z.
- Sanjana NE, Shalem O, Zhang F. Improved vectors and genome-wide libraries for CRISPR screening. *Nat Methods* 2014;11:783–4. doi:10.1038/nmeth.3047.

- Sarbassov DD, Guertin DA, Ali SM, Sabatini DM. Phosphorylation and regulation of Akt/PKB by the Rictor-mTOR complex. *Science* 2005;307:1098–101. doi:10.1126/science.1106148.
- Scherr M, Battmer K, Blömer U, Ganser A, Grez M. Quantitative determination of lentiviral vector particle numbers by real-time PCR. *Biotechniques* 2001;31:520–6.
- Schindelin J, Arganda-Carreras I, Frise E, Kaynig V, Longair M, Pietzsch T, et al. Fiji: an open-source platform for biological-image analysis. *Nat Methods* 2012;9:676–82. doi:10.1038/nmeth.2019.
- Schirris TJJ, Renkema GH, Ritschel T, Voermans NC, Bilos A, van Engelen BGM, et al. Statin-induced myopathy is associated with mitochondrial complex III inhibition. *Cell Metab* 2015;22:399–407. doi:10.1016/J.CMET.2015.08.002.
- Sebastián C, Espia M, Serra M, Celada A, Lloberas J. MacrophAging: A cellular and molecular review. *Immunobiology* 2005;210:121–6. doi:10.1016/j.imbio.2005.05.006.
- Selman C, Speakman JR, Collins AR, Mayer C, Redman P, McLaren JS, et al. Lifelong α -tocopherol supplementation increases the median life span of C57BL/6 Mice in the cold but has only minor effects on oxidative damage. *Rejuvenation Res* 2008;11:83–96. doi:10.1089/rej.2007.0586.
- Sen-Banerjee S, Mir S, Lin Z, Hamik A, Atkins GB, Das H, et al. Kruppel-Like Factor 2 as a Novel Mediator of Statin Effects in Endothelial Cells. *Circulation* 2005;112:720–6. doi:10.1161/CIRCULATIONAHA.104.525774.
- Sergio G. Exploring the complex relations between inflammation and aging (inflamm-aging): anti-inflamm-aging remodelling of inflamm-aging, from robustness to frailty. *Inflamm Res* 2008;57:558–63. doi:10.1007/s00011-008-7243-2.
- Shi X, Shi W, Li Q, Song B, Wan M, Bai S, et al. A glucocorticoid-induced leucine-zipper protein, GILZ, inhibits adipogenesis of mesenchymal cells. *EMBO Rep* 2003;4:374–80. doi:10.1038/sj.embor.embor805.
- Simon Y, Kessler SM, Gemperlein K, Bohle RM, Müller R, Haybaeck J, et al. Elevated free cholesterol in a p62 overexpression model of non-alcoholic steatohepatitis. *World J Gastroenterol* 2014;20:17839–50. doi:10.3748/wjg.v20.i47.17839.
- Sirtori CR. The pharmacology of statins. *Pharmacol Res* 2014;88:3–11. doi:10.1016/J.PHRS.2014.03.002.
- Skottheim IB, Gedde-Dahl A, Hejazifar S, Hoel K, Asberg A. Statin induced myotoxicity: the lactone forms are more potent than the acid forms in human skeletal muscle cells in vitro. *Eur J Pharm Sci* 2008;33:317–25. doi:10.1016/j.ejps.2007.12.009.
- du Souich P, Roederer G, Dufour R. Myotoxicity of statins: Mechanism of action. *Pharmacol Ther* 2017;175:1–16. doi:10.1016/j.pharmthera.2017.02.029.
- Soundararajan R, Wang J, Melters D, Pearce D. Differential activities of glucocorticoid-induced leucine zipper protein isoforms. *J Biol Chem* 2007;282:36303–13. doi:10.1074/jbc.M707287200.
- Soundararajan R, Zhang TT, Wang J, Vandewalle A, Pearce D. A novel role for glucocorticoid-induced leucine zipper protein in epithelial sodium channel-mediated sodium transport. *J Biol Chem* 2005;280:39970–81. doi:10.1074/jbc.M508658200.

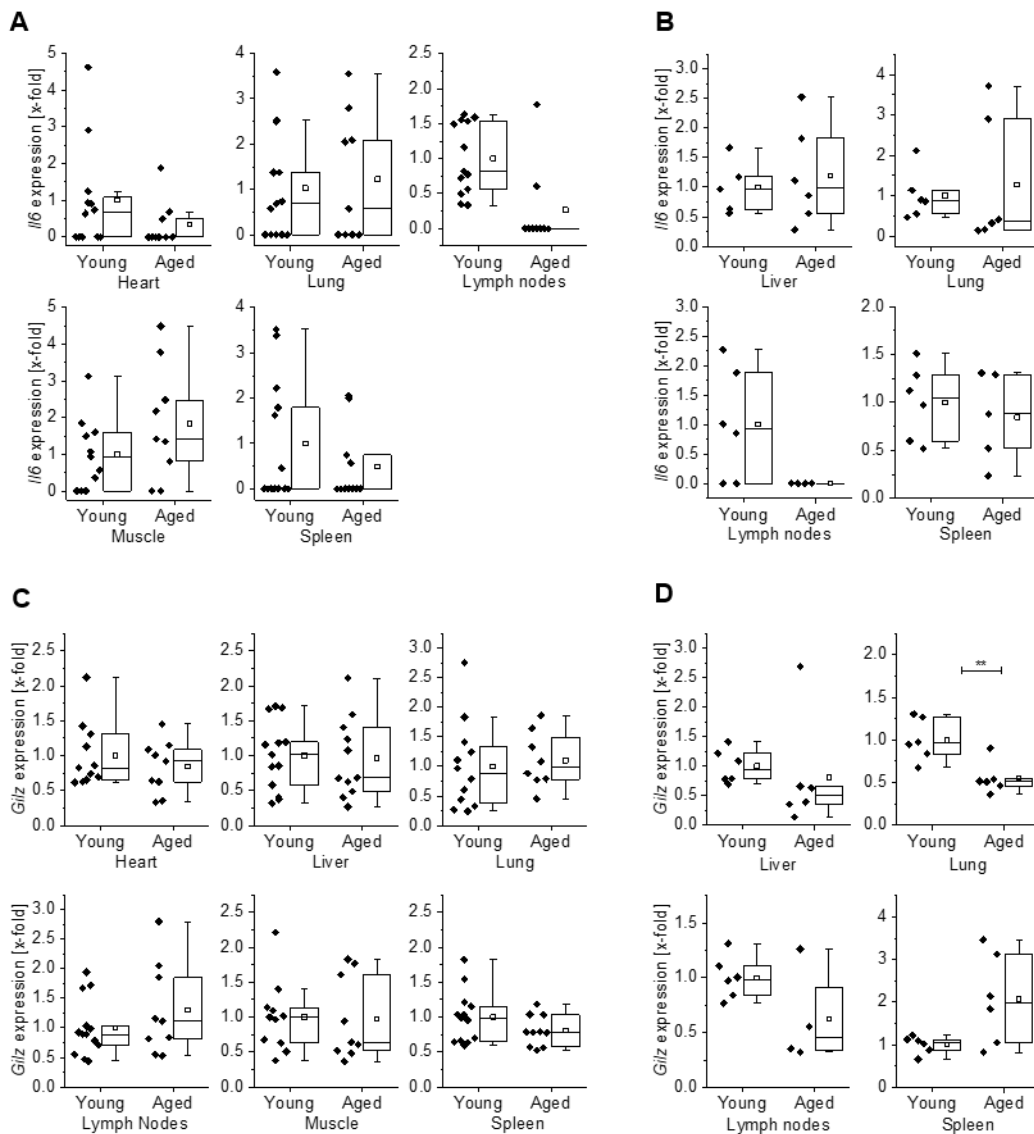
- Srinivasan M, Bayon B, Chopra N, Lahiri DK. Novel nuclear factor-kappaB targeting peptide suppresses β -amyloid induced inflammatory and apoptotic responses in neuronal cells. *PLoS One* 2016;11:e0160314. doi:10.1371/journal.pone.0160314.
- Stone NJ, Robinson JG, Lichtenstein AH, Bairey Merz CN, Blum CB, Eckel RH, et al. 2013 ACC/AHA guideline on the treatment of blood cholesterol to reduce atherosclerotic cardiovascular risk in adults. *Circulation* 2014;129:S1–45. doi:10.1161/01.cir.0000437738.63853.7a.
- Stroes ES, Thompson PD, Corsini A, Vladutiu GD, Raal FJ, Ray KK, et al. Statin-associated muscle symptoms: impact on statin therapy—European Atherosclerosis Society Consensus Panel Statement on Assessment, Aetiology and Management. *Eur Heart J* 2015;36:1012–22. doi:10.1093/eurheartj/ehv043.
- Taha DA, De Moor CH, Barrett DA, Gershkovich P. Translational insight into statin-induced muscle toxicity: from cell culture to clinical studies. *Transl Res* 2014;164:85–109. doi:10.1016/j.trsl.2014.01.013.
- Taha DA, De Moor CH, Barrett DA, Lee JB, Gandhi RD, Hoo CW, et al. The role of acid-base imbalance in statin-induced myotoxicity. *Transl Res* 2016;174:140–160.e14. doi:10.1016/J.TRSL.2016.03.015.
- Taylor F, Huffman MD, Macedo AF, Moore TH, Burke M, Davey Smith G, et al. Statins for the primary prevention of cardiovascular disease. *Cochrane Database Syst Rev* 2013. doi:10.1002/14651858.CD004816.pub5.
- Theunissen TW, Powell BE, Wang H, Mitalipova M, Faddah DA, Reddy J, et al. Systematic identification of culture conditions for induction and maintenance of naive human pluripotency. *Cell Stem Cell* 2014;15:471–87. doi:10.1016/j.stem.2014.07.002.
- Tiganescu A, Tahrani AA, Morgan SA, Otranto M, Desmoulière A, Abrahams L, et al. 11 β -Hydroxysteroid dehydrogenase blockade prevents age-induced skin structure and function defects. *J Clin Invest* 2013;123:3051–60. doi:10.1172/JCI64162.
- Tomlinson JW, Walker EA, Bujalska IJ, Draper N, Lavery GG, Cooper MS, et al. 11 β -hydroxysteroid dehydrogenase type 1: a tissue-specific regulator of glucocorticoid response. *Endocr Rev* 2004;25:831–66. doi:10.1210/er.2003-0031.
- Tousoulis D, Psarros C, Demosthenous M, Patel R, Antoniadis C, Stefanadis C. Innate and adaptive inflammation as a therapeutic target in vascular disease: the emerging role of statins. *J Am Coll Cardiol* 2014;63:2491–502. doi:10.1016/j.jacc.2014.01.054.
- Trapani L, Segatto M, La Rosa P, Fanelli F, Moreno S, Marino M, et al. 3-hydroxy 3-methylglutaryl coenzyme A reductase inhibition impairs muscle regeneration. *J Cell Biochem* 2012;113:2057–63. doi:10.1002/jcb.24077.
- Tse WKF, Jiang YJ, Wong CKC. Zebrafish transforming growth factor- β -stimulated clone 22 domain 3 (TSC22D3) plays critical roles in Bmp-dependent dorsoventral patterning via two deubiquitylating enzymes Usp15 and Otud4. *Biochim Biophys Acta - Gen Subj* 2013;1830:4584–93. doi:10.1016/j.bbagen.2013.05.006.
- Tuomisto TT, Lumivuori H, Kansanen E, Häkkinen S-K, Turunen MP, van Thienen J V., et al. Simvastatin has an anti-inflammatory effect on macrophages via upregulation of an atheroprotective transcription factor, Kruppel-like factor 2. *Cardiovasc Res* 2008;78:175–84. doi:10.1093/cvr/cvn007.

- Vaklavas C, Chatzizisis YS, Ziakas A, Zamboulis C, Giannoglou GD. Molecular basis of statin-associated myopathy. *Atherosclerosis* 2009;202:18–28. doi:10.1016/j.atherosclerosis.2008.05.021.
- Vancheri F, Backlund L, Strender L-E, Godman B, Wettermark B. Time trends in statin utilisation and coronary mortality in Western European countries. *BMJ Open* 2016;6:e010500. doi:10.1136/bmjopen-2015-010500.
- Veliça P, Bunce CM. A quick, simple and unbiased method to quantify C2C12 myogenic differentiation. *Muscle Nerve* 2011;44:366–70. doi:10.1002/mus.22056.
- Wang S, Xie X, Lei T, Zhang K, Lai B, Zhang Z, et al. Statins attenuate activation of the NLRP3 inflammasome by oxidized LDL or TNF α in vascular endothelial cells through a PXR-dependent mechanism. *Mol Pharmacol* 2017;92:256–64. doi:10.1124/mol.116.108100.
- Weber NC, Blumenthal SB, Hartung T, Vollmar AM, Kiemer AK. ANP inhibits TNF- α -induced endothelial MCP-1 expression-involvement of p38 MAPK and MKP-1. *J Leukoc Biol* 2003;74:932–41. doi:10.1189/jlb.0603254.
- Weisleder N, Zhou J, Ma J. Detection of calcium sparks in intact and permeabilized skeletal muscle fibers. *Methods Mol Biol* 2012;798:395–410. doi:10.1007/978-1-61779-343-1_23.
- World Health Organization. The top 10 causes of death 2018. <https://www.who.int/news-room/fact-sheets/detail/the-top-10-causes-of-death> (accessed March 16, 2019).
- Wynn TA, Chawla A, Pollard JW. Macrophage biology in development, homeostasis and disease. *Nature* 2013;496:445–55. doi:10.1038/nature12034.
- Yang N, Zhang W, Shi X-M. Glucocorticoid-induced leucine zipper (GILZ) mediates glucocorticoid action and inhibits inflammatory cytokine-induced COX-2 expression. *J Cell Biochem* 2008;103:1760–71. doi:10.1002/jcb.21562.
- Yuan X, Klein D, Kerscher S, West BL, Weis J, Katona I, et al. Macrophage depletion ameliorates peripheral neuropathy in aging mice. *J Neurosci* 2018;38:4610–20. doi:10.1523/JNEUROSCI.3030-17.2018.
- Zambrano E, Reyes-Castro LA, Nathanielsz PW. Aging, glucocorticoids and developmental programming. *Age (Dordr)* 2015;37:9774. doi:10.1007/s11357-015-9774-0.
- Zhang TY, Daynes RA. Macrophages from 11 -hydroxysteroid dehydrogenase type 1-deficient mice exhibit an increased sensitivity to lipopolysaccharide stimulation due to TGF-mediated up-regulation of SHIP1 expression. *J Immunol* 2007;179:6325–35. doi:10.4049/jimmunol.179.9.6325.
- Zhang TY, Ding X, Daynes RA. The expression of 11 -hydroxysteroid dehydrogenase type i by lymphocytes provides a novel means for intracrine regulation of glucocorticoid activities. *J Immunol* 2005;174:879–89. doi:10.4049/jimmunol.174.2.879.

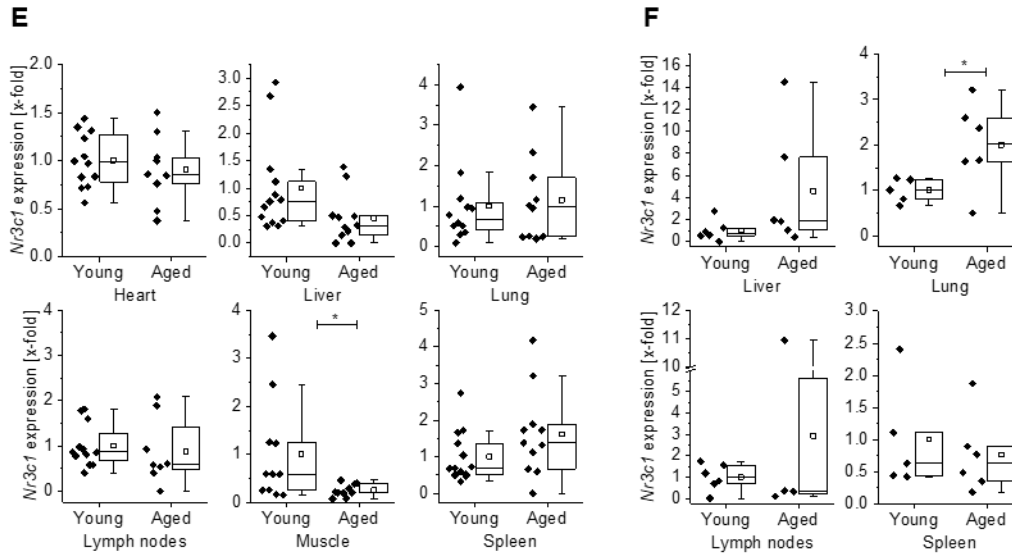
Appendix

Appendix 1

Gene expression in tissues from young and aged WT mice. *Gilz*, *Il6*, and *GR (Nr3c1)* mRNA expression levels were measured in heart, liver, lung, lymph nodes, skeletal muscle, and spleen tissues from young (10 weeks) and aged (80–100 weeks) C57BL/6 mice at the baseline (**A,C,E**, n=9–13), or in liver, lung, lymph nodes, and spleen after treatment with 5 mg/kg LPS for 4 hours (**B,D,F**, n=4–6). Gene expression was normalised against the housekeeping gene (*Ppia*) and is presented as fold change of young. Box-plots show the 25–75th percentiles (Box), mean (square), median (line) and range within 1.5 IQR (whiskers). Levels below LOD in A and B were assigned as zero-points for illustrational purposes. **P<0.01 relative to equally treated young mice.



Appendix

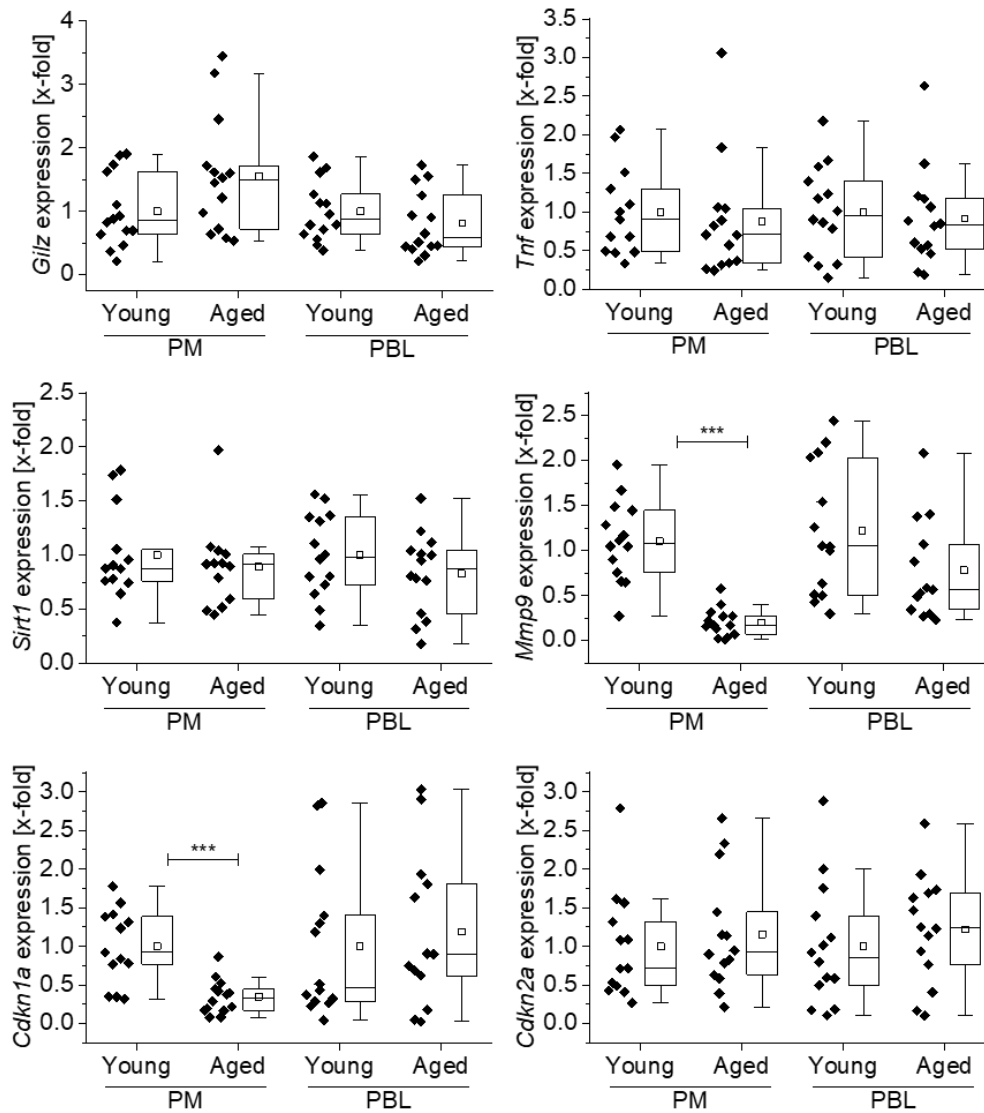


Gene expression in tissues from young and aged GILZ KO mice. mRNA expression was measured in tissues after treatment with 5 mg/kg LPS for 4 hours (n=4–6), normalised against the housekeeping gene (*Ppia*) and is presented as fold change of equally treated young WT. Data show mean (95% CI). *P<0.05 relative to equally treated young WT mice, as determined by Welch's t-test.

		Relative mRNA expression [x-fold]			
		<i>Tnf</i>	<i>Illb</i>	<i>Il6</i>	<i>Nr3c1</i>
Young KO	Liver	2.16 (0.73-3.58)	1.27 (0.43-2.10)	0.92 (0.02-1.82)	1.72 (0.17-3.26)
	Lung	0.81 (0.38-1.24)	1.05 (0.39-1.72)	1.45 (-0.25-3.15)	2.05 (0.92-3.19)*
	Lymph nodes	2.24 (0.98-3.50)	1.23 (0.44-2.02)	0.88 (-0.41-2.17)	1.27 (0.15-2.39)
	Spleen	0.63 (0.38-0.89)*	2.48 (0.07-4.90)	0.98 (-0.10-2.06)	0.79 (0.28-1.30)
Aged KO	Liver	3.51 (1.52-5.49)	1.30 (0.34-2.26)	1.49 (0.98-2.00)	11.8 (9.53-14.2)
	Lung	0.85 (0.28-1.42)	1.95 (0.39-3.51)	0.75 (-0.04-1.53)	1.22 (0.65-1.78)
	Lymph nodes	0.45 (0.27-0.63)	0.84 (0.33-1.36)	12.9 (-1.13-26.9)	1.76 (0.55-2.97)
	Spleen	0.56 (0.36-0.76)	1.60 (-0.08-3.27)	2.60 (0.36-4.83)	1.06 (0.53-1.60)

Appendix 2

Gene expression in PM/PBL from young and aged WT mice. mRNA expression levels were measured in PMs and PBLs from young (10 weeks) and aged (80–100 weeks) C57BL/6 mice (n=13–14). Gene expression was normalised against the housekeeping gene (*Ppia*) and is presented as fold change of young. Box-plots show the 25–75th percentiles (Box), mean (square), median (line) and range within 1.5 IQR (whiskers). ***P<0.001 relative to young mice.



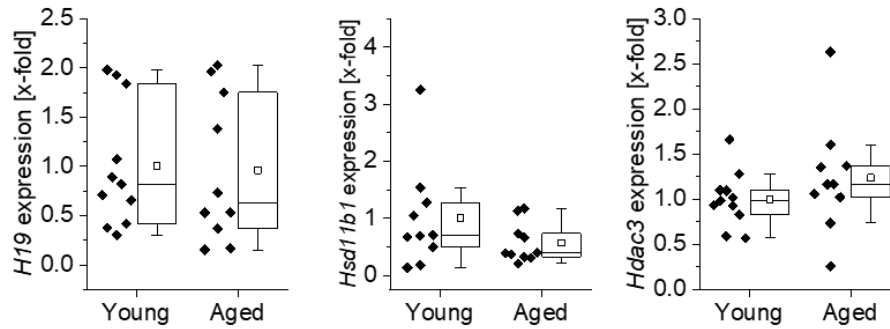
Appendix

Gene expression in PM/PBL from young GILZ KO mice. mRNA expression levels were measured in PMs and PBLs from young (10 weeks) GILZ KO mice (n=11). Gene expression was normalised against the housekeeping gene (*Ppia*) and is presented as fold change of young WT. Data show mean (95% CI). **P<0.01, ***P<0.001 relative to young WT mice, as determined by Welch's t-test.

Gene	PM	PBL
<i>Tnf</i>	1.26 (0.32-2.20)	0.66 (0.53-0.80)
<i>Mmp9</i>	1.31 (0.89-1.73)	1.31 (1.03-1.60)
<i>Nr3c1</i>	0.86 (0.73-1.00)	1.73 (1.37-2.10)**
<i>Anxa1</i>	1.66 (1.28-2.04)**	3.16 (1.88-4.44)**
<i>Dusp1</i>	1.38 (0.63-2.13)	1.04 (0.68-1.40)
<i>Sgk1</i>	1.63 (1.19-2.07)	0.91 (0.50-1.32)
<i>Hsd11b1</i>	0.62 (0.36-0.89)	0.96 (0.77-1.15)
<i>Hsd11b2</i>	1.14 (0.70-1.57)	1.12 (0.78-1.46)
<i>H6pd</i>	0.23 (0.18-0.28)***	1.06 (0.64-1.47)
<i>Cebpa</i>	0.85 (0.49-1.22)	1.10 (0.62-1.59)
<i>Cebpb</i>	0.98 (0.70-1.26)	1.23 (0.76-1.69)
<i>Cdkn1a</i>	1.02 (0.67-1.37)	1.37 (0.63-2.11)
<i>Cdkn2a</i>	1.49 (0.98-2.00)	1.89 (0.92-2.87)
<i>Sirt1</i>	0.96 (0.64-1.29)	0.87 (0.60-1.15)

Appendix 3

Gene expression in skeletal muscle from young and aged mice. mRNA expression levels were measured in skeletal muscle tissue from young (10 weeks) and aged (80–100 weeks) C57BL/6 mice (n=13–14). Gene expression was normalised against the housekeeping gene (*Ppia*) and is presented as fold change of young. Box-plots show the 25–75th percentiles (Box), mean (square), median (line) and range within 1.5 IQR (whiskers).



Acknowledgments

I would like to express my deeper gratitude to Prof. Alexandra Kiemer for inviting me to pursue my Ph.D. as part of her research group. Working in her laboratory has been an intellectually exciting, challenging, and enjoyable experience. Her guidance and trust made the successful completion of my research possible.

I thank Prof. Thorsten Lehr for accepting to take on the role of second examiner of my dissertation.

A very special acknowledgment to Dr. Jessica Hoppstädter, who was my main scientific support during these years. Thanks for the enriching dialogues, the trust in my ideas and research directions, the assistance and encouragement in every phase of this road, and the fun outside the lab. I will always appreciate having had her as my supervisor.

Thanks to all the persons that collaborated with my research project: Prof. Carlo Riccardi, Dr. Stefano Bruscoli, and the research groups of Prof. Markus R. Meyer and Prof. William K. F. Tse. I'd like to thank Anastasia Andreas from Prof. Rolf Müller's group for her assistance in providing the zebrafish embryos.

To all the members of the Pharmaceutical Biology research group, thanks for the cooperation, technical assistance, scientific exchange, and nice time. Especially to Anna Dembek and Beate Czepukojc, who were not only my colleagues but my friends all the way since the beginning. For the coffee pauses and the Friday afternoon music, for always being willing to listen and bring a set of fresh eyes when needed, thank you. It has been great to live the ups and downs of the Ph.D. life with you. Also, special thanks to Charlotte Dahlem for her valuable friendship and support, and to Rebecca Linnenberger for her help in the last stages of my work.

Thanks to Prof. Martha Fontanilla and Prof. Rosa Helena Bustos, who back in the day encouraged me to go for this dream I had of becoming a Ph.D. Thank you for always trusting I was up to the challenge.

To all my friends in both of my homes, thank you for the moral support. To the wonderful people I've met in Germany, who have always helped me and made me feel like I have a family here, too. And to the invaluable persons for whom an ocean of distance is no obstacle for being always there for me. Those who know my best and worst, have always listened to my hopes and fears, and helped me gain the strength to keep going. I am such a lucky person for having you in my life.

Acknowledgments

Most importantly, my loving gratitude to my family, for always believing in me. To my wonderful parents who I must thank for who I am, you are my driving force. Thanks for teaching me that our dreams come true when we work hard for it, for instilling the love for science into me and for being always sure that I could do it, especially when I wasn't. To David, thanks for being the best little brother, and always cheer me up with your sweetness and your trust. And to that loving, beautiful lady, who taught me so much and was always proud of me, you'll live forever in my heart. ¡los amo familia, esto es de ustedes!

At last, thank God for the wisdom and resilience that has been bestowed upon me during this research project, and indeed, throughout my life.